Master Thesis in Physics

The Harmonizable Representation of Complex-Valued Nonstationary Random Processes

Heidi Hindberg

May 2005

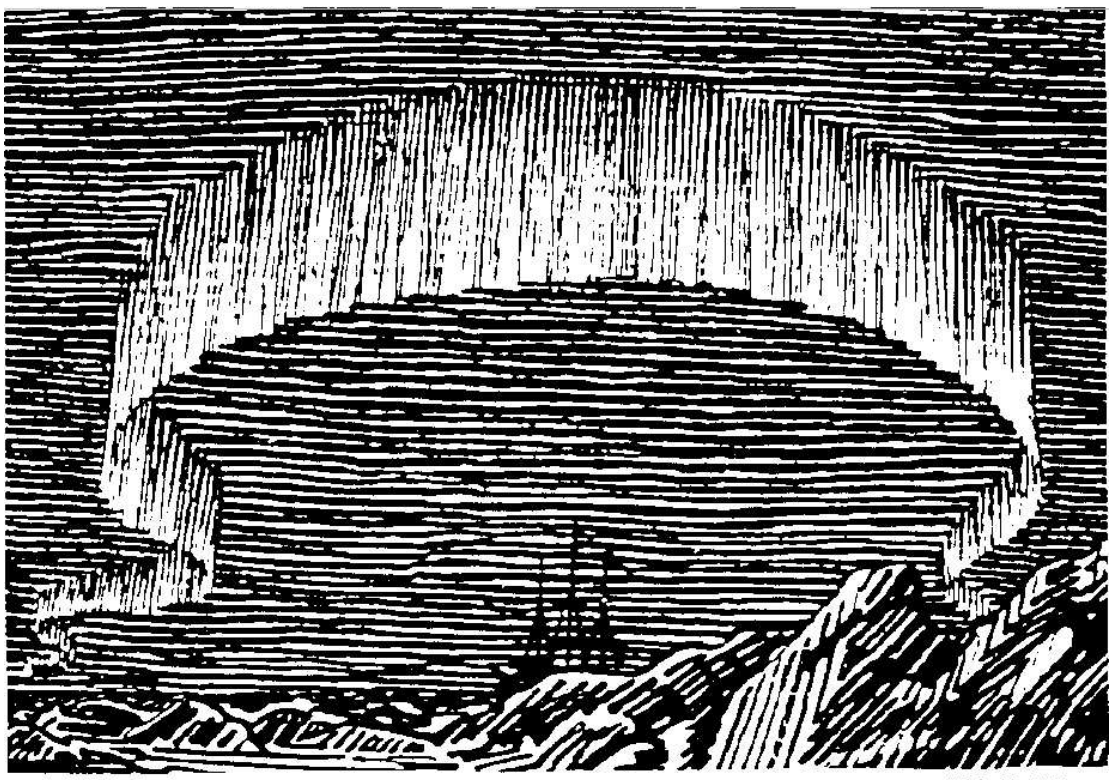

Original by F. Nansen

FACULTY OF SCIENCE
Department of Physics
University of Tromsø, N-9037 Tromsø, Norway, telephone: +47 77 64 51 50, fax no: +47 77 64 55 80

Abstract

In this thesis we study the second-order statistical moment functions that characterizes complex-valued harmonizable processes. A real-valued harmonizable process has four Hermitian second-order functions. These functions are equivalent representations of the second-order statistical quantities of the process. For a complex-valued harmonizable process, however, we need the complementary functions in addition to the Hermitian functions to completely describe the second-order statistical behavior of the process. We define and discuss the Hermitian and the complementary functions of complex-valued harmonizable processes. Exact expressions for the Hermitian and complementary second-order moment functions for some important sub-classes of complex-valued harmonizable processes are derived and discussed. We introduce, test, and characterize numerical estimators of these functions. Numerically generated data, and a real-world earthquake data set, are employed to demonstrate that the estimators work in practice. Based on the concept of widely linear mean square estimation, we propose a novel generalized measure of coherence for harmonizable random processes. This measure generalizes a recently proposed measure of coherence based on linear mean square estimation. Finally, we argue that our alternative coherence measure may in fact be beneficial for most nonstationary processes, even for real-valued harmonizable processes.

Acknowledgments

First and foremost, I thank my supervisor Professor Alfred Hanssen for excellent guidance and for sharing his seemingly never-ending enthusiasm. Thanks to Dr. Scient. Tor Arne Øigård for his help and for suffering through my lectures in my special syllabus. I thank Dr. Scient. Yngvar Larsen for providing me with computational code and for the help I got from his PhD Dissertation. A big thanks goes to my family, friends and fellow students for all their support. Especially, I thank my brother Kristian for all his help throughout my studies.

Contents

Chapter 1

Introduction

A random process is any process running along in time and controlled by probability laws. This formulation is from [Doob, 1953], which gives an introduction to the concept of random processes. Random processes are of interest in a wide range of fields and applications.

The analysis of random processes has traditionally been dominated by the assumption that the process is stationary. Among the classical texts regarding stationary processes we find [Grenander and Rosenblatt, 1984; Rosenblatt, 1985; Yaglom, 1962; Yaglom, 1987]. Stationary processes are characterized by that the probability laws governing the process do not change with time. Any stationary process is representable as the weighted sum of infinitesimal harmonic oscillators, thus connecting the concept of frequency to the process. The main advantage of the stationarity assumption is that the frequency content of a stationary process is constant as a function of time. The second-order statistical quantities of a real-valued stationary process can equivalently be represented in the time domain by the autocorrelation function, or in the frequency (Fourier) domain by the power spectral density function.

The stationarity assumption is quite limiting, and many important processes turn out to be nonstationary. Since nonstationarity is a non-property, the concept of nonstationary processes includes numerous different classes of random processes. The frequency content of a nonstationary process will vary as a function of time, such that it would be of interest to represent the process simultaneously in time and frequency. Time-frequency analysis of deterministic and random processes have been given much attention in the literature. For a treatment on time-frequency analysis for deterministic signals, see [Cohen, 1995]. Time-frequency analysis of random processes was treated in [Hlawatsch, 1998; Flandrin, 1999]. An alternative to time-frequency analysis is wavelet theory, where the process is represented simultaneous as a function of time and scale. For an introduction to wavelet theory, see e.g., [Mallat, 1998].

Harmonizable processes were introduced in [Loève, 1945; Loève, 1946]. Harmonizable processes is an important class of nonstationary processes. Recent publications regarding harmonizable processes include [Lii and Rosenblatt, 2002; Hanssen and Scharf, 2003; Scharf et al., 2005]. The second-order statistical quantities of real-valued harmonizable processes can be represented with four functions, namely the Hermitian dual-time moment function, the Hermitian dual-frequency spectral density, the Hermitian time-frequency spectral density and the Hermitian time-frequency ambiguity function.

Real-valued and complex-valued processes have conventionally been treated in the same manner, where the dual-time representation of the second-order statistical quantities is based on the correlation between the process at different time instants. However, complex-valued processes can possess correlations between the process and the complex conjugate of the process at different time instants as well [Neeser and Massey, 1993]. While the Hermitian functions will completely describe the second-order statistical quantities of a real-valued harmonizable process, this is not necessarily the case for complex-valued processes. Complex-valued harmonizable processes will also have a complementary dual-time moment function, a complementary dual-frequency spectral density, a complementary time-frequency spectral density and a complementary time-frequency ambiguity function. Interesting results concerning the second-order statistics of complex-valued processes has been published by [Picinbono and Bondon, 1997; Schreier and Scharf, 2003b; Schreier and Scharf, 2003a; Scharf et al., 2005]. The objective of this thesis is to study the second-order statistical quantities of complex-valued harmonizable random processes.

The organization of the thesis is as following. In Chapter 2, we introduce the concept of a harmonizable process, and we define the representations of the second-order statistical quantities of a harmonizable process.

In Chapter 3, we obtain expressions for the representations of the second-order statistical quantities of some general complex-valued harmonizable processes. These expressions illustrate how ignoring the complementary functions can lead to erroneous conclusions about the process under consideration.

We propose and test estimators of the moment functions, the dual-frequency spectra and the ambiguity functions of complex-valued processes in Chapter 4. These estimators are extensions of estimators proposed for real-valued harmonizable processes in [Larsen, 2003].

In Chapter 5, we implement and test estimators of the time-frequency spectral densities of complex-valued processes recently proposed in [Scharf et al., 2005].

In Chapter 6, we analyze numerically generated data and a real-world time series by the techniques of this thesis. We use the estimators from Chapter 4 and 5 to estimate the Hermitian and the complementary functions of these data sets, and we attempt at interpretations of these quantities.

We consider time-frequency and dual-frequency coherence of harmonizable processes in Chapter 7. The conventional measure of coherence is based on linear mean square estimation. We propose an alternative measure of coherence based on widely linear mean square estimation, which generalized previous coherence measures.

Chapter 2

Representation of harmonizable processes

A real-valued random process $X(t)$ is said to be wide-sense stationary (WSS) if

$$\mathbb{E}[X(t)] = \text{constant} \tag{2.1}$$
$$\mathbb{E}[X(t)X(t')] = R_{XX}(t-t'), \tag{2.2}$$

i.e., the mean value of the process is constant, and the autocorrelation function is a function only of the time difference and not of absolute time [Cramér, 1940].

The autocorrelation function in (2.2) describes the second-order statistical quantities of the real-valued process $X(t)$. If the process $X(t)$ is complex-valued, the autocorrelation function is conventionally defined as $\mathbb{E}[X(t)X^*(t')]$, see e.g., [Peebles, 2001], where the asterisk denotes complex conjugation. This function may not contain all the second-order information about the process, but for now we will assume that it does. We further assume that the process $X(t)$ has the spectral representation [Cramér, 1940]

$$X(t) = \int e^{j2\pi ft} dZ(f), \tag{2.3}$$

where $dZ(f)$ is the complex-valued increment process of $X(t)$. All limits of integration are $\pm\infty$ if not otherwise specified. Using this spectral representation, the conventional autocorrelation function of the process can be expressed by

$$\mathbb{E}[X(t)X^*(t')] = \iint e^{j2\pi ft} e^{-j2\pi f't'} \mathbb{E}[dZ(f)dZ^*(f')]\,. \tag{2.4}$$

If the process is WSS, the conventional autocorrelation function should only depend on the time difference $t-t'$. This is achieved if the increment process has uncorrelated increments [Yaglom, 1962], i.e.,

$$\mathbb{E}[dZ(f)dZ^*(f')] = \tilde{S}_{XX^*}(f)\delta(f-f')df\,df', \tag{2.5}$$

where $\delta(f)$ is Dirac's delta function. Here, $\tilde{S}_{XX^*}(f)$ is the conventional power spectral density of a WSS process. Substituting (2.5) in (2.4), the conventional autocorrelation function of $X(t)$ becomes

$$\begin{aligned} R_{XX^*}(t-t') =& \mathbb{E}[X(t)X^*(t')] \\ =& \int e^{j2\pi f(t-t')} \tilde{S}_{XX^*}(f) df. \end{aligned} \tag{2.6}$$

This is the Einstein-Wiener-Khintchine relation for WSS processes [Einstein, 1914; Wiener, 1930; Khintchine, 1934]. It states that the conventional autocorrelation function of a WSS process is related to the conventional power spectral density by a Fourier transform.

If the increment process has nonorthogonal increments, i.e.,

$$\mathbb{E}[dZ(f)dZ^*(f')] = S_{L,XX^*}(f,f')df df' \tag{2.7}$$

where $S_{L,XX^*}(f,f')$ is the Loève spectrum of the process $X(t)$, the conventional autocorrelation function becomes

$$\mathbb{E}[X(t)X^*(t')] = \iint e^{j2\pi(ft-f't')} S_{L,XX^*}(f,f')df df'. \tag{2.8}$$

A process $X(t)$ having the spectral representation in (2.3), and an increment process satisfying (2.7), belongs to the class of harmonizable nonstationary processes [Loève, 1978]. In order for the double integral in (2.8) to be convergent, $S_{L,XX^*}(f,f')$ must be a function of bounded variation in the plane [Yaglom, 1987], i.e.,

$$\iint \left| S_{L,XX^*}(f,f') \right| df df' < \infty. \tag{2.9}$$

If a process $X(t)$ has a conventional autocorrelation function of the form (2.8) and the Loève spectrum of the process is of bounded variation, the process $X(t)$ is harmonizable [Loève, 1978]. Bounded variation of the Loève spectrum is thus a necessary, but not sufficient condition for the process $X(t)$ to be harmonizable. Since stationary processes obey

$$\int |\tilde{S}_{XX^*}(f)| df < \infty, \tag{2.10}$$

stationary processes are included in the class of harmonizable processes.

2.1 Hermitian second-order statistical quantities

We define the Hermitian moment function of a general process $X(t)$ by

$$M_{XX^*}(t,\tau) = \mathbb{E}\left[X(t+\tau)X^*(t)\right]. \tag{2.11}$$

Here, t is a global time variable, and τ is a local time variable. The Hermitian moment function $M_{XX^*}(t,\tau)$ is related to the conventional autocorrelation $\mathbb{E}[X(t_1)X^*(t_2)]$ by a change of variables, given by $t = t_2$ and $\tau = t_1 - t_2$. If the process $X(t)$ is harmonizable, the Hermitian moment function can be represented as

$$\begin{aligned} M_{XX^*}(t,\tau) &= \mathbb{E}\left[\int e^{j2\pi f(t+\tau)} dZ(f) \int e^{-j2\pi f' t} dZ^*(f')\right] \\ &= \iint e^{j2\pi(f-f')t} e^{j2\pi f\tau} \mathbb{E}[dZ(f)dZ^*(f')] \\ &= \iint e^{j2\pi\nu t} e^{j2\pi f\tau} \mathbb{E}[dZ(f)dZ^*(f-\nu)] \\ &= \iint e^{j2\pi\nu t} e^{j2\pi f\tau} S_{XX^*}(\nu,f) d\nu df. \end{aligned} \tag{2.12}$$

The Hermitian dual-frequency spectral density (or Hermitian f-f spectrum) of the process is

$$S_{XX^*}(\nu,f)d\nu df = \mathbb{E}[dZ(f)dZ^*(f-\nu)]\,, \tag{2.13}$$

where f is a global frequency and ν is a local frequency relative to f. The Hermitian f-f spectrum $S_{XX^*}(\nu,f)$ is related to the Loève spectrum $S_{L,XX^*}(f_1,f_2)$ by a change of variables $f = f_1$ and $\nu = f_1 - f_2$. Consequently, the Hermitian f-f spectrum of a harmonizable process must also be a function of bounded variation.

The Hermitian moment function and the Hermitian f-f spectrum are a two-dimensional Fourier transform pair. By taking the inverse Fourier transform of the Hermitian f-f spectrum with respect to the local frequency variable ν, we obtain

$$\begin{aligned} P_{XX^*}(t,f)df &= df \int e^{j2\pi\nu t} S_{XX^*}(\nu,f) d\nu \\ &= \int e^{j2\pi\nu t} \mathbb{E}[dZ(f)dZ^*(f-\nu)] \\ &= \mathbb{E}\left[\left(\int e^{-j2\pi\nu t} dZ(f-\nu)\right)^* dZ(f)\right] \\ &= \mathbb{E}\left[\left(\int e^{j2\pi\alpha t} dZ(\alpha)\right)^* dZ(f) e^{j2\pi f t}\right] \\ &= \mathbb{E}\left[X^*(t) dZ(f) e^{j2\pi f t}\right]. \end{aligned} \tag{2.14}$$

Here, $P_{XX^*}(t,f)$ is the Hermitian time-frequency spectral density (or the Hermitian t-f spectrum) of the process $X(t)$. The Hermitian t-f spectrum is a function of global time and global frequency. Note that $S_{XX^*}(\nu,f)$ and $P_{XX^*}(t,f)$ are a Fourier transform pair in the variables t and ν.

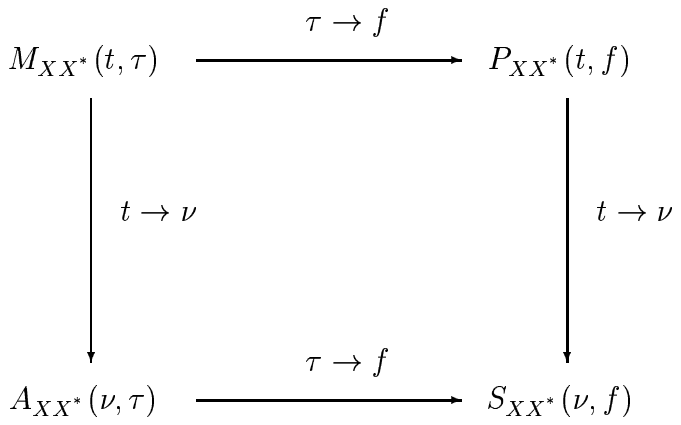

Figure 2.1: Fourier relations between the Hermitian second-order statistical quantities of a harmonizable process.

The last option is to take the inverse Fourier transform of the Hermitian f-f spectrum with respect to the global variable f,

$$\begin{aligned} A_{XX^*}(\nu,\tau)d\nu &= d\nu \int e^{j2\pi\tau f} S_{XX^*}(\nu,f)df \\ &= \mathbb{E}\left[\int e^{j2\pi f\tau} dZ(f)dZ^*(f-\nu)\right]. \end{aligned} \tag{2.15}$$

The quantity $A_{XX^*}(\nu,\tau)$ is the Hermitian ambiguity function of the process $X(t)$, which is a function of local frequency ν and local time τ. The Hermitian ambiguity function and the Hermitian f-f spectrum are a Fourier transform pair in the variables f and τ.

The Hermitian second-order statistical quantities of a harmonizable process can be represented in four different domains, and these representations are connected through Fourier transforms as illustrated in Figure 2.1 [Scharf et al., 2001]. The representations can also be seen as the expectations

$$M_{XX^*}(t,\tau) = \mathbb{E}[X(t+\tau)X^*(t)] \tag{2.16}$$

$$S_{XX^*}(\nu,f)d\nu df = \mathbb{E}[dZ(f)dZ^*(f-\nu)] \tag{2.17}$$

$$P_{XX^*}(t,f)df = \mathbb{E}\left[X^*(t)dZ(f)e^{j2\pi ft}\right] \tag{2.18}$$

$$A_{XX^*}(\nu,\tau)d\nu = \mathbb{E}\left[\int e^{j2\pi f\tau} dZ(f)dZ^*(f-\nu)\right]. \tag{2.19}$$

If we define the Hilbert space inner product between two complex-valued random variables W and Z as $\langle W,Z\rangle = \mathbb{E}[WZ^*]$, we see that the Hermitian moment function, the Hermitian f-f spectrum and the Hermitian t-f spectrum are Hilbert

space inner products [Hanssen and Scharf, 2003]

$$M_{XX^*}(t,\tau) = \langle X(t+\tau), X(t)\rangle \tag{2.20}$$
$$S_{XX^*}(\nu,f)d\nu df = \langle dZ(f), dZ(f-\nu)\rangle \tag{2.21}$$
$$P_{XX^*}(t,f)df = \left\langle dZ(f)e^{j2\pi ft}, X(t)\right\rangle. \tag{2.22}$$

Note that the Hermitian ambiguity function is not a Hilbert space inner product. If the process $X(t)$ is real-valued, the increment process will have a Hermitian symmetry $dZ^*(f) = dZ(-f)$ and the Hermitian ambiguity function will be a convolution. The expressions in (2.20)–(2.22) are valid for both real-valued and complex-valued harmonizable processes.

2.2 Complementary second-order statistical quantities

For a general complex-valued process there will be correlations between the process and its complex conjugate [Neeser and Massey, 1993]. The Hermitian moment function will not describe the second-order behavior of the process completely, so we also have to consider the quantity $\mathbb{E}[X(t+\tau)X(t)]$, which we denote the complementary moment function [Schreier and Scharf, 2003b]. Processes for which the complementary moment function is zero everywhere are called proper [Neeser and Massey, 1993]. Examples of proper processes are the analytic process obtained from any stationary process [Picinbono, 1993] and any circular process [Picinbono, 1994]. The analysis of proper complex-valued processes does not differ much from the analysis of real-valued processes. However, many complex-valued processes are improper, and the complementary functions will have to be considered. For instance, an analytic process corresponding to a real-valued, nonstationary process is improper [Schreier and Scharf, 2003b].

We defined the complementary moment function of the process $X(t)$ as

$$M_{XX}(t,\tau) = \mathbb{E}[X(t+\tau)X(t)]. \tag{2.23}$$

If $X(t)$ is harmonizable, we write the complementary moment function as

$$\begin{aligned} M_{XX}(t,\tau) &= \mathbb{E}\left[\int e^{j2\pi f(t+\tau)}dZ(f)\int e^{j2\pi f't}dZ(f')\right] \\ &= \iint e^{j2\pi(f+f')t}e^{j2\pi f\tau}\mathbb{E}[dZ(f)dZ(f')] \\ &= \iint e^{j2\pi\nu t}e^{j2\pi f\tau}\mathbb{E}[dZ(f)dZ(\nu-f)] \\ &= \iint e^{j2\pi\nu t}e^{j2\pi f\tau}S_{XX}(\nu,f)d\nu df. \end{aligned} \tag{2.24}$$

The quantity

$$S_{XX}(\nu, f)d\nu df = \mathbb{E}[dZ(f)dZ(\nu - f)] \tag{2.25}$$

is denoted the complementary dual-frequency spectral density (or the complementary f-f spectrum). The complementary f-f spectrum of a harmonizable process also have to satisfy the condition

$$\iint |S_{XX}(\nu, f)|\, d\nu df < \infty. \tag{2.26}$$

We see that the complementary moment function and the complementary f-f spectrum are a two-dimensional Fourier transform pair.

Taking the inverse Fourier transform of the complementary f-f spectrum with respect to the local variable ν yields the complementary time-frequency spectral density (or the complementary t-f spectrum) of the process

$$\begin{aligned} P_{XX}(t, f)df &= df \int e^{j2\pi\nu t} S_{XX}(\nu, f)d\nu \\ &= \mathbb{E}\left[\int e^{j2\pi\nu t} dZ(f)dZ(\nu - f)\right] \\ &= \mathbb{E}\left[\left(\int e^{j2\pi\alpha t} dZ(\alpha)\right) dZ(f)e^{j2\pi ft}\right] \\ &= \mathbb{E}\left[X(t)dZ(f)e^{j2\pi ft}\right]. \end{aligned} \tag{2.27}$$

The complementary f-f spectrum and the complementary t-f spectrum constitute a Fourier transform pair in the variables t and ν.

Finally, the inverse Fourier transform of the complementary f-f spectrum with respect to the global variable f produces the complementary ambiguity function of the process

$$\begin{aligned} A_{XX}(\nu, \tau)d\nu &= d\nu \int e^{j2\pi f\tau} S_{XX}(\nu, f)df \\ &= \mathbb{E}\left[\int e^{j2\pi f\tau} dZ(f)dZ(v - f)\right] \\ &= \mathbb{E}\left[\left(dZ(\nu)e^{j2\pi\nu\tau}\right) \star dZ(\nu)\right], \end{aligned} \tag{2.28}$$

where $\star$ denotes convolution. Thus, the complementary ambiguity function and the complementary f-f spectrum are a Fourier transform pair in the variables f and τ.

With these definitions, all the complementary functions are connected through

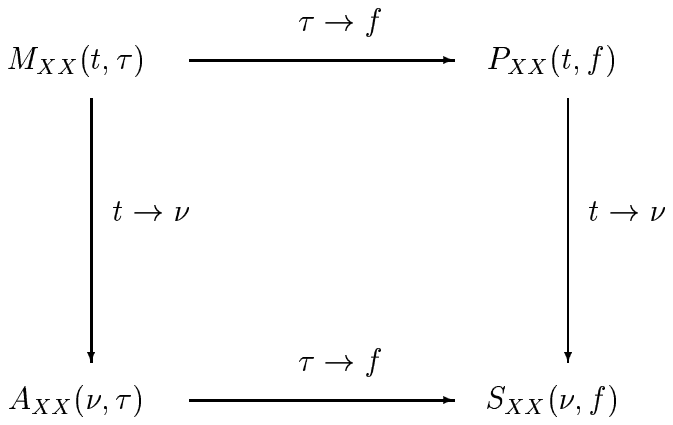

Figure 2.2: Fourier relations between the complementary second-order statistical quantities of a harmonizable process.

Fourier transforms as shown in Figure 2.2. We can also express the quantities as expectations

$$M_{XX}(t,\tau) = \mathbb{E}[X(t+\tau)X(t)] \tag{2.29}$$
$$S_{XX}(\nu,f,)d\nu df = \mathbb{E}[dZ(f)dZ(\nu-f)] \tag{2.30}$$
$$P_{XX}(t,f)df = \mathbb{E}\left[X(t)dZ(f)e^{j2\pi ft}\right] \tag{2.31}$$
$$A_{XX}(\nu,\tau)d\nu = \mathbb{E}\left[\int e^{j2\pi f\tau}dZ(f)dZ(v-f)\right]. \tag{2.32}$$

The complementary ambiguity function is a convolution. The other complementary functions can be expressed as Hilbert space inner products

$$M_{XX}(t,\tau) = \langle X(t+\tau), X^*(t)\rangle \tag{2.33}$$
$$S_{XX}(\nu,f,)d\nu df = \langle dZ(f), dZ^*(f-\nu)\rangle \tag{2.34}$$
$$P_{XX}(t,f)df = \left\langle dZ(f)e^{j2\pi ft}, X^*(t)\right\rangle. \tag{2.35}$$

For improper complex-valued processes, we now have eight possible representations of the second-order statistics of the process. In general, we need one Hermitian and one complementary function to describe the second-order behavior of the process. Note that for real-valued processes, the Hermitian and the complementary functions are identical.

2.3 Higher-order statistics

In this thesis, we will only consider the second-order statistical quantities of random processes. For a Gaussian process, the first and second-order moment function of the process will characterize the process completely [Priestley, 1988]. However, for non-Gaussian processes, the higher-order statistical quantities should also be considered. We give here references to some work on higher-order statistics for random processes.

The higher-order statistics of real-valued, stationary random processes is treated in [Nikias and Petropulu, 1993]. A bibliography regarding higher-order statistics of stationary processes is available in [Swami et al., 1997]. In [Birkelund et al., 2002], the multitaper approach to spectral estimation (see Chapter 4) was extended to polyspectra of arbitrary order for real-valued, stationary processes. The higher-order statistics of complex-valued, stationary processes was studied in [Amblard et al., 1996].

Higher-order statistics of real-valued cyclostationary time series was treated in [Dandawaté and Giannakis, 1994]. In [Gardner and Spooner, 1994; Spooner and Gardner, 1994; Izzo and Napolitano, 1998], the theory of higher-order statistics was extended to complex-valued cyclostationary time series and its relatives.

A theory of higher-order moment spectra for real-valued, harmonizable processes was presented in [Hanssen and Scharf, 2003]. Some work has also been done on higher-order time-frequency distributions of nonstationary, complex-valued processes, see e.g., [Amblard and Lacoume, 1992; Amblard and Lacoume, 1994; Fonollosa and Nikias, 1993].

Chapter 3

Some specific processes

In this Chapter, we utilize some typical nonstationary random processes to examine the eight second-order statistical quantities. Only cases where exact closed-form expressions can be derived, are considered. The intention is that these results shall serve as a library of prototypical moment functions for various interesting and important subclasses of nonstationary processes.

3.1 Stationary process

Let $X(t)$ be a WSS process with conventional autocorrelation function $R_{XX^*}(\tau)$ and conventional power density spectrum $\tilde{S}_{XX^*}(f)$. The four Hermitian second-order statistical quantities in this case become

$$M_{XX^*}(t,\tau) = R_{XX^*}(\tau) \tag{3.1}$$
$$S_{XX^*}(\nu,f) = \tilde{S}_{XX^*}(f)\,\delta(\nu) \tag{3.2}$$
$$P_{XX^*}(t,f) = \tilde{S}_{XX^*}(f) \tag{3.3}$$
$$A_{XX^*}(\nu,\tau) = R_{XX^*}(\tau)\,\delta(\nu). \tag{3.4}$$

The Hermitian moment function and the Hermitian t-f spectrum depend only on τ and f, respectively. This is what we would expect for WSS processes. The Hermitian f-f spectrum and the Hermitian ambiguity function both contain a delta function $\delta(\nu)$, concentrating these functions on the line $\nu = 0$. We can interpret (3.2) as a relation between the Hermitian f-f spectrum and the stationary, conventional power density spectrum [Hanssen and Scharf, 2003]. The Hermitian f-f spectrum of a WSS process will be non-vanishing only on the line $\nu = f - f' = 0$, which is the stationary manifold.

If $X(t)$ is a real-valued process, the Hermitian and the complementary quantities will be equal. Let us assume that $X(t)$ is an improper, complex-valued WSS process. The definition of WSS processes does not imply any conditions on

the complementary moment function. We will say that a process is second-order stationary (SOS) [Picinbono and Bondon, 1997], if it is WSS, and the complementary moment function only depends on τ, i.e., $\mathbb{E}[X(t)X(t+\tau)] = R_{XX}(\tau)$. This use of the term second-order stationary should not be confused with the conventional use of the term to denote processes that are stationary to order two, i.e., processes that have a second-order probability density function that is time-shift invariant [Peebles, 2001]. It is more common to use the term WSS for complex-valued processes that have mean value and Hermitian moment function and complementary moment function independent of t, see e.g., [Neeser and Massey, 1993; Schreier and Scharf, 2003b].

If $X(t)$ is an SOS process, the complementary functions are

$$M_{XX}(t,\tau) = R_{XX}(\tau) \tag{3.5}$$
$$S_{XX}(\nu,f) = \tilde{S}_{XX}(f)\,\delta(\nu) \tag{3.6}$$
$$P_{XX}(t,f) = \tilde{S}_{XX}(f) \tag{3.7}$$
$$A_{XX}(\nu,\tau) = R_{XX}(\tau)\,\delta(\nu), \tag{3.8}$$

where

$$R_{XX}(\tau) = \int e^{j2\pi f\tau}\tilde{S}_{XX}(f)df. \tag{3.9}$$

Both the complementary f-f spectrum and the complementary ambiguity function are concentrated on the line $\nu = 0$. Thus, $\nu = f + f' = 0$ describes the stationary manifold for the complementary functions.

3.2 Modulated stationary process

To illustrate the importance of the complementary functions of complex-valued processes, we consider a WSS real-valued process $X(t)$ with zero mean and define the complex process

$$Y(t) = e^{j2\pi f_0 t}X(t), \tag{3.10}$$

where f_0 is a constant frequency. In other words, we let the process $X(t)$ amplitude modulate the complex carrier $\exp(j2\pi f_0 t)$. The process $Y(t)$ will have the Hermitian functions

$$M_{YY^*}(t,\tau) = e^{j2\pi f_0\tau}R_{XX^*}(\tau) \tag{3.11}$$
$$S_{YY^*}(\nu,f) = \tilde{S}_{XX^*}(f-f_0)\delta(\nu) \tag{3.12}$$
$$P_{YY^*}(t,f) = \tilde{S}_{XX^*}(f-f_0) \tag{3.13}$$
$$A_{YY^*}(\nu,\tau) = e^{j2\pi f_0\tau}R_{XX^*}(\tau)\delta(\nu). \tag{3.14}$$

The mean of $Y(t)$ is obviously zero, and from (3.11) we see that the Hermitian moment function of $Y(t)$ is independent of t. Thus $Y(t)$ is a WSS process. However, the complementary functions of $Y(t)$ are

$$M_{YY}(t,\tau) = e^{j2\pi f_0(2t+\tau)} R_{XX}(\tau) \tag{3.15}$$
$$S_{YY}(\nu, f) = \tilde{S}_{XX}(f - f_0)\delta(\nu - 2f_0) \tag{3.16}$$
$$P_{YY}(t, f) = e^{j4\pi f_0 t}\, \tilde{S}_{XX}(f - f_0) \tag{3.17}$$
$$A_{YY}(\nu,\tau) = e^{j2\pi f_0 \tau}\, R_{XX}(\tau)\delta(\nu - 2f_0). \tag{3.18}$$

Since the complementary moment function depends on t, the process $Y(t)$ is not an SOS process. Hence, WS stationarity does not imply SO stationarity. In this case the complementary functions suggests that the process is cyclostationary (see Section 3.3). Note that since $X(t)$ is real-valued, we have $R_{XX^*}(\tau) = R_{XX}(\tau)$.

If now $X(t)$ is a complex-valued, SOS process with zero mean, the second-order statistical quantities of $Y(t)$ are still as in (3.11)–(3.18), but with $R_{XX^*}(\tau) \neq R_{XX}(\tau)$. Even if $X(t)$ is an SOS process, $Y(t)$ will not be an SOS process.

Finally, if $X(t)$ is a complex-valued, WSS but not SOS process with zero mean, the Hermitian functions of $Y(t)$ are as in (3.11)–(3.14). The complementary functions will be

$$M_{YY}(t,\tau) = e^{j2\pi f_0(2t+\tau)} M_{XX}(t,\tau) \tag{3.19}$$
$$S_{YY}(\nu, f) = S_{XX}(\nu - 2f_0, f - f_0) \tag{3.20}$$
$$P_{YY}(t, f) = e^{j4\pi f_0 t} P_{XX}(t, f - f_0) \tag{3.21}$$
$$A_{YY}(\nu,\tau) = e^{j2\pi f_0 \tau} A_{XX}(\nu - 2f_0, \tau). \tag{3.22}$$

Again we see that the Hermitian functions suggests that $Y(t)$ is a stationary process, but the complementary functions are highly nonstationary.

3.3 Cyclostationary process

A complex-valued process $X(t)$ is said to be cyclostationary [Bennett, 1958], or periodically correlated [Gladyshev, 1961], with a period $T_0 = 1/f_0$, if the mean of the process is periodic with period T_0, and the Hermitian moment function and/or the complementary moment function is periodic in t with period T_0. In mathematical terms, this is

$$\mathbb{E}[X(t + T_0)] = \mathbb{E}[X(t)] \tag{3.23}$$
$$M_{XX^*}(t + T_0, \tau) = M_{XX^*}(t,\tau) \tag{3.24}$$
$$M_{XX}(t + T_0, \tau) = M_{XX}(t,\tau). \tag{3.25}$$

In order for $X(t)$ to be cyclostationary, it has to satisfy (3.23) and at least one of (3.24) and (3.25). WSS processes have a constant mean value and a Hermitian moment function that does not depend on t, thus WSS and, by definition, SOS processes are included in the class of cyclostationary processes.

If the Hermitian moment function of a cyclostationary process is periodic in t, it has a Fourier series expansion in t such that

$$M_{XX^*}(t,\tau) = \sum_k e^{j2\pi k f_0 t} R^{(k)}_{XX^*}(\tau), \tag{3.26}$$

where

$$R^{(k)}_{XX^*}(\tau) = \frac{1}{T_0}\int_0^{T_0} e^{-j2\pi k f_0 t} M_{XX^*}(t,\tau)dt. \tag{3.27}$$

If we further assume that the process is harmonizable cyclostationary [Yaglom, 1987], the function $R^{(k)}_{XX^*}(\tau)$ has the representation

$$R^{(k)}_{XX^*}(\tau) = \int e^{j2\pi f\tau} \tilde{S}^{(k)}_{XX^*}(f)df. \tag{3.28}$$

Thus, the Hermitian moment function of a harmonizable cyclostationary process $X(t)$ is

$$M_{XX^*}(t,\tau) = \iint e^{j2\pi\nu t} e^{j2\pi f\tau} \sum_k \delta(\nu - kf_0)\tilde{S}^{(k)}_{XX^*}(f)df\,d\nu, \tag{3.29}$$

which can be simplified to

$$M_{XX^*}(t,\tau) = \sum_k e^{j2\pi k f_0 t} \int e^{j2\pi f\tau} \tilde{S}^{(k)}_{XX^*}(f)df. \tag{3.30}$$

By comparing (3.29) with (2.12), we find the Hermitian f-f spectrum of $X(t)$,

$$S_{XX^*}(\nu, f) = \sum_k \delta(\nu - kf_0)\, \tilde{S}^{(k)}_{XX^*}(f). \tag{3.31}$$

Thus, the spectral measure is concentrated on the lines $\nu = kf_0$. Since $X(t)$ is a harmonizable process, the Hermitian t-f spectrum and the Hermitian ambiguity function are easily obtained as

$$P_{XX^*}(t,f) = \sum_k e^{j2\pi k f_0 t} \tilde{S}^{(k)}_{XX^*}(f) \tag{3.32}$$

and

$$A_{XX^*}(\nu,\tau) = \sum_k \delta(\nu - kf_0) \int e^{j2\pi f\tau} \tilde{S}^{(k)}_{XX^*}(f)df. \tag{3.33}$$

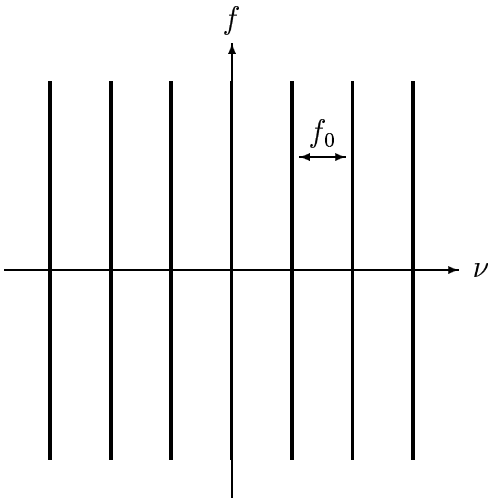

Figure 3.1: The lines of support in the f-ν plane for cyclostationary processes.

The Hermitian ambiguity function is also concentrated on the lines $\nu = kf_0$. If the complementary moment function is periodic in t with period T_0, the complementary functions of $X(t)$ are as in (3.29)–(3.33) with the change of index $XX^* \to XX$.

Cyclostationary processes are nonstationary, but, as the name suggests, they are closely related to stationary processes. The f-f spectrum of a stationary process is non-zero only on the stationary manifold. Cyclostationary processes are an extension of this where the f-f spectrum is non-zero only on the lines $\nu = kf_0$ as illustrated in Figure 3.1. The function $\tilde{S}^{(k)}_{XX^*}(f)$ on the line $\nu = kf_0$ bears some resemblance to a conventional power spectral density of a stationary process. However, it is not a power spectral density, since $\tilde{S}^{(k)}_{XX^*}(f)$ in general is a complex-valued function. If we replace the f-axis with a τ-axis in Figure 3.1, we get the lines of support of the ambiguity function of a cyclostationary process. Consequently, to determine if a process is cyclostationary, we can examine the f-f spectrum or the ambiguity function for this line concentration.

3.4 Oscillatory process

Since cyclostationary processes are closely related to stationary processes, we may describe them as weakly nonstationary processes. Another class of weakly nonstationary processes are processes with evolutionary spectral representations, also called oscillatory processes. Oscillatory processes were introduced in [Granger and Hatanaka, 1964] and, in more detail, in [Priestley, 1965]. An oscillatory

process $X(t)$ has a spectral representation

$$X(t) = \int e^{j2\pi ft} A(t,f)\, dZ(f), \tag{3.34}$$

where $Z(f)$ has uncorrelated increments, i.e.,

$$\mathbb{E}[dZ(f)dZ^*(f')] = \delta(f-f')\, \tilde{S}_{XX^*}(f) df df'. \tag{3.35}$$

This spectral representation differs from the stationary spectral representation only in the function $A(t,f)$, which is a "slowly varying" function of t satisfying

$$\int |A(t,f)|^2\, \tilde{S}_{XX^*}(f) df < \infty, \quad \forall t. \tag{3.36}$$

In order for $A(t,f)$ to vary slowly enough in t, it has to obey the representation

$$A(t,f) = \int e^{j2\pi t\theta}\, dK(\theta, f), \tag{3.37}$$

where the differential is with respect to θ and $|dK(\theta,f)|$ has an absolute maximum at $\theta = 0$ for any fixed f [Priestley, 1965]. The function $A(t,f) = 1$ everywhere obviously satisfy these conditions. Stationary processes are therefore included in the class of oscillatory processes.

An oscillatory process $X(t)$ has the Hermitian functions

$$M_{XX^*}(t,\tau) = \int e^{j2\pi\alpha\tau} A(t+\tau,\alpha) A^*(t,\alpha)\, \tilde{S}_{XX^*}(\alpha) d\alpha \tag{3.38}$$

$$S_{XX^*}(\nu,f) = \int dK(f-\alpha,\alpha)\, dK^*(\nu+f-\alpha,\alpha) \tilde{S}_{XX^*}(\alpha) d\alpha \tag{3.39}$$

$$P_{XX^*}(t,f) = \int e^{j2\pi(f-\alpha)t} A^*(t,\alpha)\, dK(f-\alpha,\alpha) \tilde{S}_{XX^*}(\alpha) d\alpha \tag{3.40}$$

$$A_{XX^*}(\nu,\tau) = \iint e^{j2\pi(\alpha+\beta)\tau}\, dK(\beta,\alpha)\, dK^*(\beta-\nu,\alpha) \tilde{S}_{XX^*}(\alpha) d\alpha. \tag{3.41}$$

If $X(t)$ is a complex-valued process, we should assume weak nonstationarity of the complementary functions also, i.e.,

$$\mathbb{E}[dZ(f)dZ(f')] = \delta(f+f') \tilde{S}_{XX}(f) df df'. \tag{3.42}$$

Now, $A(t,f)$ should also satisfy the condition

$$\int A(t,f) A(t,-f) \tilde{S}_{XX}(f) df < \infty, \quad \forall t. \tag{3.43}$$

The complementary functions of $X(t)$ are

$$M_{XX}(t,\tau) = \int e^{j2\pi\alpha\tau} A(t+\tau,\alpha)A(t,-\alpha)\,\tilde{S}_{XX}(\alpha)d\alpha \tag{3.44}$$

$$S_{XX}(\nu,f) = \int dK(f+\alpha,\alpha)dK(\nu-\alpha-f,-\alpha)\tilde{S}_{XX}(\alpha)d\alpha \tag{3.45}$$

$$P_{XX}(t,f) = \int e^{-j2\pi\alpha t} A(t,-\alpha)dK(f-\alpha,\alpha)\tilde{S}_{XX}(\alpha)d\alpha \tag{3.46}$$

$$A_{XX}(\nu,\tau) = \iint e^{j2\pi(\alpha+\theta)\tau} dK(\theta,\alpha)dK(v-\theta,-\alpha)\tilde{S}_{XX}(\alpha)d\alpha. \tag{3.47}$$

We have obtained expressions of the second-order statistical quantities of an oscillatory process, but compared to the processes we have considered so far, these expressions do not offer much in the way of interpretation. This class of processes will not be considered any further in this thesis.

3.5 Linear, time-invariant system

We will examine the output process $Y(t)$ from a linear, time-invariant system with impulse response $h(t)$ and transfer function $H(f)$, when the input is a complex-valued process $X(t)$. The process $Y(t)$ is then defined as

$$Y(t) = h(t) \star X(t). \tag{3.48}$$

The Hermitian second-order statistical quantities of $Y(t)$, when $X(t)$ is WSS, are

$$M_{YY^*}(t,\tau) = h(\tau) \star h^*(-\tau) \star R_{XX^*}(\tau) \tag{3.49}$$

$$S_{YY^*}(\nu,f) = |H(f)|^2\, S_{XX^*}(f)\delta(\nu) \tag{3.50}$$

$$P_{YY^*}(t,f) = |H(f)|^2\, S_{XX^*}(f) \tag{3.51}$$

$$A_{YY^*}(\nu,\tau) = [h(\tau) \star h^*(-\tau) \star R_{XX^*}(\tau)]\,\delta(\nu). \tag{3.52}$$

From these quantities we see that the output process is a WSS process. If $X(t)$ is not SO stationary, the complementary moment function of $X(t)$ depends on t and $Y(t)$ will not be an SOS process. But if $X(t)$ is an SOS process, we have the complementary functions

$$M_{YY}(t,\tau) = h(\tau) \star h(-\tau) \star R_{XX}(\tau) \tag{3.53}$$

$$S_{YY}(\nu,f) = H(f)H(-f)\tilde{S}_{XX}(f)\delta(\nu) \tag{3.54}$$

$$P_{YY}(t,f) = H(f)H(-f)\tilde{S}_{XX}(f) \tag{3.55}$$

$$A_{YY}(\nu,\tau) = [h(\tau) \star h(-\tau) \star R_{XX}(\tau)]\,\delta(\nu). \tag{3.56}$$

Thus, if a complex-valued, SOS process is sent through a linear, time-invariant system, the output process of the system will also be an SOS process. If the input process is harmonizable and the absolute value of the transfer function is uniformly bounded, the output process will also be harmonizable [Yaglom, 1987].

3.6 Linear, time-variant system

Harmonizable processes are nonstationary, so we should not restrict ourselves to time-invariant systems. One way to describe a linear, time-variant system is

$$Y(t) = \int h(t,u)X(t-u)\,du, \tag{3.57}$$

where $X(t)$ is the input process and $h(t,u)$ is a time-varying impulse response [Yaglom, 1987]. Here, t is the time the impulse response is observed and $t-u$ is the time the impulse was introduced to the system. Thus, this impulse response is a function of two time variables, the global time t and the local time u. We define

$$P_h(t,f) = \int e^{-j2\pi fu}h(t,u)du \tag{3.58}$$

and

$$S_h(\nu,f) = \iint e^{-j2\pi fu}e^{-j2\pi\nu t}h(t,u)dtdu. \tag{3.59}$$

If $X(t)$ is a harmonizable process, all eight second-order quantities of $Y(t)$ can be expressed as functions of $P_h(t,f)$, $S_h(\nu,f)$ and the f-f spectra of $X(t)$. The Hermitian functions of $Y(t)$ are

$$M_{YY^*}(t,\tau) = \iint e^{j2\pi f\tau}e^{j2\pi\nu t}P_h(t+\tau,f)P_h^*(t,f-\nu)S_{XX^*}(\nu,f)d\nu df \tag{3.60}$$

$$S_{YY^*}(\nu,f) = \iint S_h(f-\beta,\beta)S_h^*(\alpha-\beta+f-\nu,\beta-\alpha)S_{XX^*}(\alpha,\beta)d\alpha d\beta \tag{3.61}$$

$$P_{YY^*}(t,f) = \iint e^{j2\pi(\alpha-\beta+f)t}S_h(f-\beta,\beta)P_h^*(t,\beta-\alpha)S_{XX^*}(\alpha,\beta)d\alpha d\beta \tag{3.62}$$

$$A_{YY^*}(\nu,\tau) = \iiint e^{j2\pi(\beta+\lambda)\tau}S_h(\lambda,\beta)S_h^*(\lambda+\alpha-\nu,\beta-\alpha)S_{XX^*}(\alpha,\beta)d\lambda d\alpha d\beta. \tag{3.63}$$

Likewise, we find the complementary functions of $Y(t)$ to be

$$M_{YY}(t,\tau) = \iint e^{j2\pi f\tau} e^{j2\pi\nu t} P_h(t+\tau, f) P_h(t, \nu - f) S_{XX}(\nu, f) d\nu df \tag{3.64}$$

$$S_{YY}(\nu, f) = \iint S_h(f-\beta, \beta) S_h(\nu - \alpha + \beta - f, \alpha - \beta) S_{XX}(\alpha, \beta)\, d\alpha d\beta \tag{3.65}$$

$$P_{YY}(t, f) = \iint e^{j2\pi(\alpha-\beta+f)t} S_h(f-\beta, \beta) P_h(t, \alpha - \beta) S_{XX}(\alpha, \beta) d\alpha d\beta \tag{3.66}$$

$$A_{YY}(\nu,\tau) = \iiint e^{j2\pi(\beta+\lambda)\tau} S_h(\lambda, \beta) S_h(\nu - \alpha - \lambda, \alpha - \beta) S_{XX}(\alpha, \beta) d\lambda d\alpha d\beta. \tag{3.67}$$

The input process is harmonizable. If now

$$\iint |P_h(t+\tau, f) P_h^*(t, f-\nu) S_{XX^*}(\nu, f)|\, d\nu df < \infty \quad \forall t, \tau \tag{3.68}$$

and

$$\iint |P_h(t+\tau, f) P_h(t, \nu - f) S_{XX}(\nu, f)|\, d\nu df < \infty \quad \forall t, \tau, \tag{3.69}$$

the output process $Y(t)$ is also harmonizable [Yaglom, 1987]. Consequently, for the time-varying system described by (3.58), an SOS input process results in a harmonizable output process. Under some wide conditions the output process $Y(t)$ will be harmonizable even if the input process $X(t)$ is not [Cambanis and Liu, 1970].

3.7 Harmonizable process with stationary additive noise

Many systems introduce additive noise to random processes such that

$$Y(t) = X(t) + N(t), \tag{3.70}$$

where $X(t)$ is a general random process and $N(t)$ is a random noise process. The noise is often assumed to be a real-valued WSS process or a complex-valued SOS process. Let $N(t)$ be a complex-valued SOS process with conventional autocorrelation function $R_{NN^*}(\tau)$, conventional power spectral density $\tilde{S}_{NN^*}(f)$ and complementary functions $R_{NN}(\tau)$ and $\tilde{S}_{NN}(f)$. If $X(t)$ is a harmonizable process, and the noise and the process are statistically independent, the Hermitian

functions of $Y(t)$ will be

$$M_{YY^*}(t,\tau) = M_{XX^*}(t,\tau) + R_{NN^*}(\tau) \tag{3.71}$$
$$S_{YY^*}(\nu,f) = S_{XX^*}(\nu,f) + \tilde{S}_{NN^*}(f)\delta(\nu) \tag{3.72}$$
$$P_{YY^*}(t,f) = P_{XX^*}(t,f) + \tilde{S}_{NN^*}(f) \tag{3.73}$$
$$A_{YY^*}(\nu,\tau) = A_{XX^*}(\nu,\tau) + R_{NN^*}(\tau)\delta(\nu). \tag{3.74}$$

The complementary functions of $Y(t)$ are obtained by replacing all the Hermitian functions in (3.71)–(3.74) with their complementary equivalents. In the f-f spectra and in the ambiguity functions, the noise in $Y(t)$ is concentrated on the stationary manifold. When analyzing the process $Y(t)$ we are only interested in information about $X(t)$, and in these two domains only the stationary part of $X(t)$ is corrupted by noise. Therefore, by doing the analysis in the dual-frequency domain or through the ambiguity function, we are able to retrieve most of the information uncorrupted by noise.

3.7.1 White Gaussian noise process

A real-valued process $N(t)$ is called a white process if its conventional power spectral density $\tilde{S}_{NN^*}(f)$ is constant for all f [Proakis and Salehi, 2002]. For a real-valued white process $N(t)$, the second-order statistical quantities are

$$M_{NN^*}(t,\tau) = C\delta(\tau) \tag{3.75}$$
$$S_{NN^*}(\nu,f) = C\delta(\nu) \tag{3.76}$$
$$P_{NN^*}(t,f) = C \tag{3.77}$$
$$A_{NN^*}(\nu,\tau) = C\delta(\tau)\delta(\nu), \tag{3.78}$$

where $C \in \mathbb{R}$ is a constant. Obviously, real-valued white processes are WSS processes. From the moment function we see that the white process at any two different times $t_1 \neq t_2$ is uncorrelated if $N(t)$ is zero-mean. If the zero-mean, white process is also a Gaussian process, these values will also be independent. In communication systems, the thermal noise is often assumed to be a zero-mean, white Gaussian process [Proakis and Salehi, 2002]. We will in this thesis use the term white Gaussian noise process for a real-valued, stationary, zero-mean, white Gaussian process.

3.8 Chirp with random phase

A signal that is used in many areas of signal processing is a linear frequency modulation (FM), also called a chirp. A chirp is usually defined as a deterministic signal, but in order to form a random process, we will introduce a random phase. The chirp process can be expressed as

$$X(t) = \exp\left[j\pi\left(2\alpha t + \beta t^2 + 2\Psi\right)\right], \tag{3.79}$$

where Ψ is a random variable. The variable α determines the starting instantaneous frequency of the chirp and the variable β is the chirp rate. From (3.79) we determine the Hermitian moment function as

$$M_{XX^*}(t,\tau) = \exp\left[j\pi(\beta\tau^2 + 2\beta\tau t + 2\alpha\tau)\right]. \tag{3.80}$$

By a two dimensional Fourier transform of (3.80) we obtain the function

$$S_{XX^*}(\nu, f) = \frac{1}{\beta}\exp\left[\frac{j\pi}{\beta}(\nu^2 + 2\alpha\nu - 2f\nu)\right]. \tag{3.81}$$

For $X(t)$ to be a harmonizable process, it is necessary that the f-f spectra are functions of bounded variation. But if $X(t)$ is harmonizable, its Hermitian f-f spectrum is given by (3.81), and we see that

$$\iint |S_{XX^*}(\nu, f)|\, d\nu df = \iint \left|\beta^{-1}\right| d\nu df. \tag{3.82}$$

Since $\beta \neq 0$ is a constant, $S_{XX^*}(\nu, f)$ is not a function of bounded variation and we must conclude that the chirp process is not harmonizable.

To obtain the function in (3.81) we did a two dimensional Fourier transform where we let both time variables go from $-\infty$ to ∞. When dealing with actual processes, however, the time has to be limited and the representation of the process should be

$$X(t) = \Pi_T(t) \cdot \exp\left[j\pi\left(2\alpha t + \beta t^2 + \Psi\right)\right], \tag{3.83}$$

where

$$\Pi_T(t) = \begin{cases} 1 & -\frac{T}{2} \leq t < \frac{T}{2} \\ 0 & \text{otherwise} \end{cases} \tag{3.84}$$

is a rectangular pulse. The parameter T will then control the limits of integration, i.e., the time interval the process is defined for. With these limits we can only find closed form expressions for the moment functions, and not for the other six second-order functions.

3.9 Chirp with Gaussian envelope and random phase

We now consider a modification of the chirp process as follows. Introduce a Gaussian envelope to define a modulated chirp process

$$X(t) = \exp\left[-\pi\mu\,(t-m)^2\right]\exp\left[j\pi\left(\beta t^2 + 2\alpha t + 2\Psi\right)\right], \tag{3.85}$$

where Ψ is a random variable. This is a chirp with starting instantaneous frequency α, chirp rate β and Gaussian envelope centered at $t = m$ and $1/\mu$ is a width measure of the Gaussian envelope. The Hermitian moment function of $X(t)$ is

$$\begin{aligned} M_{XX^*}(t,\tau) =& \exp\left\{-\pi\mu\left[(t+\tau-m)^2+(t-m)^2\right]\right\} \\ & \times \exp\left[j\pi\left(\beta\tau^2+2\beta\tau t+2\alpha\tau\right)\right], \end{aligned} \tag{3.86}$$

and the two-dimensional Fourier transform of this function is

$$\begin{aligned} S_{XX^*}(\nu,f) =& \frac{1}{\theta}\exp\left\{\frac{-\pi\mu}{\theta^2}\left[(\nu+\alpha+m\beta-f)^2+(\alpha+m\beta-f)^2\right]\right\} \\ & \times \exp\left\{\frac{j\pi\beta}{\theta^2}\left[\left(\nu+\alpha-f-\mu^2 m/\beta\right)^2\right]\right\} \\ & \times \exp\left\{\frac{-j\pi\beta}{\theta^2}\left[\left(f+\mu^2 m/\beta-\alpha\right)^2\right]\right\}, \end{aligned} \tag{3.87}$$

where $\theta^2 = \mu^2 + \beta^2$. Here, $S_{XX^*}(\nu, f)$ is a function of bounded variation, it is the Hermitian f-f spectrum of $X(t)$. We now find the Hermitian t-f spectrum

$$\begin{aligned} P_{XX^*}(t,f) =& \frac{e^{\frac{j}{2}\arctan(\beta/\mu)}}{\sqrt{\theta}}\exp\left\{\frac{-\pi\mu}{\theta^2}\left[(\alpha-f+m\beta)^2+\theta^2(t-m)^2\right]\right\} \\ & \times \exp\left[-j\pi\left(\beta t^2+2\alpha t-2tf-\frac{\mu^2 m^2}{\beta}\right)\right] \\ & \times \exp\left[\frac{-j\pi\beta}{\theta^2}\left(\alpha-f-\frac{\mu^2 m}{\beta}\right)^2\right], \end{aligned} \tag{3.88}$$

and the Hermitian ambiguity function

$$\begin{aligned} A_{XX^*}(\nu,\tau) =& \frac{1}{\sqrt{2\mu}}\exp\left[j\pi\left(2\alpha\tau+\tau\nu+2m\beta\tau-2m\nu\right)\right] \\ & \times \exp\left[-\frac{\pi}{2\mu}\left(\nu^2-2\beta\tau\nu+\theta^2\tau^2\right)\right] \end{aligned} \tag{3.89}$$

of the process.

Figure 3.2 shows the real part of the Hermitian second-order quantities of the process $X(t)$ with $\alpha = -0.3$, $\beta = 0.005$, $\mu = 3 \times 10^{-5}$ and Ψ uniformly distributed on $[0, 1/2]$. The chirp has an instantaneous frequency [Flandrin, 1999]

$$f_i = \alpha + \beta t \tag{3.90}$$

at each time instant t. Here, the time goes from $t = 0$ to $t = 100$, such that the instantaneous frequency of the process will increase linearly with time from -0.3

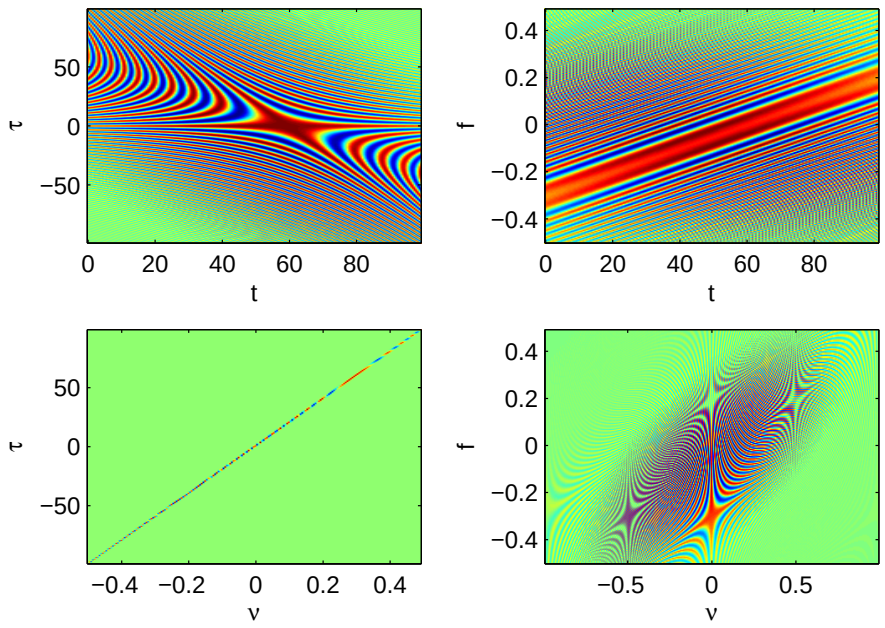

Figure 3.2: Hermitian second-order statistical quantities of a chirp with Gaussian envelope. Top left: $\Re\{M_{XX^*}(t,\tau)\}$. Top right: $\Re\{P_{XX^*}(t,f)\}$. Bottom left: $\Re\{A_{XX^*}(\nu,\tau)\}$. Bottom right: $\Re\{S_{XX^*}(\nu,f)\}$.

to 0.2. We see that the strong red line in the Hermitian t-f spectrum concurs with this. The Hermitian ambiguity function is concentrated on a straight line, and the gradient of this line is

$$\frac{\partial A_{XX^*}(\nu,\tau)}{\partial \nu} = \frac{1}{\beta}. \tag{3.91}$$

Because of the complex conjugation in the definition of the Hermitian moment function, the random phase will cancel out for the Hermitian functions. This is not the case for the complementary functions. We define the characteristic function of Ψ as

$$\Phi_\Psi(x) = \mathbb{E}\left[e^{j2\pi x\Psi}\right]. \tag{3.92}$$

Thus, the complementary moment function is

$$\begin{aligned} M_{XX}(t,\tau) =& \Phi_\Psi(2)\exp\left\{-\pi\mu\left[(t+\tau-m)^2+(t-m)^2\right]\right\} \\ &\times \exp\left[j\pi\left(2\beta t^2+2\beta t\tau+\beta\tau^2+2\alpha\tau+4\alpha t\right)\right], \end{aligned} \tag{3.93}$$

from which we find the complementary f-f spectrum

$$\begin{aligned} S_{XX}(\nu, f) =& \frac{\Phi_\Psi(2)\, e^{j \arctan(\beta/\mu)}}{\theta} \exp\left[\frac{-j\pi\beta}{\theta^2}\left(\nu + \mu^2 m/\beta - \alpha - f\right)^2\right] \\ & \times \exp\left\{\frac{-j\pi\beta}{\theta^2}\left[\left(f + \mu^2 m/\beta - \alpha\right)^2 - 2\theta^2\mu^2 m^2/\beta^2\right]\right\} \\ & \times \exp\left\{\frac{-\pi\mu}{\theta^2}\left[(\nu - \alpha - m\beta - f)^2 + (\alpha + m\beta - f)^2\right]\right\}. \end{aligned} \tag{3.94}$$

Note that $S_{XX}(\nu, f)$ is also a function of bounded variation. The complementary t-f spectrum and the complementary ambiguity function are

$$\begin{aligned} P_{XX}(t, f) =& \frac{\Phi_\Psi(2)\, e^{\frac{j}{2} \arctan(\beta/\mu)}}{\sqrt{\theta}} \exp\left[\frac{-j\pi\beta}{\theta^2}\left(\alpha - f - \frac{\mu^2 m}{\beta}\right)^2\right] \\ & \times \exp\left[j\pi\left(\beta t^2 + 2\alpha t + 2tf + \frac{\mu^2 m^2}{\beta}\right)\right] \\ & \times \exp\left\{\frac{-\pi\mu}{\theta^2}\left[(\alpha - f + m\beta)^2 + \theta^2\,(t - m)^2\right]\right\} \end{aligned} \tag{3.95}$$

and

$$\begin{aligned} A_{XX}(\nu, \tau) =& \frac{\Phi_\Psi(2)\, e^{j \arctan(\beta/\mu)/2}}{\sqrt{2\theta}} \exp\left\{\frac{-\pi\mu}{2\theta^2}\left[\theta^2\tau^2 + (\nu - 2\alpha - 2m\beta)^2\right]\right\} \\ & \times \exp\left[\frac{j\pi}{2\beta}\left(\beta^2\tau^2 + 2\beta\tau\nu + 4\mu^2 m^2\right)\right] \\ & \times \exp\left[\frac{-j\pi\beta}{2\theta^2}(\nu + 2\mu^2 m/\beta - 2\alpha)^2\right], \end{aligned} \tag{3.96}$$

respectively.

We see some strong features in Figure 3.3, which shows the real part of the complementary functions of $X(t)$ with $\alpha = -0.3$, $\beta = 0.005$, $\mu = 3 \times 10^{-5}$ and Ψ uniformly distributed on $[0, 1/2]$. However, we are not able to relate these features directly to this process.

Both the Hermitian and the complementary f-f spectrum of the chirp with Gaussian envelope are functions of bounded variation. Strictly speaking this is not sufficient to conclude that the chirp process with Gaussian envelope is harmonizable, but it strongly suggests that $X(t)$ is harmonizable.

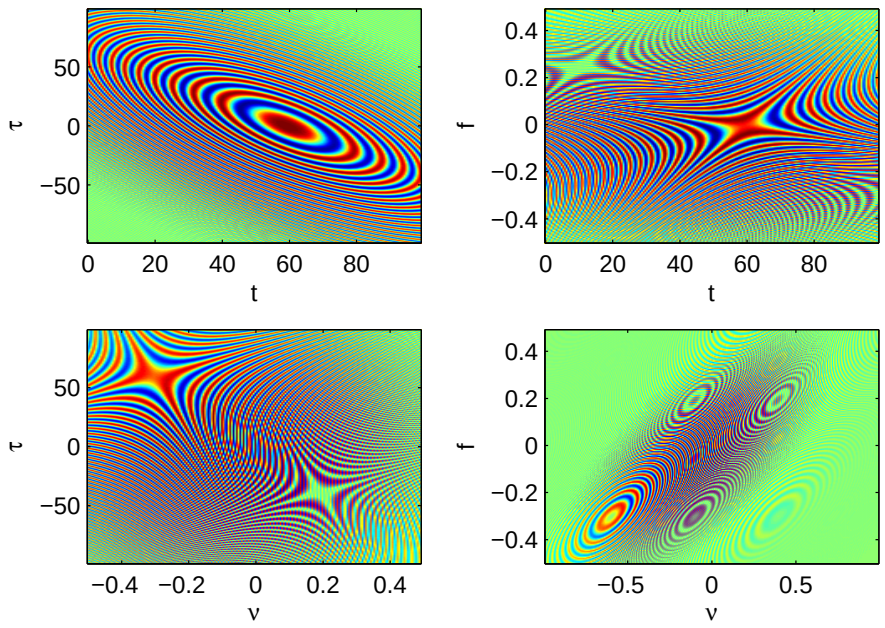

Figure 3.3: Complementary second-order statistical quantities of a chirp with Gaussian envelope. Top left: $\Re\{M_{XX}(t,\tau)\}$. Top right: $\Re\{P_{XX}(t,f)\}$. Bottom left: $\Re\{A_{XX}(\nu,\tau)\}$. Bottom right: $\Re\{S_{XX}(\nu,f)\}$

3.10 Analytic process corresponding to a stationary process

An analytic process is a complex-valued process that only has positive frequencies. The analytic process $Y(t)$ corresponding to the real-valued process $X(t)$ is

$$Y(t) = X(t) + j\mathcal{H}\{X(t)\}, \tag{3.97}$$

where $\mathcal{H}\{X(t)\}$ denotes the Hilbert transform of $X(t)$ [Bracewell, 1986]. If $X(t)$ is a real-valued WSS process with spectral representation as in (2.3), the process $Y(t)$ has the spectral representation

$$Y(t) = 2\int_0^\infty e^{j2\pi ft}\, dZ(f), \tag{3.98}$$

where $dZ(f)$ is the increment process of $X(t)$. Since $X(t)$ is WSS, $dZ(f)$ has uncorrelated increments, i.e.,

$$\mathbb{E}[dZ(f)dZ^*(f')] = \delta(f-f')\tilde{S}_{XX^*}(f)df\,df'. \tag{3.99}$$

The Hermitian quantities of $Y(t)$ are

$$M_{YY^*}(t,\tau) = 4\int_0^\infty e^{j2\pi f\tau}\,\tilde{S}_{XX^*}(f)df \tag{3.100}$$

$$S_{YY^*}(\nu,f) = \begin{cases} 4\tilde{S}_{XX^*}(f)\delta(\nu) & f \geq 0 \\ 0 & f < 0 \end{cases} \tag{3.101}$$

$$P_{YY^*}(t,f) = \begin{cases} 4\tilde{S}_{XX^*}(f) & f \geq 0 \\ 0 & f < 0 \end{cases} \tag{3.102}$$

$$A_{YY^*}(\nu,\tau) = 4\delta(\nu)\int_0^\infty e^{j2\pi f\tau}\,\tilde{S}_{XX^*}(f)df. \tag{3.103}$$

Since the Hermitian moment function of $Y(t)$ is independent of t, $Y(t)$ is a WSS process. But $Y(t)$ has complex values, so we should also consider the complementary functions. The process $X(t)$ is real-valued, thus its corresponding increment process $dZ(f)$ will have a Hermitian symmetry $dZ^*(f) = dZ(-f)$. We use the spectral representation in (3.98) to obtain the complementary moment function as

$$\begin{aligned} M_{YY}(t,\tau) &= 4\,\mathbb{E}\left[\int_0^\infty\int_0^\infty e^{j2\pi f(t+\tau)}e^{j2\pi f't}dZ(f)dZ(f')\right] \\ &= 4\,\mathbb{E}\left[\int_0^\infty\int_0^\infty e^{j2\pi f(t+\tau)}e^{j2\pi f't}dZ(f)dZ^*(-f')\right] \\ &= 4\int_0^\infty\int_0^\infty e^{j2\pi f(t+\tau)}e^{j2\pi f't}\delta(f+f')\tilde{S}_{XX^*}(f)df\,df'. \end{aligned} \tag{3.104}$$

The delta function in the last line is zero everywhere except when $f = -f'$. Since both f and f' are non-negative, we will never have $f = -f'$ and the complementary moment function is zero everywhere. Thus the analytic process $Y(t)$ corresponding to a real-valued WSS process $X(t)$ is a proper WSS process. If a general analytic process is an SOS process, it will also be proper [Picinbono and Bondon, 1997]. We see in (3.100)–(3.103) that the Hermitian functions of $Y(t)$ only depend on $\tilde{S}_{XX^*}(f)$ for $f \geq 0$.

3.11 Analytic process corresponding to a harmonizable process

Analytic processes obtained from real-valued processes are used in many systems, e.g., single-sideband amplitude modulation [Proakis and Salehi, 2002]. In such systems the noise is often assumed to be stationary, but the information signal will in general be nonstationary. Let

$$X(t) = \int e^{j2\pi ft}dZ(f) \tag{3.105}$$

be a real-valued harmonizable process with

$$\mathbb{E}[dZ(f)dZ^*(f-\nu)] = S_{XX^*}(\nu, f)d\nu df. \tag{3.106}$$

The analytic process $Y(t)$ corresponding to $X(t)$ has the spectral representation

$$Y(t) = 2\int_0^\infty e^{j2\pi ft}\, dZ(f). \tag{3.107}$$

This representation suggests that $Y(t)$ is a harmonizable process with an increment process

$$dZ_Y(f) = 2u(f)dZ(f), \tag{3.108}$$

where $u(f)$ is the unit step function

$$u(f) = \begin{cases} 1 & f \geq 0 \\ 0 & f < 0. \end{cases} \tag{3.109}$$

This gives us the Hermitian functions

$$M_{YY^*}(t,\tau) = 4\iint u(\beta)u(\beta-\alpha)e^{j2\pi\alpha t}e^{j2\pi\beta\tau}S_{XX^*}(\alpha,\beta)d\alpha d\beta \tag{3.110}$$

$$S_{YY^*}(\nu, f) = \begin{cases} 4\, S_{XX^*}(\nu, f) & f \geq 0, \nu \leq f \\ 0 & \text{otherwise} \end{cases} \tag{3.111}$$

$$P_{YY^*}(t, f) = \begin{cases} 4\int u(f-\alpha)e^{j2\pi\alpha t}S_{XX^*}(\alpha, f)d\alpha & f \geq 0 \\ 0 & \text{otherwise} \end{cases} \tag{3.112}$$

$$A_{YY^*}(\nu,\tau) = 4\int u(\beta)u(\beta-\nu)e^{j2\pi\beta\tau}S_{XX^*}(\nu,\beta)d\beta. \tag{3.113}$$

Since $Y(t)$ is a complex-valued process, we have to consider the complementary functions as well. The complementary moment function of $Y(t)$ is

$$M_{YY}(t,\tau) = 4\iint u(\beta)u(\alpha-\beta)e^{j2\pi\alpha t}e^{j2\pi\beta\tau}S_{XX^*}(\alpha,\beta)d\alpha d\beta. \tag{3.114}$$

Clearly this function is non-vanishing, thus an analytic process corresponding to a harmonizable real-valued process is improper. The other complementary functions are

$$S_{YY}(\nu, f) = \begin{cases} 4\, S_{XX^*}(\nu, f) & \nu \geq f, f \geq 0 \\ 0 & \text{otherwise} \end{cases} \tag{3.115}$$

$$P_{YY}(t, f) = \begin{cases} 4\int u(\alpha-f)e^{j2\pi\alpha t}S_{XX^*}(\alpha, f)d\alpha & f \geq 0 \\ 0 & \text{otherwise} \end{cases} \tag{3.116}$$

$$A_{YY}(\nu,\tau) = 4\int u(\beta)u(\nu-\beta)e^{j2\pi\beta\tau}S_{XX^*}(\nu,\beta)d\beta. \tag{3.117}$$

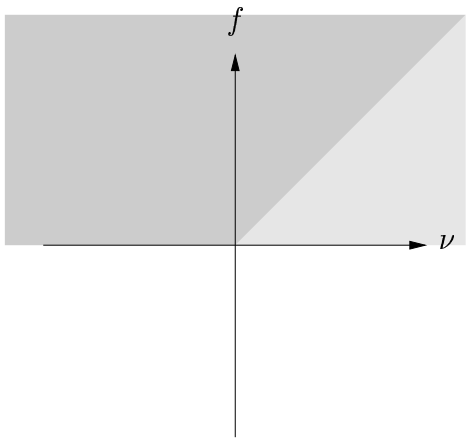

Figure 3.4: The darker shaded area is the area in the f-ν plane where $S_{YY^*}(\nu, f)$ is non-zero. The lighter shaded area is the area in the f-ν plane where $S_{YY}(\nu, f)$ is non-zero.

In Figure 3.4, the darker shaded area is the area of the f-ν plane where the Hermitian f-f spectrum of $Y(t)$ is nonzero and proportional to the f-f spectrum of $X(t)$. Likewise, the lighter shaded area is the area of the f-ν plane where the complementary f-f spectrum of $Y(t)$ is non-zero and proportional to the f-f spectrum of $X(t)$. When we generate an analytic process $Y(t)$ from a real-valued harmonizable process $X(t)$, we are interested in the part of $X(t)$ corresponding to positive frequencies. We see from Figure 3.4 that we need both the f-f spectrum and the complementary f-f spectrum of $Y(t)$ to describe our area of interest.

Chapter 4

Estimators

Consider the random process

$$X(t) = \cos(2\pi f_0 t + \Psi), \tag{4.1}$$

where the phase Ψ is a random variable. If we randomly draw a phase Ψ_1, we obtain the realization

$$x(t) = \cos(2\pi f_0 t + \Psi_1). \tag{4.2}$$

Here, $x(t)$ is a deterministic time function. In practice, we will not know the exact expression of the random process, we will only have available realizations (often just one) of the process. Since the realizations are deterministic, we cannot determine exactly the statistical quantities of the process based on its realizations. In this case, we have to estimate the Hermitian and the complementary functions from the realizations.

4.1 Discrete-time processes

So far we have looked at random processes in continuous-time. A discrete-time harmonizable process $X[k]$ has the spectral representation

$$X[k] = \int_{-1/2}^{1/2} e^{j2\pi fk} dZ(f), \tag{4.3}$$

where $dZ(f)$ is the increment process of $X[k]$ [Yaglom, 1987]. We define the Hermitian second-order quantities of a discrete-time harmonizable process as

$$M_{XX^*}[k,\kappa] = \mathbb{E}[X[k+\kappa]X^*[k]] \tag{4.4}$$

$$S_{XX^*}(\nu, f)d\nu df = \mathbb{E}[dZ(f)dZ^*(f-\nu)] \tag{4.5}$$

$$P_{XX^*}[k, f)df = \mathbb{E}\left[X^*[k]dZ(f)e^{j2\pi fk}\right] \tag{4.6}$$

$$A_{XX^*}(\nu,\kappa]d\nu = \mathbb{E}\left[\int_{-1/2}^{1/2} e^{j2\pi f\kappa} dZ(f)dZ^*(f-\nu)\right], \tag{4.7}$$

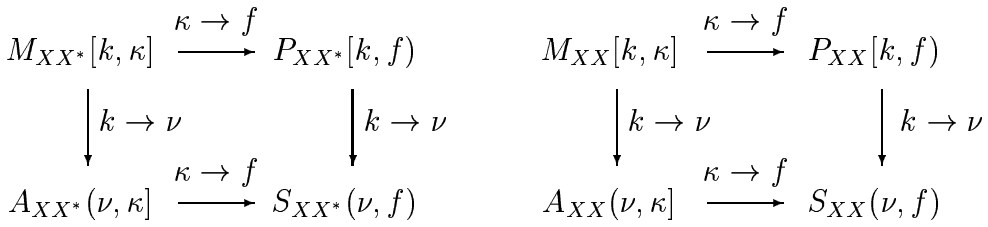

Figure 4.1: Fourier relations between the second-order representations of a discrete-time harmonizable process.

and the complementary second-order quantities are defined as

$$M_{XX}[k,\kappa] = \mathbb{E}[X[k+\kappa]X[k]] \tag{4.8}$$

$$S_{XX}(\nu,f)d\nu df = \mathbb{E}[dZ(f)dZ(\nu-f)] \tag{4.9}$$

$$P_{XX}[k,f)df = \mathbb{E}\left[X[k]dZ(f)e^{j2\pi fk}\right] \tag{4.10}$$

$$A_{XX}(\nu,\kappa]d\nu = \mathbb{E}\left[\int_{-1/2}^{1/2} e^{j2\pi f\kappa}dZ(f)dZ(\nu-f)\right]. \tag{4.11}$$

Here, k is a discrete global time variable, κ is a discrete local time variable, f is a continuous global frequency variable, and ν is a continuous local frequency variable. The quantities are connected through discrete-time Fourier transforms as shown in Fig 4.1. Note that discrete variables are delimited by a square bracket and continuous variables are delimited by a parenthesis.

4.1.1 Sampling

For continuous-time processes, we often only have a sampled realization of the process. The samples of the process $X(t)$ at $t = k\Delta t$, $k \in \mathbb{Z}$, have the spectral representation in (4.3) with the increment process

$$dZ(f) = 2f_N \sum_{n=-\infty}^{\infty} dZ_X(2f_N(f+n)), \tag{4.12}$$

where $dZ_X(f)$ is the increment process of the continuous-time process $X(t)$. Here, $f_N = 1/2\Delta t$ is the Nyquist frequency. If the process $X(t)$ is bandlimited to $(-f_B, f_B]$, and if we sample the process such that $f_N \geq f_B$, then $dZ(f)$ contains only one term, $dZ_X(2f_N f)$. If $f_N < f_B$, or if the process is not bandlimited, contributions of $dZ_X(f)$ for $|f| > f_N$ will be folded back into the interval $(-1/2, 1/2]$. This phenomenon is known as aliasing [Shannon, 1949]. Thus, to avoid aliasing, the sampling frequency $f_s = 1/\Delta t$ must be at least twice the highest frequency

component of the process, which is the Nyquist criterion [Nyquist, 1924].

In all our numerical examples, we will use $\Delta t = 1$, i.e., a sampling frequency $f_s = 1$. Thus, to avoid aliasing, the process under consideration should only have frequencies in the interval $(-1/2, 1/2]$.

4.2 Estimators of the moment functions

We assume that we have K samples $x[k]$, $k = 0, \ldots, K-1$, of a realization of a complex-valued harmonizable process $X(t)$ with zero mean.

A general estimator of the Hermitian moment function is [Martin and Flandrin, 1985]

$$\widehat{M}_{XX^*}[k, \kappa] = \sum_u \Phi[u, \kappa] x[k+u] x^*[k+\kappa+u]. \tag{4.13}$$

The complementary moment function will likewise have an estimator

$$\widehat{M}_{XX}[k, \kappa] = \sum_u \Phi[u, \kappa] x[k+u] x[k+\kappa+u]. \tag{4.14}$$

Here, $\Phi[u, \kappa]$ is a data window that corresponds to a smoothing of the products $x[k+u]x^*[k+\kappa+u]$ and $x[k+u]x[k+\kappa+u]$ in the global time direction. In [Larsen, 2003], it was stated that for white processes, the moment function is singular on the line $\tau = 0$ and for broadband processes, the moment function is expected to decay rapidly as a function of κ. We therefore do not want to smooth in the local time direction.

4.3 Estimators of the ambiguity functions

The Hermitian ambiguity function is often estimated by means of a tapered Fourier transform of the Hermitian moment function estimator [Larsen, 2003],

$$\widehat{A}_{XX^*}(\nu, \kappa] = \sum_k v[k, \kappa] e^{-j2\pi\nu k} \sum_u \Phi[u, \kappa] x[k+u] x^*[k+\kappa+u]. \tag{4.15}$$

We estimate the complementary ambiguity function in the same manner,

$$\widehat{A}_{XX}(\nu, \kappa] = \sum_k v[k, \kappa] e^{-j2\pi\nu k} \sum_u \Phi[u, \kappa] x[k+u] x[k+\kappa+u]. \tag{4.16}$$

The columns of $v[k, \kappa]$ are data tapers. Data tapers (also called data windows) are used with the discrete Fourier transform to reduce spectral leakage [Percival and Walden, 1993]. Spectral leakage may cause a bias in the amplitude and the

position of a harmonic estimate. Hence, data tapers should have low sidelobe levels and the transition to the low sidelobes from the main lobe should be very rapid, or equivalently, the dynamic range should be large. For an extensive treatment of data windows in conjunction with Fourier transformations, see [Harris, 1978].

4.4 Dual-frequency spectra

In order to estimate the f-f spectrum, we need an estimate of the increment process of the process. The multitaper approach to spectral estimation was introduced in [Thomson, 1982]. This approach involves solving an integral equation using an eigenfunction expansion.

4.4.1 Discrete Prolate Spheroidal Wave Functions and Sequences

In [Slepian, 1978] it was shown that the eigenfunctions of the Dirichlet kernel are fundamental to the study of time- and frequency-limited systems. The phase-shifted Dirichlet kernel is defined as

$$D_K(f) = \sum_{k=0}^{K-1} e^{-j2\pi fk} = \frac{\sin(K\pi f)}{\sin(\pi f)} e^{j2\pi f(K-1)}. \tag{4.17}$$

The eigenfunctions $V_n(f; K, W)$ of the kernel are known as discrete prolate spheroidal wave functions (DPSWF) [Slepian, 1978] and are solutions to the equation

$$\int_{-W}^{W} D_K(f - f')V_n(f'; K, W)df' = \lambda_n(K, W)V_n(f; K, W). \tag{4.18}$$

Here, W is a bandwidth defining a local frequency interval $(f - W, f + W)$. For notational convenience, we will not show the dependency on the parameters K and W in the following. The integral equation (4.18) will only have K non-zero eigenvalues, and we order them such that

$$\lambda_0 > \lambda_1 > \ldots \lambda_{K-1} > 0. \tag{4.19}$$

The DPSWFs are doubly orthogonal

$$\int_{-W}^{W} V_n(f)V_m(f)df = \lambda_n \int_{-1/2}^{1/2} V_n(f)V_m(f)df = \lambda_n \delta[n - m]. \tag{4.20}$$

The inverse Fourier transform of the DPSWFs,

$$v_n[k] = \int_{-1/2}^{1/2} V_n(f)e^{j2\pi fk}df, \tag{4.21}$$

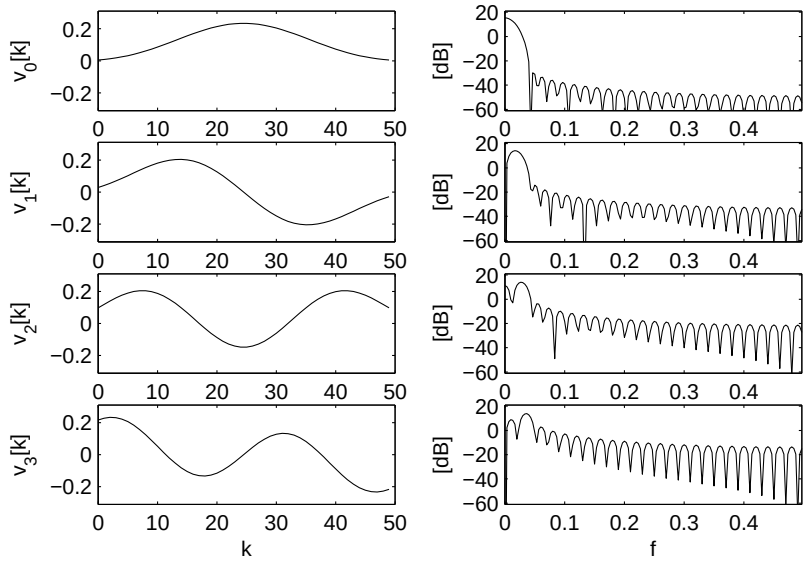

Figure 4.2: Left panel: The four DPSS tapers $v_n[k]$ with largest eigenvalues λ_n for K=50 samples and with a bandwidth $W = 2/K$. Right panel: The corresponding energy spectra.

are the discrete prolate spheroidal sequences (DPSS) [Slepian, 1978]. The DPSS are real-valued sequences, and they are also doubly orthogonal

$$\sum_{k=0}^{K-1} v_n[k]v_m[k] = \lambda_n \sum_{k=-\infty}^{\infty} v_n[k]v_m[k] = \lambda_n \delta[n-m]. \tag{4.22}$$

In multitaper spectral estimation, the DPSS are used as data tapers [Thomson, 1982]. The following considerations are by and large from [Larsen, 2003]. If we consider all functions which are a Fourier transform of a sequence of length K, the eigenfunction $V_0(f)$ corresponding to the largest eigenvalue will have the largest fractional energy in the band $(-W, W)$. The eigenfunction $V_1(f)$ corresponding to the second largest eigenvalue will have the largest fractional energy in the band $(-W, W)$ of all functions which are a Fourier transform of a sequence of length K, and are orthogonal to $V_0(f)$. It can be shown that the $N = \lfloor 2KW \rfloor$ largest eigenvalues have values close to one, while the remaining have values close to zero. The amount of spectral leakage is $1 - \lambda_n$, such that using only the N eigenfunctions corresponding to large eigenvalues ensures that the spectral leakage is kept low.

Figure 4.2 shows the four DPSS tapers $v_n[k]$ with largest eigenvalues λ_n for $K = 50$ samples and a time-bandwidth product $KW = 2$ in the left panel

and their corresponding energy spectra in the right panel. Only the first DPSS is non-negative like conventional bell-shaped data tapers. Note also that as the eigenvalue decreases, the sidelobe levels increases.

4.4.2 Estimator of the increment process

A discrete-time process $X[k]$ has the spectral representation in (4.3). We want to estimate $dZ(f)$ from the K samples of a realization f the process. By taking the finite discrete Fourier transform of the samples, we have

$$y(f) = \sum_{k=0}^{K-1} e^{-j2\pi fk} x[k]. \tag{4.23}$$

Since $y(f)$ can be inverted to recover the data, there is no information lost in the transformation. Substituting the process with its spectral representation, we have

$$\begin{aligned} y(f) &= \int_{-1/2}^{1/2} \sum_{k=0}^{K-1} e^{-j2\pi(f-f')k} dZ(f') \\ &= \int_{-1/2}^{1/2} D_K(f-f') dZ(f'). \end{aligned} \tag{4.24}$$

Now (4.24) can be seen as a Fredholm integral equation of the first kind for $dZ(f)$. This equation cannot be solved exactly, but it has several approximate solutions. The multitaper approach to spectral estimation uses an approximate solution based on eigenfunction expansions. The estimate [Thomson, 1982]

$$\widehat{Z}(f; f_0) = \sum_{n=0}^{N-1} V_n(f-f_0) \frac{Z_n(f_0)}{\lambda_n}, \tag{4.25}$$

where

$$Z_n(f) = \sum_{k=0}^{K-1} x[k] v_n[k] e^{-j2\pi fk}, \tag{4.26}$$

will be a high-resolution estimate of $dZ(f)$ which is valid for $f_0 - W < f < f_0 + W$.

4.4.3 Estimators of the dual-frequency spectra

We may now estimate the Hermitian f-f spectrum at $(\nu, f) = (f_1 - f_2, f_1)$ by averaging the sample covariance matrix of the estimate of the increment process over $(-W, W) \times (-W, W)$ around each point (f_1, f_2) [Larsen, 2003]. This procedure yields

$$\begin{aligned} \widehat{S}_{XX^*}(\nu, f) &= \widehat{S}_{XX^*}(f_1 - f_2, f_1) \\ &= \int_{-W}^{W} \int_{-W}^{W} \widehat{Z}(f_1 + \xi_1; f_1) \widehat{Z}^*(f_2 + \xi_2, f_2) H(\xi_1, \xi_2) d\xi_1 d\xi_2. \end{aligned} \tag{4.27}$$

We choose to smooth over a bandwidth $2W$ along the stationary manifold, i.e., $H(\xi_1, \xi_2) = \delta(\xi_1 - \xi_2)/\lfloor 2WK \rfloor$. Then

$$\begin{aligned}
\widehat{S}_{XX^*}(\nu, f) &= \frac{1}{\lfloor 2WK \rfloor} \int_{-W}^{W} \widehat{Z}(f_1 + \xi_1; f_1) \widehat{Z}^*(f_2 + \xi_1, f_2) d\xi_1 \\
&= \frac{1}{N} \sum_{n=0}^{N-1} \sum_{m=0}^{N-1} \frac{Z_n(f_1) Z_m^*(f_2)}{\lambda_n \lambda_m} \int_{-W}^{W} V_n(\xi_1) V_m^*(\xi_1) d\xi_1 \\
&= \frac{1}{N} \sum_{n=0}^{N-1} \sum_{m=0}^{N-1} \frac{\delta[n-m]}{\lambda_n} Z_n(f_1) Z_m^*(f_2) \\
&= \frac{1}{N} \sum_{n=0}^{N-1} \frac{Z_n(f_1) Z_n^*(f_2)}{\lambda_n},
\end{aligned} \tag{4.28}$$

where we have used that the DPSWFs are orthogonal. This estimator was proposed in [Thomson, 1982].

If we use the same procedure to estimate the complementary f-f spectrum, we have an estimator

$$\begin{aligned}
\widehat{S}_{XX}(\nu, f) &= \widehat{S}_{xx}(f_1 + f_2, f_1) \\
&= \int_{-W}^{W} \int_{-W}^{W} \widehat{Z}(f_1 + \xi_1; f_1) \widehat{Z}(f_2 + \xi_2, f_2) H(\xi_1, \xi_2) d\xi_1 d\xi_2.
\end{aligned} \tag{4.29}$$

Again, we want to do the smoothing over a bandwidth $2W$ along the stationary manifold. The stationary manifold of the complementary f-f spectrum is the line $\nu = f_1 + f_2 = 0$, we now choose $H(\xi_1, \xi_2) = \delta(\xi_1 + \xi_2)/\lfloor 2WK \rfloor$. Since the DPSS are real-valued, the DPSWF will have a Hermitian symmetry $V_n(f) = V_n^*(-f)$. We estimate the complementary f-f spectrum with

$$\begin{aligned}
\widehat{S}_{XX}(\nu, f) &= \frac{1}{\lfloor 2WK \rfloor} \int_{-W}^{W} \widehat{Z}(f_1 + \xi_1; f_1) \widehat{Z}(f_2 - \xi_1, f_2) d\xi_1 \\
&= \frac{1}{N} \sum_{n=0}^{N-1} \sum_{m=0}^{N-1} \frac{Z_n(f_1) Z_m(f_2)}{\lambda_n \lambda_m} \int_{-W}^{W} V_n(\xi_1) V_m(-\xi_1) d\xi_1 \\
&= \frac{1}{N} \sum_{n=0}^{N-1} \sum_{m=0}^{N-1} \frac{Z_n(f_1) Z_m(f_2)}{\lambda_n \lambda_m} \int_{-W}^{W} V_n(\xi_1) V_m^*(\xi_1) d\xi_1 \\
&= \frac{1}{N} \sum_{n=0}^{N-1} \frac{Z_n(f_1) Z_n(f_2)}{\lambda_n}.
\end{aligned} \tag{4.30}$$

Multitaper spectral analysis was described in great detail in [Percival and Walden,

1993]. The following statements are from this book. For multitaper analysis, typical choices of the time-bandwidth product KW are values between 2 and 4, although values larger than 4 are sometimes of interest. For a fixed K, increasing KW increases the number of tapers with good leakage properties, thus reducing the variance of the estimate. However, increasing KW also decreases the resolution of the estimate.

4.5 Testing the estimators

The estimators outlined here for the Hermitian functions are known to work for real-valued processes. We want to assess whether our estimators of the complementary functions work properly. Our implementation of these estimators are based on code from [Larsen, 2003]. Consider a real-valued chirp process in noise,

$$Y(t) = \cos\left[\pi(\beta t^2 + 2\alpha t)\right] + N(t), \tag{4.31}$$

where $N(t)$ is a white Gaussian noise process. If we define a complex-valued process $X(t) = \exp\left[j\pi(\beta t^2 + 2\alpha t)\right] + N(t)$, we see that

$$Y(t) = \frac{X(t) + X^*(t)}{2}. \tag{4.32}$$

The moment function of $Y(t)$ will be

$$\begin{aligned} M_{YY^*}(t,\tau) &= \mathbb{E}\left[Y(t+\tau)Y^*(t)\right] \\ &= \frac{1}{4}\left[M_{XX^*}(t,\tau) + M^*_{XX^*}(t,\tau) + M_{XX}(t,\tau) + M^*_{XX}(t,\tau)\right]. \end{aligned} \tag{4.33}$$

By Fourier transforms we get similar expressions for the f-f spectrum

$$S_{YY^*}(\nu,f) = \frac{1}{4}\left[S_{XX^*}(\nu,f) + S^*_{XX^*}(-\nu,-f) + S_{XX}(\nu,f) + S^*_{XX}(-\nu,-f)\right], \tag{4.34}$$

and the ambiguity function

$$A_{YY^*}(\nu,\tau) = \frac{1}{4}\left[A_{XX^*}(\nu,\tau) + A^*_{XX^*}(-\nu,\tau) + A_{XX}(\nu,\tau) + A^*_{XX}(-\nu,\tau)\right]. \tag{4.35}$$

We generated $K = 100$ samples $y[k] = Y(k)$ and $x[k] = X(k)$, $k = 0, \ldots, K-1$, with $\alpha = -0.3$, $\beta = 0.005$ and a noise process with standard deviation $\sigma = 0.05$. Figure 4.3 shows the available samples $y[k]$.

We use the estimator in (4.13) to estimate the Hermitian moment functions

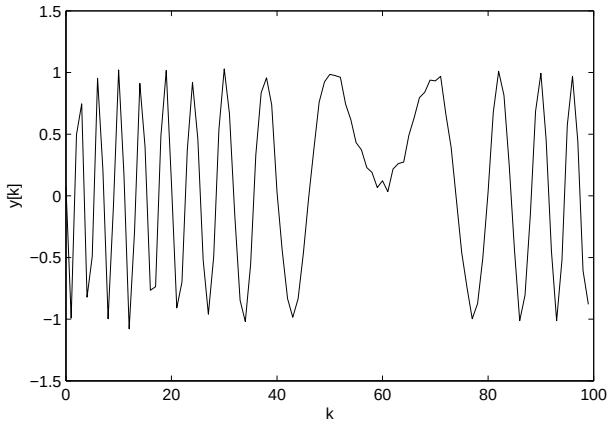

Figure 4.3: Samples $y[k]$ of the real-valued noisy chirp process.

of $Y(t)$ and $X(t)$ and the estimator in (4.14) to estimate the complementary moment function of $X(t)$. The kernel

$$\Phi[u,\kappa] = \begin{cases} 1/N_t & u = 0,\ldots,N_t-1 \\ 0 & \text{otherwise} \end{cases} \tag{4.36}$$

is applied with $N_t = 15$. This is a moving average of N_t samples in the k-direction. In Figure 4.4 we compare the estimate of $M_{YY^*}(t,\tau)$ obtained from (4.13) with the estimate of $M_{YY^*}(t,\tau)$ based on estimates of the moment functions of $X(t)$, as in (4.33).

We estimate the Hermitian f-f spectra of $Y(t)$ and $X(t)$ with (4.28), and the complementary f-f spectrum of $X(t)$ with (4.30). We use a time-bandwidth product $KW = 5/2$. In Figure 4.5 we compare the estimate of $S_{YY^*}(\nu,f)$ obtained from (4.28) with the estimate of $S_{YY^*}(\nu,f)$ based on estimates of the f-f spectra of $X(t)$, as in (4.34).

The Hermitian ambiguity functions of $Y(t)$ and $X(t)$ are estimated with (4.15) and the complementary ambiguity function of $X(t)$ is estimated with (4.16). The data taper

$$v[k] = 0.5 - 0.5\cos\left(\frac{2\pi(k+1)}{N+1}\right) \quad k = 0,\ldots,N-1, \tag{4.37}$$

know as a Hann window [Harris, 1978], is used for all κ. In Figure 4.6 we compare the estimate of $A_{YY^*}(\nu,\tau)$ obtained from (4.15) with the estimate of $A_{YY^*}(\nu,\tau)$ based on estimates of the ambiguity functions of $X(t)$, as in (4.35).

The estimates of the three Hermitian statistical quantities of $Y(t)$ obtained by

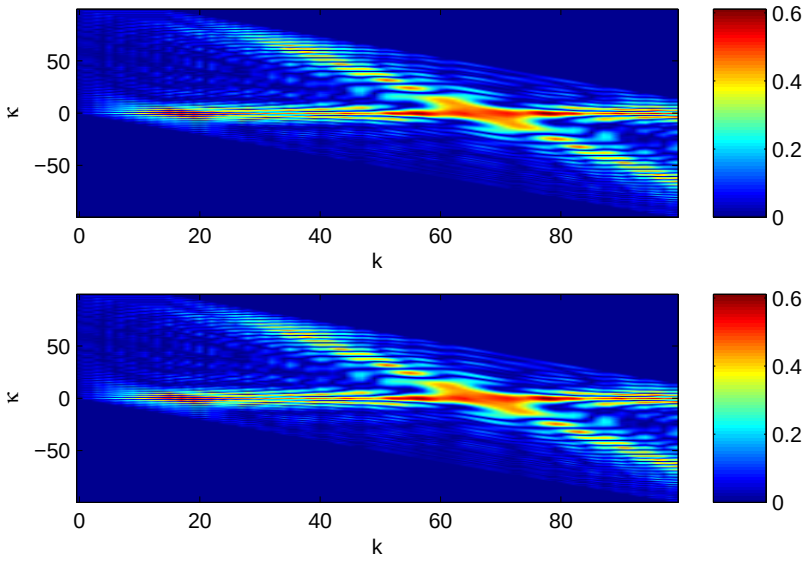

Figure 4.4: $|\widehat{M}_{YY^*}[k,\kappa]|$. Top: Estimate based on $y[k]$. Bottom: Estimate based on $x[k]$.

analyzing the real-valued time series $y[k]$ are identical to the estimates obtained by analyzing the complex-valued time series $x[k]$ and using the relations (4.33)–(4.35). This suggests that the estimators of the complementary quantities are correct.

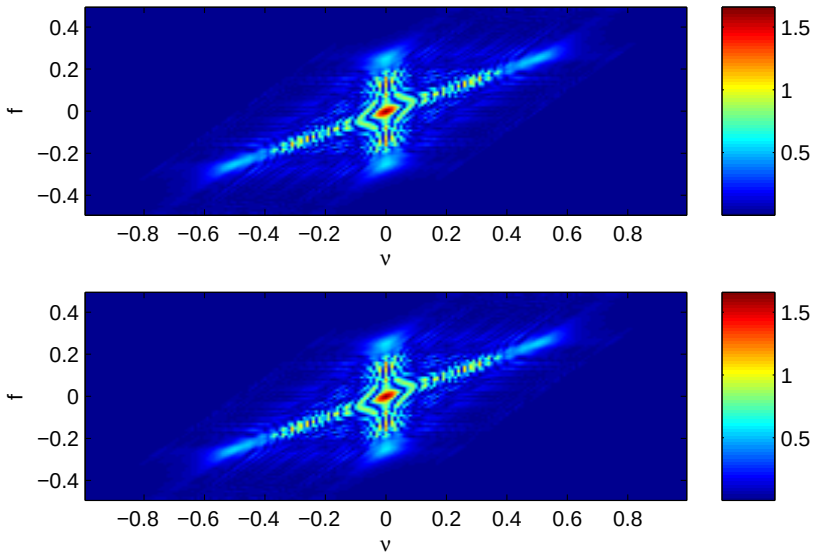

Figure 4.5: $|\widehat{S}_{YY^*}(\nu, f)|$. Top: Estimate based on $y[k]$. Bottom: Estimate based on $x[k]$.

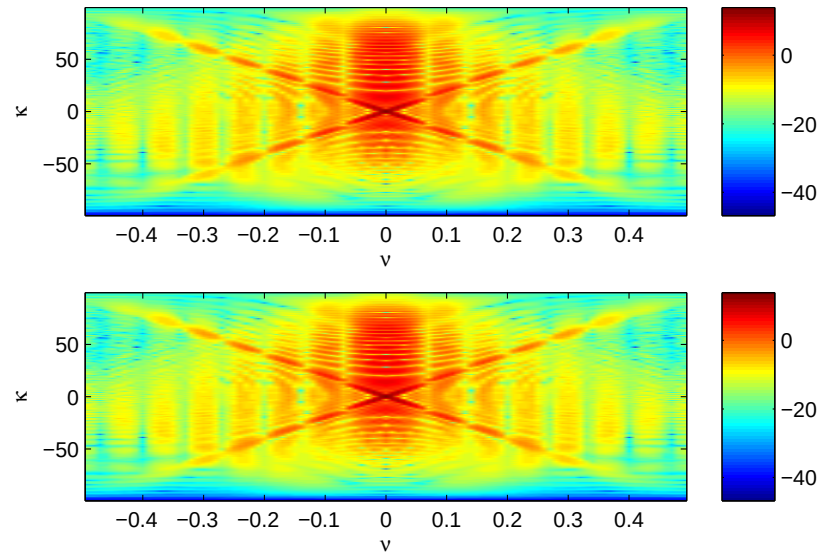

Figure 4.6: $|\widehat{A}_{XX^*}(\nu, \kappa]|$ on a log scale. Top: Estimate based on $y[k]$. Bottom: Estimate based on $x[k]$.

Chapter 5

Estimation of the time-frequency spectrum

Estimation of the time-frequency behavior of a process has been given much attention in the literature. One of the more popular approaches to time-frequency analysis is the Wigner-Ville time-frequency distribution, introduced by Wigner in [Wigner, 1932] in quantum mechanics, and by Ville in [Ville, 1948] in signal theory. The Wigner-Ville distribution has many desirable properties, but it is not clear what property of the process the distribution actually measures. The common assumption is that the Wigner-Ville is an energy density. However, this cannot be true since the Wigner-Ville distribution can attain negative values. Time-frequency analysis of synthetic aperture sonar data using the Wigner-Ville distribution and its relatives was presented in [Hindberg et al., 2004].

The Hermitian time-frequency spectrum of complex-valued processes can be estimated using multitaper by the baseband complex demodulate [Thomson, 1989]. However, there is no equivalent way to estimate the complementary t-f spectrum.

To estimate the Hermitian and the complementary t-f spectrum of a process, we define

$$V_{XX^*}(t,f)df = \mathbb{E}\left[X(t)\left(e^{j2\pi ft}dZ(f)\right)^*\right] \tag{5.1}$$

$$V_{XX}(t,f)df = \mathbb{E}\left[X(t)\left(e^{j2\pi ft}dZ^*(-f)\right)^*\right]. \tag{5.2}$$

Here, $V_{XX^*}(t,f)$ is the Hermitian Rihaczek time-frequency distribution (HR-TFD) [Rihaczek, 1968] and $V_{XX}(t,f)$ is the complementary Rihaczek time-frequency distribution (CR-TFD) [Schreier and Scharf, 2003b]. The relationship between these time-frequency representations and the t-f spectra are then

$$P_{XX^*}(t,f) = (V_{XX^*}(t,f))^* \tag{5.3}$$

$$P_{XX}(t,f) = V_{XX}(t,-f). \tag{5.4}$$

Time-frequency analysis favors the use of analytic processes since it reduces the number of cross-terms that cause interference in the distribution [Flandrin, 1999]. For analytic processes, the HR-TFD will only be non-zero for positive frequencies and the CR-TFD only for negative frequencies. This is consistent with the Hermitian and complementary t-f spectrum of the process being non-zero only for positive frequencies, as we showed in Section 3.11.

Note that the HR-TFD and the CR-TFD are generally complex-valued. The following quote is from [Scharf et al., 2005]: "We interpret the Rihaczek distribution of stochastic signals as a distribution of correlation over time and frequency, rather than a distribution of energy. This resolves concerns about the meaning of negative or complex energy." It was also shown in [Scharf et al., 2005] that the Rihaczek distribution determines the time-varying Wiener filter for estimating the process from its increment process.

5.1 Estimation of the Rihaczek distributions

The HR-TFD and the CR-TFD are bilinear time-frequency distributions that are covariant to shifts in time and frequency. They are therefore members of Cohen's class [Cohen, 1966], and the discrete-time version of Cohen's class can be used to estimate these distributions [Martin and Flandrin, 1985]. The HR-TFD is estimated with

$$\widehat{V}_{XX^*}[k,f] = \sum_{m=-\infty}^{\infty} \sum_{\mu=-\infty}^{\infty} x[k+m]\phi[m,\mu]x^*[k+m-\mu]e^{-j2\pi\mu f}, \tag{5.5}$$

and we estimate the CR-TFD with

$$\widehat{V}_{XX}[k,f] = \sum_{m=-\infty}^{\infty} \sum_{\mu=-\infty}^{\infty} x[k+m]\phi[m,\mu]x[k+m-\mu]e^{-j2\pi\mu f}. \tag{5.6}$$

Here, m is a global time variable and μ is a local time variable. In [Scharf et al., 2005], a factorized kernel

$$\phi[m,\mu] = w_1[m]w_2[\mu]w_3^*[m-\mu] \tag{5.7}$$

was suggested as a suitable dual-time kernel for these estimators. We will now implement and test these estimators. We use the estimators in (5.5) and (5.6) along with the relations in (5.3) and (5.4) to estimate the Hermitian and complementary t-f spectrum of analytic processes.

5.2 Choice of windows

Inserting the kernel (5.7) in (5.5) and (5.6), we obtain

$$\begin{aligned}\widehat{V}_{XX^*}[k,f) = &\sum_{m=\infty}^{\infty} x[k+m]w_1[m] \\ &\times \int_{-\pi}^{\pi} W_2(f') \left(F_3[k, f-f')e^{j2\pi m(f-f')}\right)^* df'\end{aligned} \tag{5.8}$$

and

$$\begin{aligned}\widehat{V}_{XX}[k,f) = &\sum_{m=\infty}^{\infty} x[k+m]w_1[m] \\ &\times \int_{-\pi}^{\pi} W_2(f') \left(F_3^*[k, -(f-f'))e^{j2\pi m(f-f')}\right)^* df'.\end{aligned} \tag{5.9}$$

Here, $W_2(f)$ is the Fourier transform of $w_2[\mu]$, and

$$F_3[k,f) = \sum_{m=-\infty}^{\infty} w_3[m]x[m+k]e^{-j2\pi mf} \tag{5.10}$$

is the Short-Time Fourier Transform (STFT) of $x[k]$ using window w_3. The window w_3 should be a smooth data taper to stabilize the STFT, and the windows w_1 and w_2 should be localized to concentrate the estimator in time and frequency, respectively [Scharf et al., 2005]. There are many possible ways of choosing these windows and the parameters associated with the windows to fulfill this, and we have no way of determining what the optimal choice would be. We will consider two kernels composed of two different sets of windows.

5.2.1 Hamming and Gaussian windows

We start by selecting w_3 to be the smooth data taper

$$w_3[n] = 0.54 - 0.46\cos\left(\frac{2\pi n}{N+1}\right) \quad n = 0, \ldots, N-1 \tag{5.11}$$

known as the Hamming window [Harris, 1978]. The Gaussian window [Harris, 1978] is defined by

$$w[n] = \exp\left(\frac{-n^2}{2\sigma^2}\right) \quad n = 0, \ldots, N-1. \tag{5.12}$$

The choice of σ controls the width of the window itself and the width of the Fourier transform of the window. By choosing a small value of σ, the window

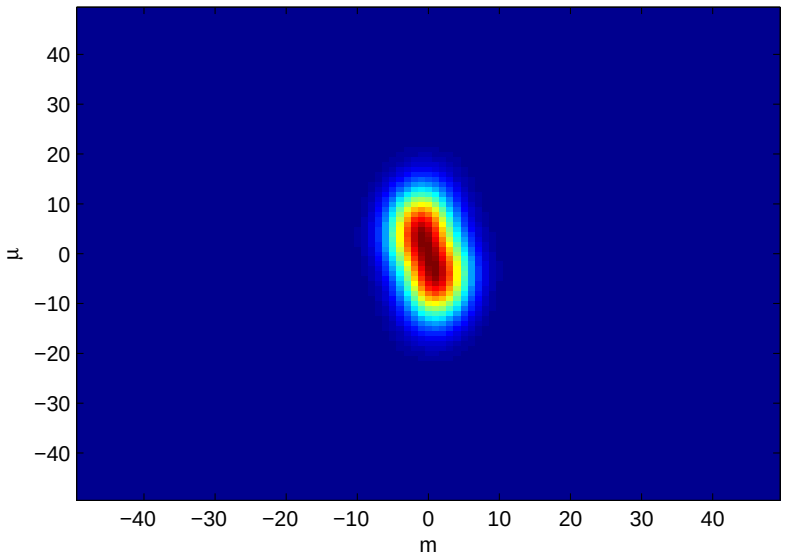

Figure 5.1: The kernel $\phi[m, \mu]$ with w_3 as a Hamming window and w_1 and w_2 as Gaussian windows with $\sigma_1^2 = 10$ and $\sigma_2^2 = 40$, respectively.

will be concentrated in time. Likewise, a large value of σ gives a narrow window in the Fourier domain. We choose w_1 to be a Gaussian window with $\sigma_1^2 = 10$ and w_2 to be a Gaussian window with $\sigma_2^2 = 40$. Figure 5.1 shows the resulting total kernel $\phi[m, \mu]$ with these windows.

We will generate numerical data from some processes which have well-known time-frequency behavior, to examine how the estimators work with these windows. In the following, $N(t)$ is a white Gaussian noise process with standard deviation $\sigma_N = 0.05$.

First, we consider the process

$$X(t) = \cos(2\pi f_0 t) + N(t) + j\mathcal{H}\left\{\cos(2\pi f_0 t) + N(t)\right\}. \tag{5.13}$$

The process $X(t)$ is a complex-valued, analytic process corresponding to a cyclostationary real-valued process. We generated $K = 100$ samples $x[k]$, $k = 0, \ldots, K-1$, of $X(t)$ with $f_0 = 0.3$.

Figure 5.2 shows the estimates of the Hermitian and complementary spectrum based on these samples. We see that the Hermitian t-f spectrum is concentrated on the line $f = f_0$, and it is reasonably constant as a function of time. This is what we would expect for this process, since $X(t)$ consists of a pure tone with frequency f_0 and $N(t)$ which has a constant t-f spectrum. The complementary t-f spectrum has its largest values at frequency f_0.

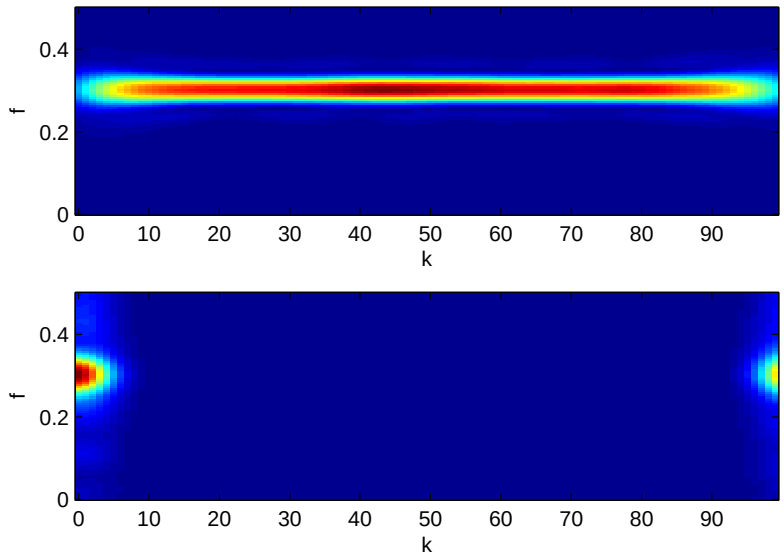

Figure 5.2: Estimates of the t-f spectra of the process in (5.13). Top: $|\widehat{P}_{XX^*}[k,f)|$. Bottom: $|\widehat{P}_{XX}[k,f)|$.

The process

$$X(t) = \cos\left[\pi(2\alpha t + \beta t^2)\right] + N(t) + j\mathcal{H}\left\{\cos\left[\pi(2\alpha t + \beta t^2)\right] + N(t)\right\}. \quad (5.14)$$

is a complex-valued, analytic process corresponding to a real-valued chirp in white Gaussian noise. We generated $K = 100$ samples $x[k]$, $k = 0, \ldots, K-1$, of $X(t)$, with $\alpha = 0.15$ and $\beta = 0.0025$.

The estimates of the Hermitian and the complementary t-f spectrum based on these samples are shown in Figure 5.3. The chirp has a starting instantaneous frequency of $\alpha = 0.15$, and the frequency will increase as a linear function of time such that at $k = K-1$, the instantaneous frequency of the chirp will be 0.4. We see that this behavior is reflected in our estimate of the Hermitian t-f spectrum.

We will estimate the t-f spectra of the two-tone process in noise,

$$\begin{aligned} X(t) = &\cos(2\pi f_1 t) + \cos(2\pi f_2 t) + N(t) \\ &+ j\mathcal{H}\left\{\cos(2\pi f_1 t) + \cos(2\pi f_2 t) + N(t)\right\}. \end{aligned} \quad (5.15)$$

The process $X(t)$ consists of two distinct tones at frequencies f_1 and f_2.

We generated $K = 100$ samples $x[k]$, $k = 0, \ldots, K-1$, of $X(t)$ with $f_1 = 0.2$ and $f_2 = 0.3$.

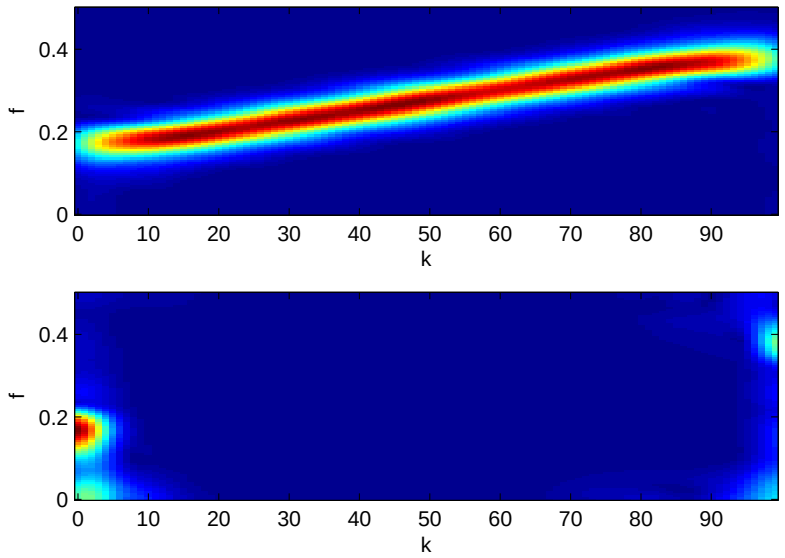

Figure 5.3: Estimates of the t-f spectra of the process in (5.14). Top: $|\widehat{P}_{XX^*}[k,f)|$. Bottom: $|\widehat{P}_{XX}[k,f)|$.

We see in Figure 5.4 that the Hermitian t-f spectrum is indeed concentrated on the lines $f = 0.2$ and $f = 0.3$. The spectrum is, however, no longer constant as a function of time. There is a pulsation of the lines which is periodic with frequency $f_2 - f_1 = 0.1$. Since the estimator is a quadratic function of the samples, this pulsation is probably due to interference between the two sinusoidal components of the process, a process commonly referred to as a "beat". By increasing σ_1^2 and decreasing σ_2^2, we can reduce the interference in the estimate. However, this will give an estimate with poorer overall resolution.

Except for the interference in the two-component process, the estimated Hermitian t-f spectra in this section have been consistent with what we would expect for the different processes. However, we had no such intuition regarding the complementary t-f spectra. From the figures in this section, we see that the estimate of the complementary t-f spectrum appears to fill in the parts that are missing on the edges of the estimate of the Hermitian t-f spectrum.

This choice of windows seems to work quite well for single-component processes, but for multi-component processes we may experience interference in the estimates.

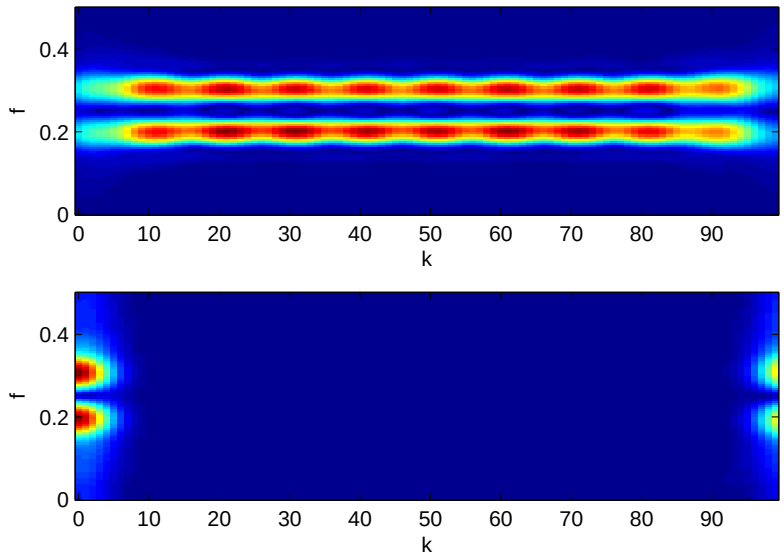

Figure 5.4: Estimates of the t-f spectra of the process in (5.15). Top: $|\widehat{P}_{XX^*}[k,f)|$. Bottom: $|\widehat{P}_{XX}[k,f)|$.

5.2.2 Kaiser-Bessel windows

We introduced the DPSS in Section 4.4.1, and stated that they are good choices for data windows. We want to use the DPSS of order zero, $v_0[k]$, for all the data windows in the kernel of the estimators of the t-f spectra. Here, the choice of the time-bandwidth product KW of the DPSS should differ for the different windows.

A problem with the DPSS is that they do not have a closed form expression. We will therefore use an approximation of the DPSS of order zero called the Kaiser-Bessel window [Kaiser, 1966]. This window is defined by

$$v[n] = \frac{I_0\left[\pi\alpha\sqrt{1-\left(\frac{n}{N/2}\right)^2}\right]}{I_0\left(\pi\alpha\right)} \tag{5.16}$$

where $I_0(x)$ is the modified Bessel function of the first kind of order zero. The parameter α in (5.16) corresponds to the time-bandwidth product KW of the DPSS that the Kaiser-Bessel window is an approximation to. Figure 5.5 shows the window and its energy spectrum for the Kaiser-Bessel window and the DPSS of order zero. The Kaiser-Bessel window has a maximum value of one, but here we have scaled the Kaiser-Bessel window to have the same maximum value as the corresponding DPSS.

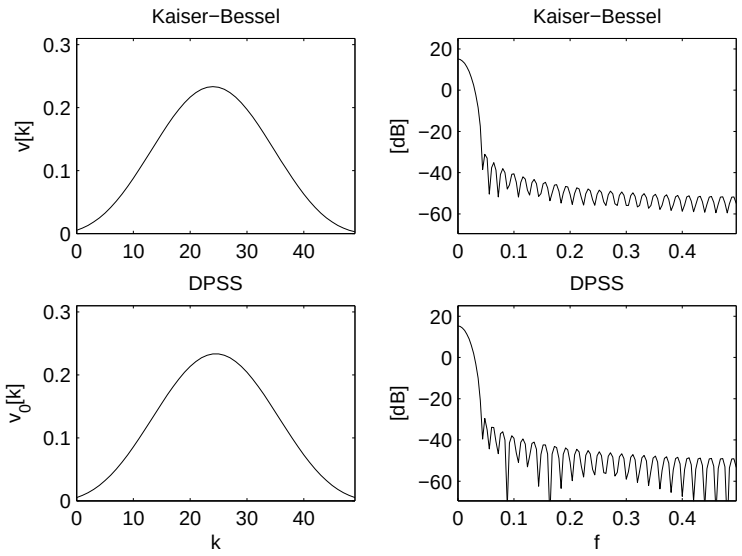

Figure 5.5: Comparison between the DPSS of order zero and the Kaiser-Bessel window for $K = 50$ samples and a bandwidth $W = 4/K$. Top: The Kaiser-Bessel window (left) and its energy spectrum (right). Bottom: The DPSS of order zero (left) and its energy spectrum (right).

In Figure 5.6 we show four different kernels of the Rihaczek estimators constructed from three Kaiser-Bessel windows. The notation KW_i is used for the

Kernel	KW_1	KW_2	KW_3
$\phi_1[m,\mu]$	4	2	3
$\phi_2[m,\mu]$	6	4	5
$\phi_3[m,\mu]$	8	4	6
$\phi_4[m,\mu]$	16	8	12

Table 5.1: The time-bandwidth products of four kernels constructed from three Kaiser-Bessel windows.

time-bandwidth product of window w_i in the kernel. The time-bandwidth products of each kernel are specified in Table 5.1. We see that as the time-bandwidth products of the windows increase, the size of the kernel decreases.

All the time-bandwidth products in Table 5.1 were chosen such that $KW_1 > KW_3 > KW_2$. The larger the value of KW_i, the narrower the window w_i will be in time. Likewise, the smaller the value of KW_i, the narrower the window w_i will be in frequency. If w_3 is supposed to stabilize the STFT, and w_1 and w_2 are used to concentrate the estimate in time and frequency respectively, we should have the ordering $KW_1 > KW_3 > KW_2$. Exactly how the ratio between

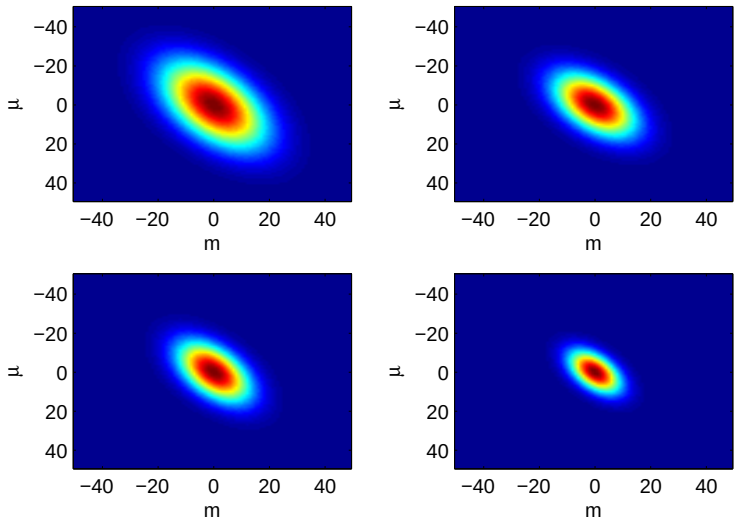

Figure 5.6: Kernels based on three Kaiser-Bessel windows. Top left: The kernel $\phi_1[m,\mu]$ with $KW_1 = 4$, $KW_2 = 2$ and $KW_3 = 3$. Top right: The kernel $\phi_2[m,\mu]$ with $KW_1 = 6$, $KW_2 = 4$ and $KW_3 = 5$. Bottom left: The kernel $\phi_3[m,\mu]$ with $KW_1 = 8$, $KW_2 = 4$ and $KW_3 = 6$. Bottom right: The kernel $\phi_4[m,\mu]$ with $KW_1 = 16$, $KW_2 = 8$ and $KW_3 = 12$.

the time-bandwidth products should be, will have to be determined through trial and error for any given data set.

We estimate the t-f spectra of the chirp process in Section 5.2.1 with the four kernels in Table 5.1. Figure 5.7 and Figure 5.8 shows the magnitude of the estimates of the Hermitian and complementary t-f spectrum obtained with the different kernels. The localization of the estimate improves as the kernel decreases in size. But we also see that the magnitude of the estimate depends on the size of the kernel, the magnitude decreases as the kernel decreases in size. Note that the magnitude of $|\widehat{P}_{XX}[k,f)|$ is much smaller than the magnitude of $|\widehat{P}_{XX^*}[k,f)|$.

Of the kernels in Table 5.1, $\phi_4[m,\mu]$ gave the best localization of the chirp. We will use this kernel to estimate the t-f spectra of the other two processes considered in Section 5.2.1. The t-f spectra of the single tone are shown in Figure 5.9. These estimates are quite similar to the estimates in Figure 5.2 obtained with the previous kernel. Figure 5.10 shows the t-f spectra of the process consisting of two tones. Here, the Kaiser-Bessel kernel has improved the estimates dramatically, and the interference between the two tones has disappeared altogether.

The kernel consisting of three Kaiser-Bessel windows with $KW_1 > KW_3 > KW_2$ gave us good estimates of the t-f spectra both for single-component and two-

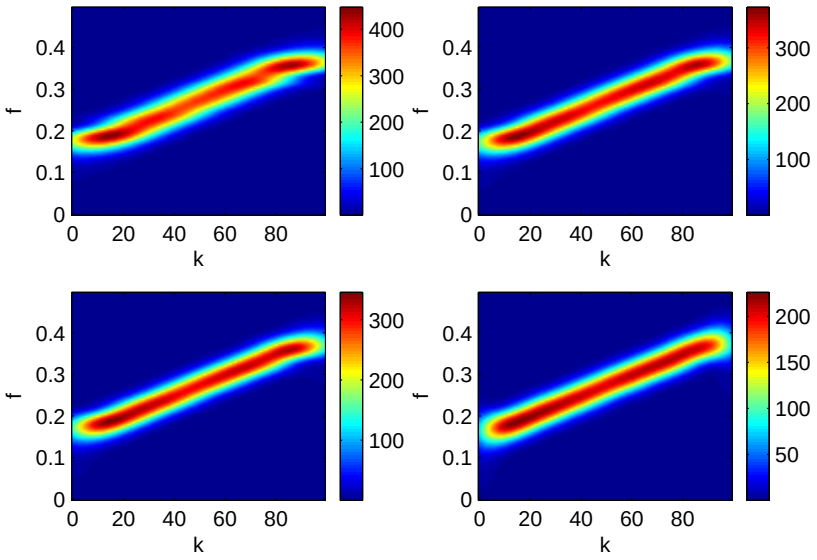

Figure 5.7: Estimates of the Hermitian t-f spectrum of a chirp process using the kernels in Figure 5.6. Top left: $|\widehat{P}_{XX^*}[k,f)|$ with kernel $\phi_1[m,\mu]$. Top right: $|\widehat{P}_{XX^*}[k,f)|$ with kernel $\phi_2[m,\mu]$. Bottom left: $|\widehat{P}_{XX^*}[k,f)|$ with kernel $\phi_3[m,\mu]$. Bottom right: $|\widehat{P}_{XX^*}[k,f)|$ with kernel $\phi_4[m,\mu]$.

component processes.

5.3 Statistical properties

We estimated the Hermitian and complementary t-f spectrum of a process by estimating the HR-TFD and the CR-TFD of the process. From (5.5) and (5.6) we have

$$\mathbb{E}\left[\widehat{V}_{XX^*}[k,f)\right] = \sum_{m=-\infty}^{\infty} \int_0^{1/2} V_{XX^*}[m,\alpha)\Phi[m-k,f-\alpha)d\alpha \tag{5.17}$$

$$\mathbb{E}\left[\widehat{V}_{XX}[k,f)\right] = \sum_{m=-\infty}^{\infty} \int_{-1/2}^{0} V_{XX}[m,\alpha)\Phi[m-k,f-\alpha)d\alpha \tag{5.18}$$

where $\Phi[m,f)$ is the discrete-time Fourier transform of the kernel $\phi[m,\mu]$ with respect to the variable μ. Thus, the expected value of the estimators are a time-frequency smoothed version of the HR-TFD and the CR-TFD [Scharf et al., 2005].

We will use Monte Carlo simulation to approximate the expected values of the estimators of the t-f spectra. We consider the process in (5.14). We generate $K = 50$ samples $x[k]$, $k = 0,\ldots,K-1$, with $\alpha = 0.15$, $\beta = 0.0051$ and $N(t)$

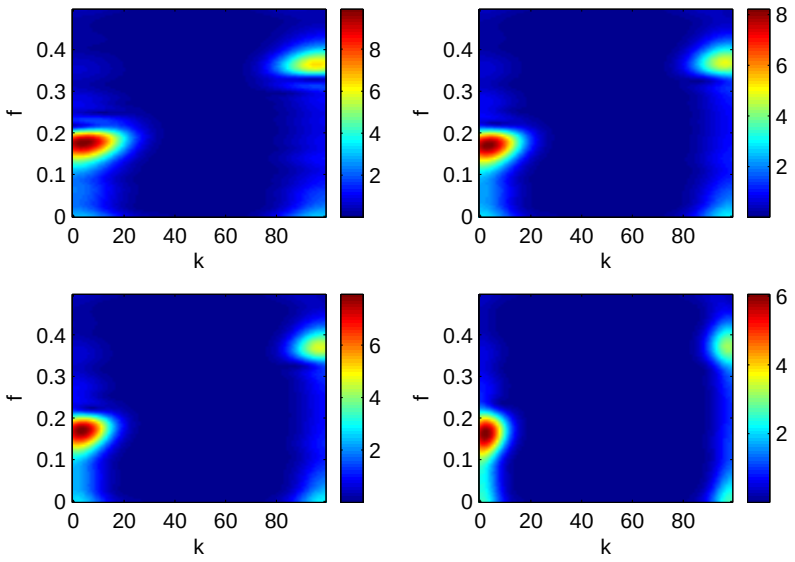

Figure 5.8: Estimates of the complementary t-f spectrum of a chirp process using the kernels in Figure 5.6. Top left: $|\widehat{P}_{XX}[k,f)|$ with kernel $\phi_1[m,\mu]$. Top right: $|\widehat{P}_{XX}[k,f)|$ with kernel $\phi_2[m,\mu]$. Bottom left: $|\widehat{P}_{XX}[k,f)|$ with kernel $\phi_3[m,\mu]$. Bottom right: $|\widehat{P}_{XX}[k,f)|$ with kernel $\phi_4[m,\mu]$.

with standard deviation $\sigma_N = 0.05$. The estimates $\widehat{P}^{(1)}_{XX^*}[k,f)$ and $\widehat{P}^{(1)}_{XX}[k,f)$ are calculated from these samples. We generate K new samples and calculate $\widehat{P}^{(2)}_{XX^*}[k,f)$ and $\widehat{P}^{(2)}_{XX}[k,f)$ based on these samples. This is repeated $L = 1000$ times, and we estimate the expected values by

$$\overline{\widehat{P}}_{XX^*}[k,f) = \frac{1}{L}\sum_{i=1}^{L} \widehat{P}^{(i)}_{XX^*}[k,f) \tag{5.19}$$

$$\overline{\widehat{P}}_{XX}[k,f) = \frac{1}{L}\sum_{i=1}^{L} \widehat{P}^{(i)}_{XX}[k,f). \tag{5.20}$$

From Figure 5.11 we see that the approximated expected value of the t-f spectra are time- and frequency-smoothed versions of the spectra themselves.

We can also use Monte Carlo simulation to estimate the variance of the esti-

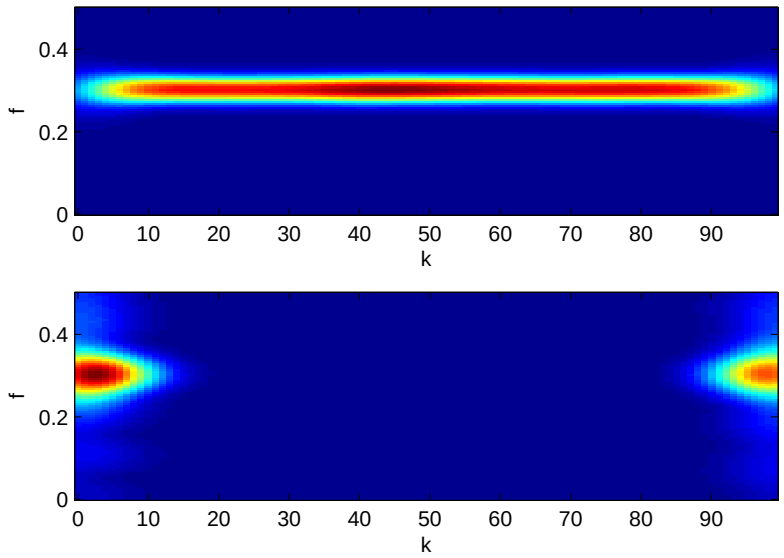

Figure 5.9: Estimates of the t-f spectra of the process in (5.13) with the kernel $\phi_4[m, \mu]$. Top: $|\widehat{P}_{XX^*}[k, f)|$. Bottom: $|\widehat{P}_{XX}[k, f)|$.

mators of the t-f spectra. This numerical approximation is

$$\overline{\mathrm{Var}}\left\{\widehat{P}_{XX^*}[k, f)\right\} = \frac{1}{L}\sum_{i=1}^{L}\left|\widehat{P}^{(i)}_{XX^*}[k, f)\right|^2 - \left|\overline{\widehat{P}}_{XX^*}[k, f)\right|^2 \tag{5.21}$$

$$\overline{\mathrm{Var}}\left\{\widehat{P}_{XX}[k, f)\right\} = \frac{1}{L}\sum_{i=1}^{L}\left|\widehat{P}^{(i)}_{XX}[k, f)\right|^2 - \left|\overline{\widehat{P}}_{XX}[k, f)\right|^2. \tag{5.22}$$

Figure 5.12 shows the Monte Carlo estimate of the variance of the estimators. The variance of $\widehat{P}_{XX^*}[k, f)$ is largest in the area where the magnitude of each estimate $\widehat{P}^{(i)}_{XX^*}[k, f)$ is largest. This is also true for the variance of $\widehat{P}_{XX}[k, f)$.

An approximate expression for the variance of the estimate of the Hermitian t-f spectrum was derived in [Scharf et al., 2005] as

$$\begin{aligned}\mathrm{Var}\left\{\widehat{P}_{XX^*}[k, f)\right\} \approx \sum_{m=-\infty}^{\infty}\Bigg[&\int_0^{1/2}|\Phi[m-k, f-\alpha)|^2|P_{XX^*}[k, \alpha)|^2 d\alpha \\ &+ \int_0^{1/2}\Phi[m-k, f+\alpha)\Phi^*[m-k, f-\alpha) \\ &\times |P_{XX}[k, \alpha)|^2 d\alpha\Bigg].\end{aligned} \tag{5.23}$$

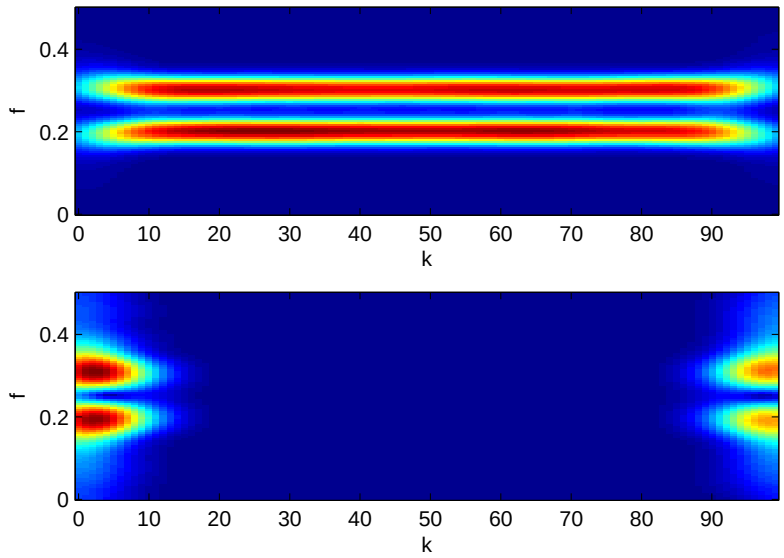

Figure 5.10: Estimates of the t-f spectra of the process in (5.15) with kernel $\phi_4[m, \mu]$. Top: $|\widehat{P}_{XX^*}[k, f)|$. Bottom: $|\widehat{P}_{XX}[k, f)|$.

This approximation assumes quasistationary processes whose time of stationarity is much greater than the correlation time. Since analytic, SOS processes are proper, this assumption on the complementary functions will result in approximately zero variance for the estimate of the complementary t-f spectrum. We examine the quasistationary process

$$X(t) = \exp\left[j(2\pi f_0 t + \Psi)\right], \tag{5.24}$$

which is a pure tone with a random phase. Here, $f_0 = 0.2$ and Ψ is uniformly distributed on $[-\pi, \pi]$.

We estimated $\mathrm{Var}\left\{\widehat{P}_{XX^*}[k, f)\right\}$ for this process with (5.23) and with Monte Carlo simulation using $L = 1000$ iterations and $K = 50$ samples for each iteration. From Figure 5.13, we see that the two estimates of the variance are qualitatively alike.

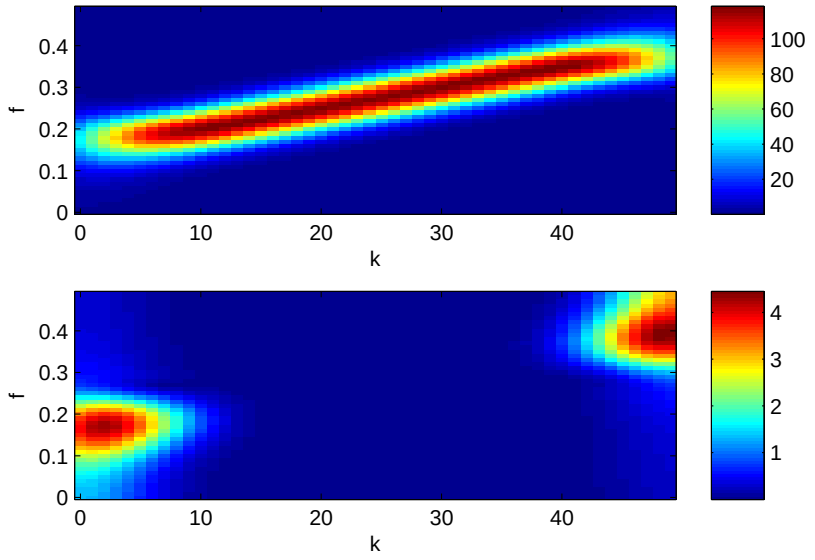

Figure 5.11: Expected value of the estimators of the t-f spectra approximated with Monte Carlo simulation. Top: $\left|\overline{\widehat{P}}_{XX^*}[k,f)\right|$. Bottom: $\left|\overline{\widehat{P}}_{XX}[k,f)\right|$.

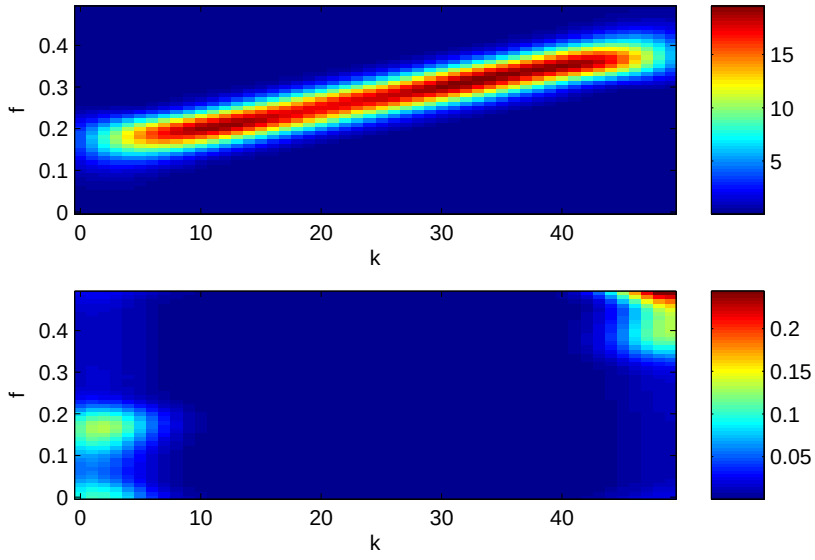

Figure 5.12: Variance of the estimators of the t-f spectra approximated with Monte Carlo simulation. Top: $\overline{\text{Var}}\left\{\widehat{P}_{XX^*}[k,f)\right\}$. Bottom: $\overline{\text{Var}}\left\{\widehat{P}_{XX}[k,f)\right\}$

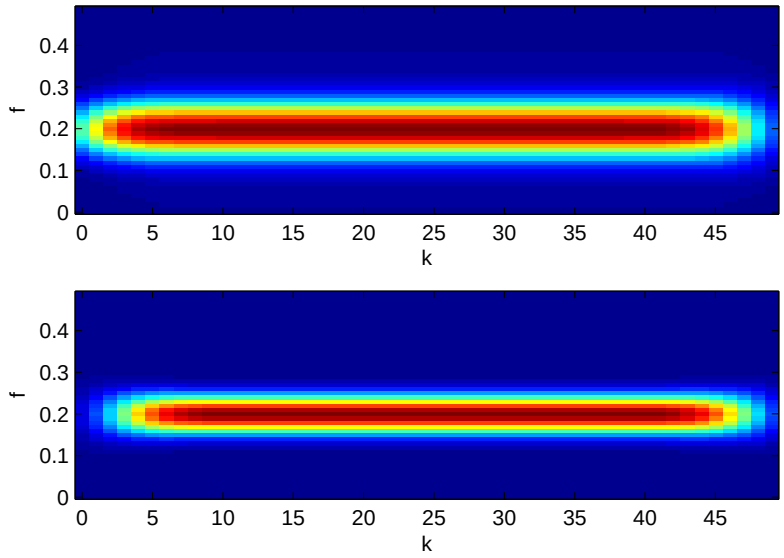

Figure 5.13: Variance for the estimator of the Hermitian t-f spectrum of the process in (5.24). Top: Variance approximated with (5.23). Bottom: Variance estimated with Monte Carlo simulation.

Chapter 6

Numerical examples

We have derived exact theoretical expressions of the Hermitian and the complementary functions of some random processes. In this chapter, we will estimate these functions with the estimators outlined in the previous chapters. We will use the estimation procedure discussed in Section 4.5 for the moment functions and the ambiguity functions. The f-f spectra are estimated by (4.28) and (4.30) and the t-f spectra are estimated by (5.5) and (5.6). For each process, we have chosen the number of samples N_t to average over for the moment functions, the time-bandwidth product KW for the estimate of the f-f spectra, and the kernel in the estimates of the t-f spectra. In the following, $N(t)$ is the analytic process corresponding to a white Gaussian noise process with standard deviation $\sigma_N = 0.05$. Thus, $N(t)$ is proper, and its complementary functions are zero everywhere.

6.1 Single tone process

We start off by looking at the noisy single-tone process

$$X(t) = \exp(j2\pi f_0 t) + N(t). \tag{6.1}$$

This is a cyclostationary process, since the mean-value and the complementary moment function of $X(t)$ is periodic in t, with period $T = 1/f_0$. The Hermitian moment function is independent of t.

Figure 6.1 and Figure 6.2 shows the estimates of the Hermitian and the complementary second-order statistical quantities, respectively. The estimates are based on $K = 100$ samples $x[k]$, $k = 0, \ldots, K-1$, of the process $X(t)$ with $f_0 = 0.1$. Note that we should average over at least one period in the estimates of the moment functions, i.e., $N_t \geq 10$. Here, we have chosen $N_t = 15$, $KW = 5/2$ and the Kaiser-Bessel kernel with $KW_1 = 16$, $KW_2 = 8$ and $KW_3 = 12$.

The moment functions are non-zero only in the area of the k-κ plane where both

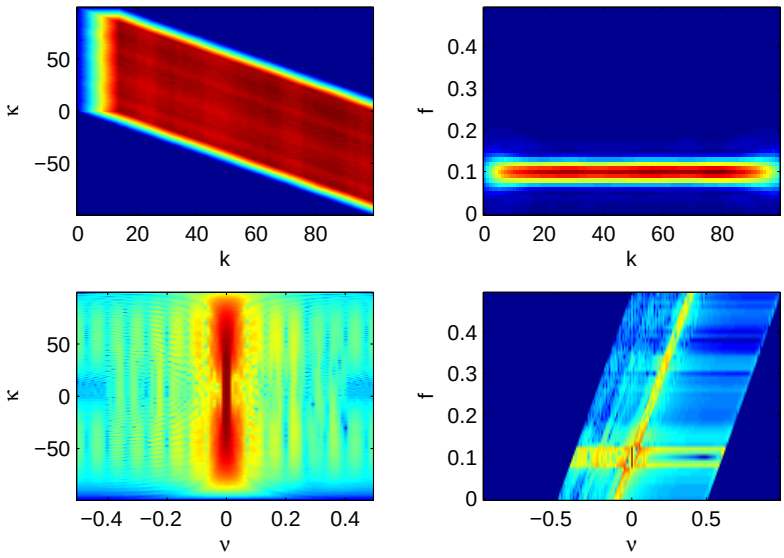

Figure 6.1: Estimates of the Hermitian second-order statistical quantities of the noisy single-tone process. Top left: $|\widehat{M}_{XX^*}[k,\kappa]|$. Top right: $|\widehat{P}_{XX^*}[k,f)|$. Bottom left: $|\widehat{A}_{XX^*}(\nu,\kappa]|$ on a log scale. Bottom right: $|\widehat{S}_{XX^*}(\nu,f)|$ on a log scale.

k and $k+\kappa$ have values between zero and $K-1$. In this area, the magnitude of $\widehat{M}_{XX^*}[k,\kappa]$ is reasonably constant except for on the edges, whereas $\widehat{M}_{XX}[k,\kappa]$ has its largest values on these edges. The single tone is a straight line at $f=f_0$ in the estimate of the Hermitian t-f spectrum. The estimate of the complementary t-f spectrum has its values at frequency f_0 for $k=0$ and $k=K-1$. Since the Hermitian moment function is independent of t, the Hermitian ambiguity function will be concentrated around the stationary manifold. Likewise, the complementary ambiguity function should have its values on $\nu=0$ and $\nu=2f_0$ because of the periodicity of the complementary moment function. Furthermore, $\widehat{S}_{XX^*}(\nu,f)$ has a spike at $(0,f_0)$ and $\widehat{S}_{XX}(\nu,f)$ has a spike at $(2f_0,f_0)$. We see that all the estimates are consistent with the theoretical results.

6.2 Two-tone process

Our next example is the two-tone process in noise,

$$X(t)=\exp(j2\pi f_1 t)+\exp(j2\pi f_2 t)+N(t). \tag{6.2}$$

It is easy to show that the mean value, the Hermitian and the complementary moment function of this process is periodic in t with period $T=1/f_0$, where $f_0=f_2-f_1$. Thus, $X(t)$ is a cyclostationary process. The moment functions are also periodic in τ with the same period.

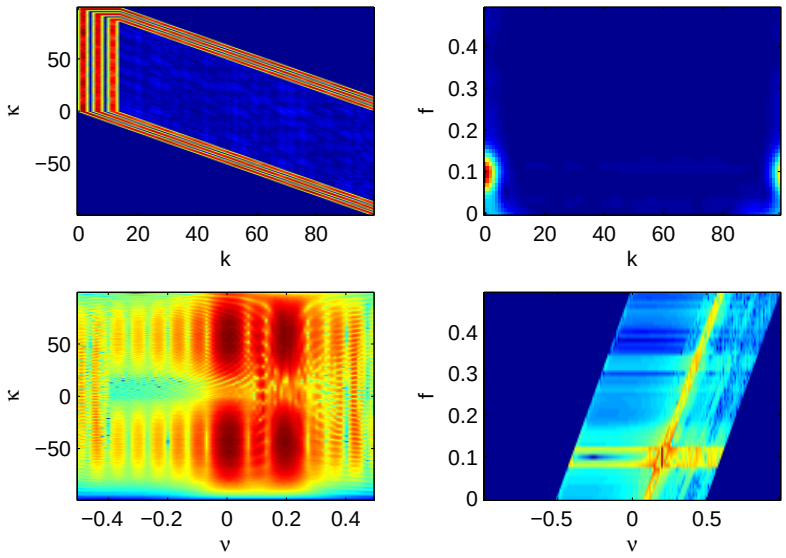

Figure 6.2: Estimates of complementary second-order statistical quantities of the noisy single-tone process. Top left: $|\widehat{M}_{XX}[k,\kappa]|$. Top right: $|\widehat{P}_{XX}[k,f)|$. Bottom left: $|\widehat{A}_{XX}(\nu,\kappa]|$ on a log scale. Bottom right: $|\widehat{S}_{XX}(\nu,f)|$ on a log scale.

The estimates presented in Figure 6.3 and 6.4 are based on $K = 100$ samples $x[k]$, $k = 0,\ldots,K-1$, of the process with $f_1 = 0.1$ and $f_2 = 0.2$. Again, we should average over at least one period T in the estimates of the moment functions. However, for this process we should avoid values of N_t that are multiples of the period, i.e., $N_t \neq nT$, where $n \in \mathbb{N}$. Here, $N_t = 15$, $KW = 5/2$ and the kernel is the Kaiser-Bessel kernel with $KW_1 = 16$, $KW_2 = 8$ and $KW_3 = 12$.

We see an interference pattern in $\widehat{M}_{XX^*}[k,\kappa]$, where the magnitude drops every tenth sample in both directions. Again, $\widehat{M}_{XX^*}[k,\kappa]$ has its smallest values and $\widehat{M}_{XX}[k,\kappa]$ has its highest values on the edges of the area defined by the samples. The estimate of the complementary moment functions also exhibits periodic drops in the magnitude. Because of the periodicity of the Hermitian moment function, the lines of support for the Hermitian ambiguity function and the Hermitian f-f spectrum are $\nu = \pm f_0$ and $\nu = 0$. Likewise, the complementary ambiguity function and the complementary f-f spectrum are non-zero only on $\nu = 2f_1$, $\nu = 2f_2$ and $\nu = f_1 + f_2$. The estimates of the ambiguity functions have their values concentrated on these lines. But $\widehat{A}_{XX}(\nu,\kappa]$ also has values on $\nu = 0$, this is most likely due to a weakness in the estimator. There are four spikes in $\widehat{S}_{XX^*}(\nu,f)$ and four spikes in $\widehat{S}_{XX^*}(\nu,f)$ located where we would expect them. In the estimate of the Hermitian t-f spectrum, the two tones are the two straight

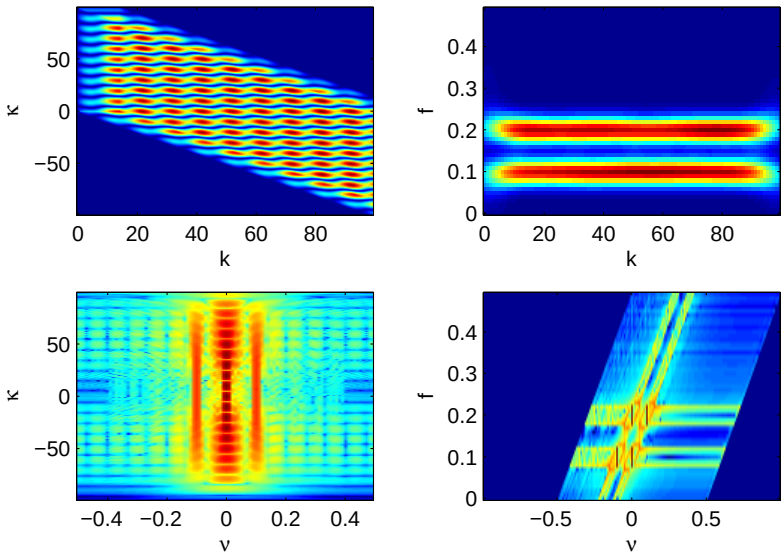

Figure 6.3: Estimates of the Hermitian second-order statistical quantities of the noisy two-tone process. Top left: $|\widehat{M}_{XX^*}[k,\kappa]|$. Top right: $|\widehat{P}_{XX^*}[k,f)|$. Bottom left: $|\widehat{A}_{XX^*}(\nu,\kappa]|$ on a log scale. Bottom right: $|\widehat{S}_{XX^*}(\nu,f)|$ on a log scale.

lines at $f = f_1$ and $f = f_2$, and the complementary t-f spectrum fills in the values missing on the edges.

6.3 Chirp process

We estimate the second-order statistical quantities of the chirp process

$$X(t) = \exp\left[j\pi(2\alpha t + \beta t^2 + \Psi)\right]. \tag{6.3}$$

We generated $K = 100$ samples $x[k]$, $k = 0, \ldots, K-1$, of the process with $\alpha = 0.15$, $\beta = 0.0025$ and Ψ uniformly distributed on $[-1, 1]$. The estimates of the Hermitian quantities are shown in Figure 6.5, and the estimate of the complementary quantities are shown in Figure 6.6. For the estimates, we have used $KW = 5/2$, $N_t = 15$ and the Kaiser-Bessel kernel with $KW_1 = 16$, $KW_2 = 8$ and $KW_3 = 12$.

Here, $\widehat{A}_{XX^*}(\nu,\kappa]$ has values on the stationary manifold and on a line with gradient

$$\frac{\partial \widehat{A}_{XX^*}(\nu,\kappa]}{\partial \nu} = \frac{1}{\beta}. \tag{6.4}$$

We see the chirp as a linear function in the Hermitian t-f spectrum estimate, and $\widehat{P}_{XX}[k,f)$ has its values at the beginning and at the end of this line. The

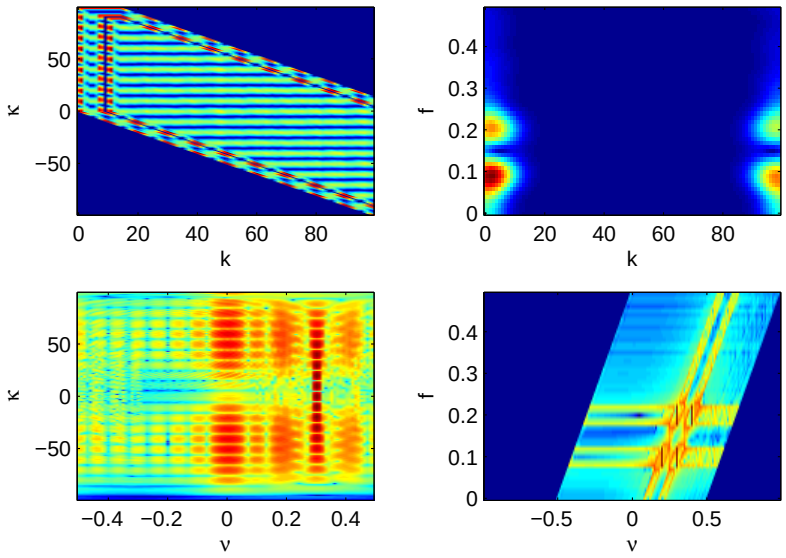

Figure 6.4: Estimates of complementary second-order statistical quantities of the noisy two-tone process. Top left: $|\widehat{M}_{XX}[k,\kappa]|$. Top right: $|\widehat{P}_{XX}[k,f)|$. Bottom left: $|\widehat{A}_{XX}(\nu,\kappa]|$ on a log scale. Bottom right: $|\widehat{S}_{XX}(\nu,f)|$ on a log scale.

estimate of the Hermitian f-f spectrum is concentrated in an area around $\nu = 0$ and the estimate of the Hermitian moment function is concentrated in an area around $\tau = 0$. This suggests that for this process, there is a strong relationship between neighboring samples and between neighboring frequencies. In $\widehat{S}_{XX}(\nu, f)$ the chirp again appears as a linear function starting at frequency $f = \alpha$ and ending at frequency $f = 0.4$, only now as a function of the local frequency variable ν instead of the global time k. For this process, no further insight was gained through the estimates of the complementary moment function and the complementary ambiguity function.

6.4 Sinusoidal frequency modulation

We now consider the sinusoidal FM process

$$X(t) = \exp\left\{j2\pi\left[f_c t + \sin\left(2\pi f_m t\right)\right]\right\} + N(t), \tag{6.5}$$

where f_c is the carrier frequency, and f_m is the modulation frequency. We use the code from [Auger et al., 1996] to generate $K = 250$ samples $x[k]$, $k = 0, \ldots, K-1$ of a sinusoidal FM with $f_c = 0.3$ and a modulation sinusoid with period $K/2$, minimum frequency 0.1 and maximum frequency 0.4. For this process, which is a single-component process, the kernel from Section 5.2.1 gave the best localization in the estimates of the t-f spectra. The parameters for the other estimators are

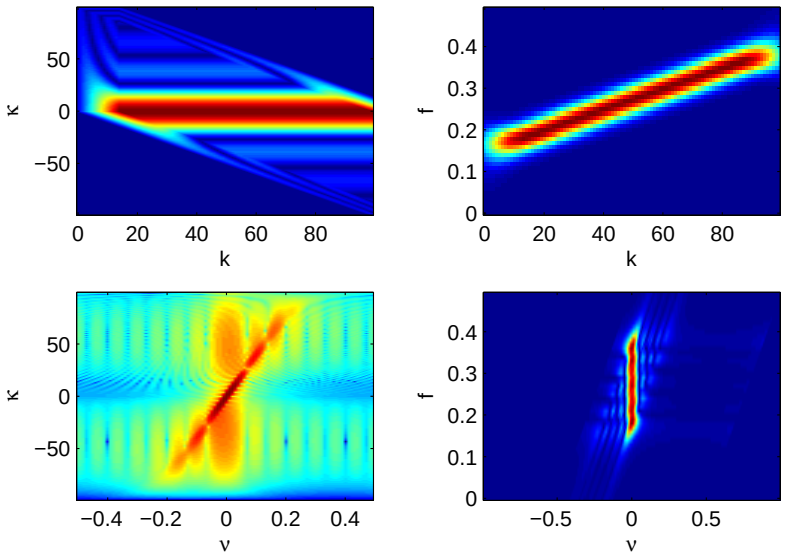

Figure 6.5: Estimates of the Hermitian second-order statistical quantities of the chirp process. Top left: $|\widehat{M}_{XX^*}[k,\kappa]|$. Top right: $|\widehat{P}_{XX^*}[k,f)|$. Bottom left: $|\widehat{A}_{XX^*}(\nu,\kappa]|$ on a log scale. Bottom right: $|\widehat{S}_{XX^*}(\nu,f)|$.

$KW = 5/2$ and $N_t = 30$. Figure 6.7 shows the estimates of the Hermitian functions of $X(t)$ and Figure 6.8 shows the estimates of the complementary functions of $X(t)$.

The estimate of the Hermitian moment function shows us that two samples that are $K/2 = 125$ samples apart have a strong correlation, since the sinusoidal FM has a period of 125 samples. The diagonal lines connecting the strongest values in $\widehat{M}_{XX^*}[k,\kappa]$ displays the correlation between samples where the modulation sinusoid has different orientation. We see two periods of a sinusoid with maximum frequency 0.4 and minimum frequency 0.1 in the estimate of the Hermitian t-f spectrum, and the estimate of the complementary t-f spectrum has its largest values at the edges. Note that the position in k for $\kappa = 0$ of the circles in $\widehat{M}_{XX}[k,\kappa]$ corresponds to the position of the maxima and the minima of the modulation sinusoid in $\widehat{P}_{XX}[k,f)$. In $\widehat{A}_{XX^*}(\nu,\kappa]$, we see two sinusoids as a function of κ. These sinusoids have the same period as the modulation sinusoid and an amplitude equal to the difference between the maximum and the minimum frequency of the modulation sinusoid. The two sinusoids oscillate around the line $\nu = 0$. The estimate of the complementary ambiguity function also has these two sinusoids, but here they oscillate around $\nu = 0.5$, which is the sum of the minimum and the maximum frequency of the modulation sinusoid. But half of the sinusoids have been folded back to oscillate around $\nu = -0.5$ due to aliasing. The estimates of the f-f spectra have their values in the frequency range we expect, and they have

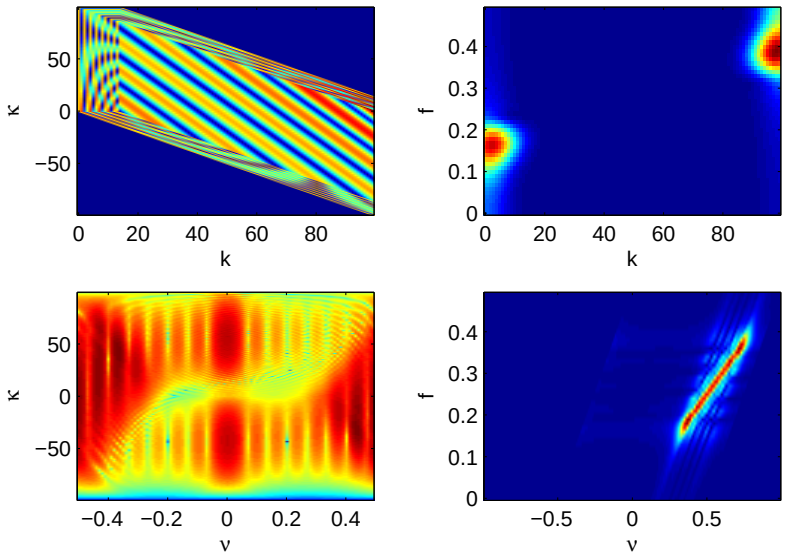

Figure 6.6: Estimates of complementary second-order statistical quantities of the chirp process. Top left: $|\widehat{M}_{XX}[k,\kappa]|$. Top right: $|\widehat{P}_{XX}[k,f)|$. Bottom left: $|\widehat{A}_{XX}(\nu,\kappa]|$ on a log scale. Bottom right: $|\widehat{S}_{XX}(\nu,f)|$.

their maximal values at $f = 0.1$ and $f = 0.4$. But for this process, it is hard to characterize the process from its f-f spectra.

6.5 Fractional Brownian motion

Fractional Brownian motion (FBM) provides a useful model for processes with long-term dependence. The FBM process is a real-valued, nonstationary, harmonizable process. An FBM process $X(t)$ is commonly defined as [Mandelbrot and Van Ness, 1968]

$$\begin{aligned} X(t) - X(0) = &\frac{1}{\Gamma(H+1/2)}\left[\int_{-\infty}^{0}\left((t-s)^{H-1/2} - (-s)^{H-1/2}\right)dY(s)\right. \\ &\left. + \int_{0}^{t}(t-s)^{H-1/2}dY(s)\right]. \end{aligned} \tag{6.6}$$

Here, $Y(t)$ is standard Brownian motion, $dY(t)$ is a differential increment of $Y(t)$ and $H \in (0,1)$ is the Hurst parameter. When $H = 1/2$, $X(t)$ is a standard Brownian motion process. It can be shown that for $H \in (0,1/2)$, $X(t)$ will fluctuate more than $Y(t)$ and for $H \in (1/2,1)$, $X(t)$ will be smoother than $Y(t)$.

The f-f spectrum and the t-f spectrum of an FBM process was found in [Øigård,

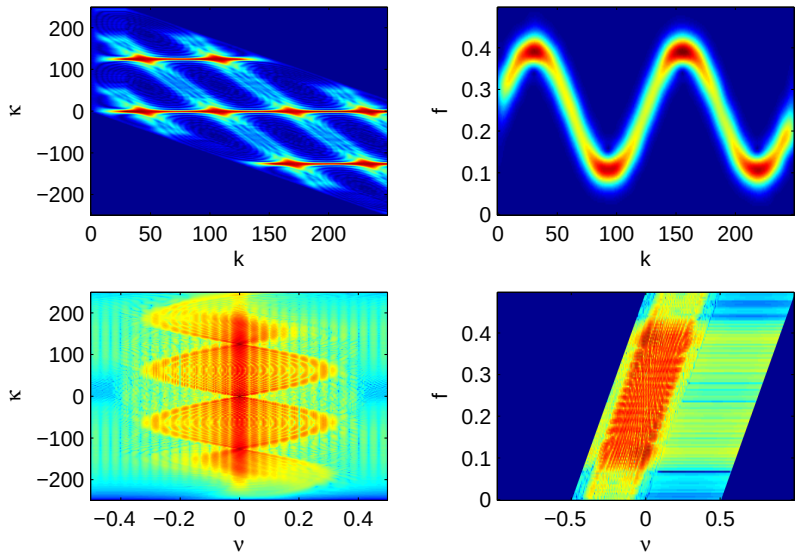

Figure 6.7: Estimates of the Hermitian second-order statistical quantities of a noisy sinusoidal FM process. Top left: $|\widehat{M}_{XX^*}[k,\kappa]|$. Top right: $|\widehat{P}_{XX^*}[k,f)|$. Bottom left: $|\widehat{A}_{XX^*}(\nu,\kappa]|$ on a log scale. Bottom right: $|\widehat{S}_{XX^*}(\nu,f)|$ on a log scale.

2004] to be

$$\begin{aligned} S_{XX^*}(\nu,f) =& (2\pi)^{(2-2H)}\big[|f-\nu|^{-(2H+1)}\delta(\nu) - |\nu|^{-(2H+1)}\delta(f-\nu) \\ & - |f-\nu|^{-(H+1/2)}\delta(f)|\nu|^{-(H+1/2)}\big] \end{aligned} \tag{6.7}$$

and

$$\begin{aligned} P_{XX^*}(t,f) =& \frac{2\pi\Gamma(1-2H)\cos(\pi H)}{H}|t|^{2H}\delta(f) \\ & - 2(2\pi)^{-2H} j\sin(\pi f t)e^{j\pi f t}|f|^{-(2H+1)}, \end{aligned} \tag{6.8}$$

respectively. We see that the f-f spectrum has its values on the three discrete lines of support $f=0$, $\nu=0$ and $f=\nu$. Note also that the t-f spectrum has a delta function $\delta(f)$ in the first term. We will only consider the f-f spectrum and the t-f spectrum of this process.

We generated $K=250$ samples of FBM processes with different values of H using the code from [Lowen, 2000]. Figure 6.9 shows the samples of the FBM processes with $H=0.1$, $H=0.5$ and $H=0.8$. Figures 6.10–6.12 show a section of the estimates of the f-f spectra with $KW=5$ for the three FBM process. The estimates are concentrated on the lines $f=0$ and $\nu=f$, as expected. The line $\nu=0$ is also present in the estimates, but it is difficult to see since it is only

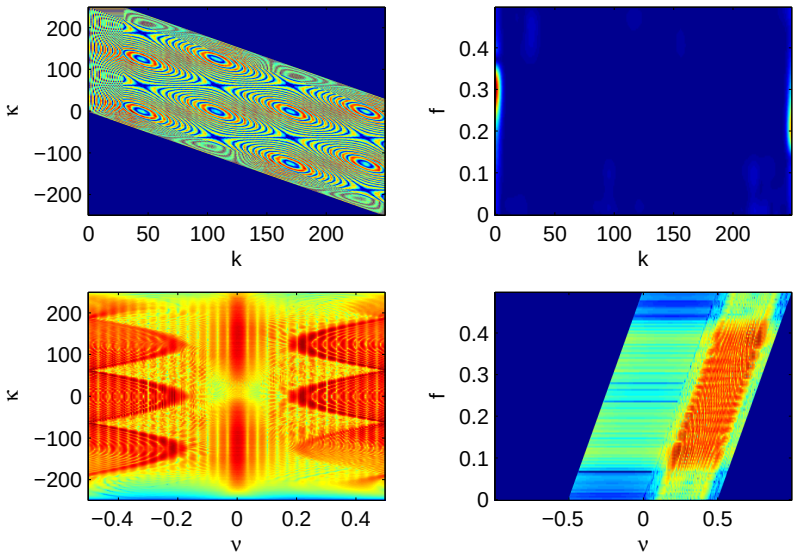

Figure 6.8: Estimates of complementary second-order statistical quantities of a noisy sinusoidal FM process. Top left: $|\widehat{M}_{XX}[k,\kappa]|$. Top right: $|\widehat{P}_{XX}[k,f)|$. Bottom left: $|\widehat{A}_{XX}(\nu,\kappa]|$ on a log scale. Bottom right: $|\widehat{S}_{XX}(\nu,f)|$ on a log scale.

one pixel wide. Note that as H increases, $\widehat{S}_{XX^*}(\nu,f)$ becomes more concentrated around the point $f=0$, $\nu=0$, which follows from (6.7).

Since an FBM process is real-valued, the t-f spectrum will have the symmetry $P_{XX^*}(t,f)=P^*_{XX^*}(t,-f)$, so we only consider the t-f spectrum for positive frequencies. The estimate of the t-f spectrum of the FBM processes with $H=0.1$, $H=0.5$ and $H=0.8$ are shown in Figures 6.13–6.15. The Kaiser-Bessel kernel with $KW_1=16$, $KW_2=8$ and $KW_3=12$ was used in the estimates. Here, the t-f spectrum has its largest values at $f=0$ for all three values of H. Due to the second term in (6.8), the value of H will control how fast the Hermitian t-f spectrum decays as f increases. This is reflected in our estimates.

6.6 Earthquake data

We will analyze a real world time series. The time series in Figure 6.16 contains the number of earthquakes of magnitude larger than 7.0 on the Richter's scale for each year from year 1900 to year 2003 inclusive. The data can be downloaded from the Earthquake Data Base System of the U.S. Geological Survey at *http://neic.usgs.gov/neis/eqlists/7up.html*.

The f-f spectrum of the time series is estimated using a time-bandwidth product

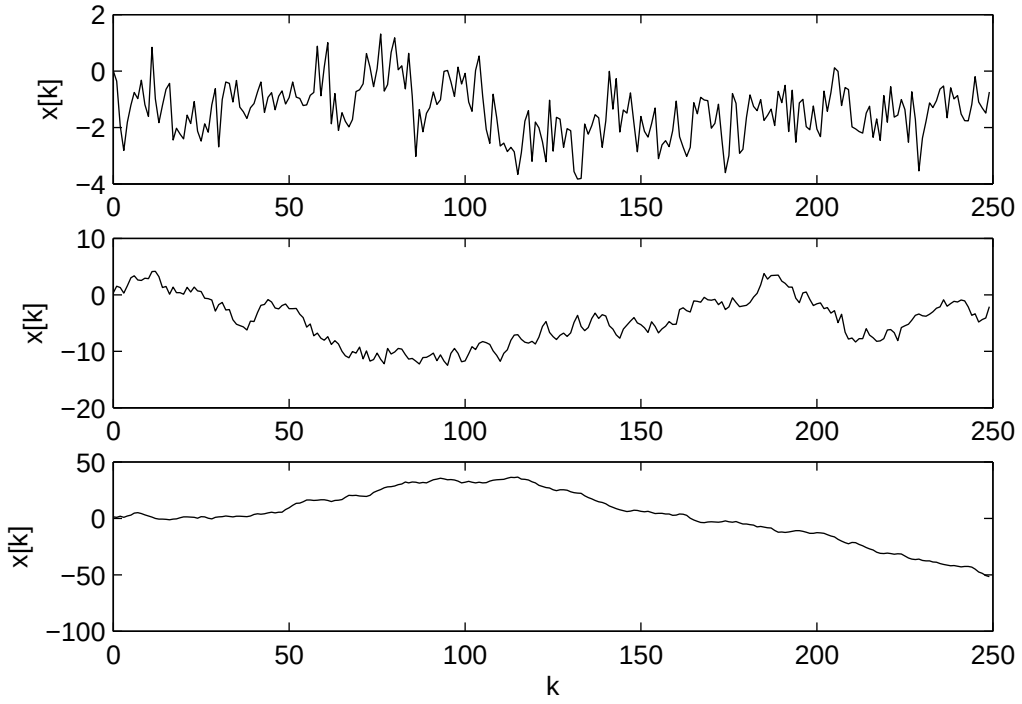

Figure 6.9: Samples of FBM processes with different values of H. Top: $H = 0.1$. Middle: $H = 0.5$. Bottom: $H = 0.8$.

$KW = 5/2$. From Figure 6.17 we see that the estimate of the f-f spectrum of the data has the same structure as the estimated f-f spectrum for the FBM processes. This time series was also analyzed in [Øigård, 2004], where the Hurst parameter was estimated based on $\widehat{S}_{XX^*}(\nu, f)$ to be $\widehat{H} = 0.29$. We use an average of $N_t = 10$ samples to estimate the moment function and the ambiguity function of the time series. These estimates are displayed in Figure 6.18, where $k = 0$ denotes the year 1900, $k = 1$ the year 1901 and so on. Here, $|\widehat{A}_{XX^*}(\nu, \kappa]|$ has its largest values on the stationary manifold $\nu = 0$. The estimate of the moment function has large values around the years 1913, 1949 and 1975. Figure 6.19 shows the estimates of the t-f spectrum for the time series using the Kaiser-Bessel kernel with $KW_1 = 16$, $KW_2 = 8$ and $KW_3 = 12$. The estimate has the same structure as the estimates of the t-f spectra for the FBM processes.

The f-f spectrum and the t-f spectrum of the earthquake data have the same structure as the spectra of an FBM process. The earthquake data cannot be a realization of an FBM process, since the earthquake data do not attain negative values. Even so, there seems to be some sort of connection between the time series and FBM due to their similarities in terms of spectral correlations.

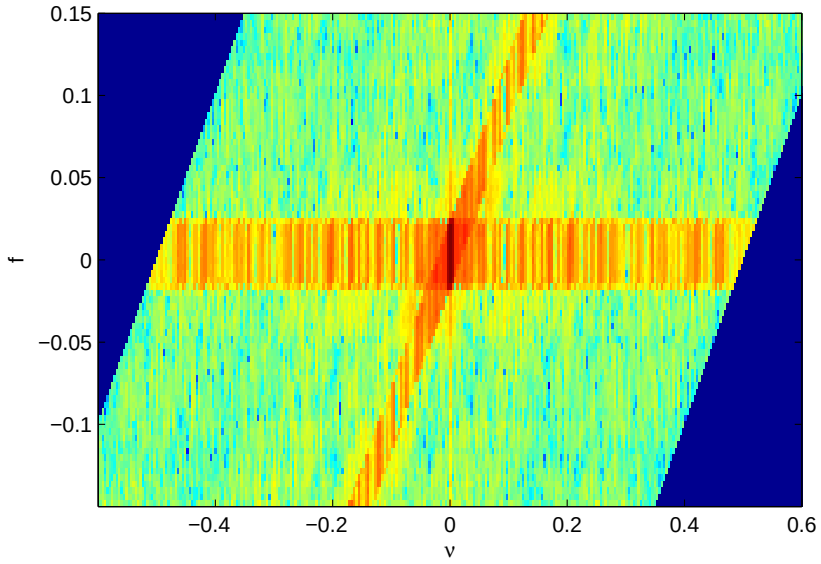

Figure 6.10: The estimate $|\widehat{S}_{XX^*}(\nu, f)|$ on a log scale for an FBM process $X(t)$ with $H = 0.1$.

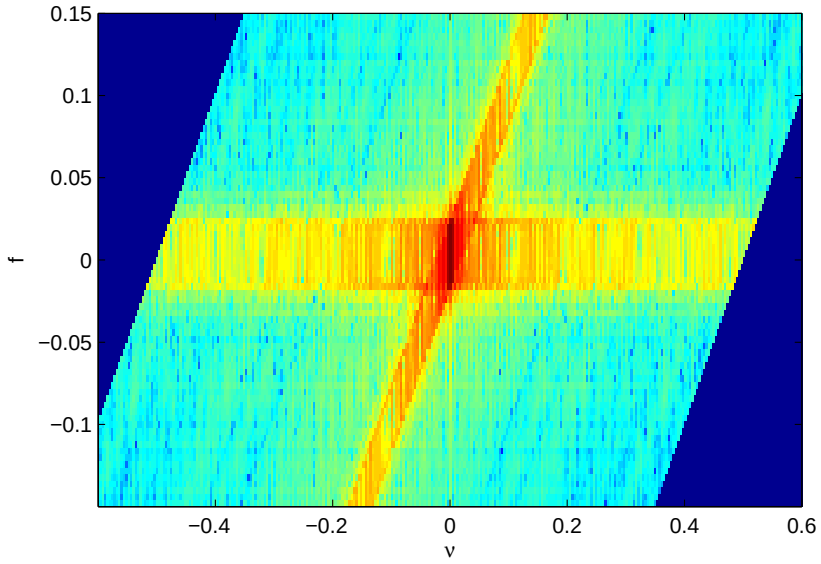

Figure 6.11: The estimate $|\widehat{S}_{XX^*}(\nu, f)|$ on a log scale for an FBM process $X(t)$ with $H = 0.5$.

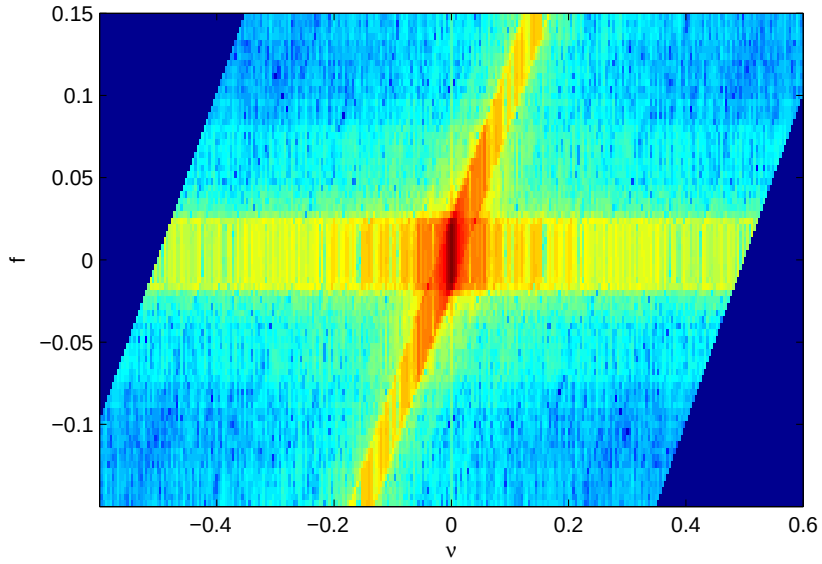

Figure 6.12: The estimate $|\widehat{S}_{XX^*}(\nu, f)|$ on a log scale for an FBM process $X(t)$ with $H = 0.8$.

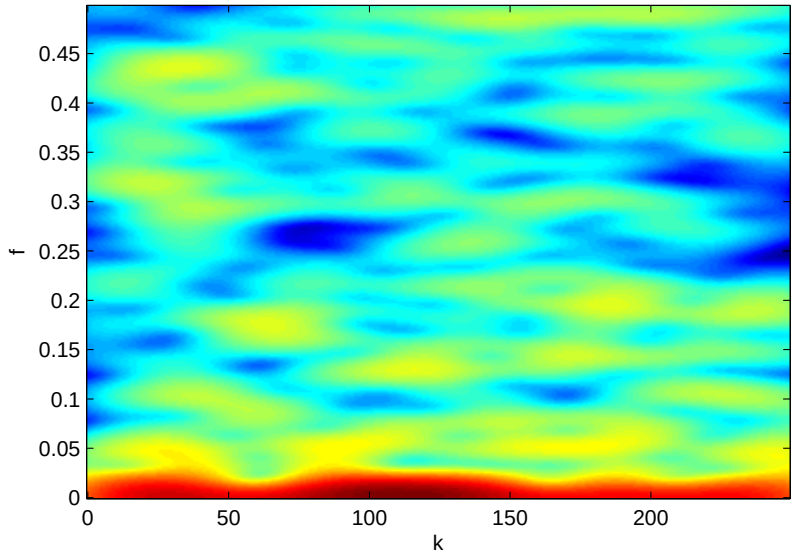

Figure 6.13: The estimate $|\widehat{P}_{XX^*}[k, f)|$ on a log scale for an FBM process with $H = 0.1$.

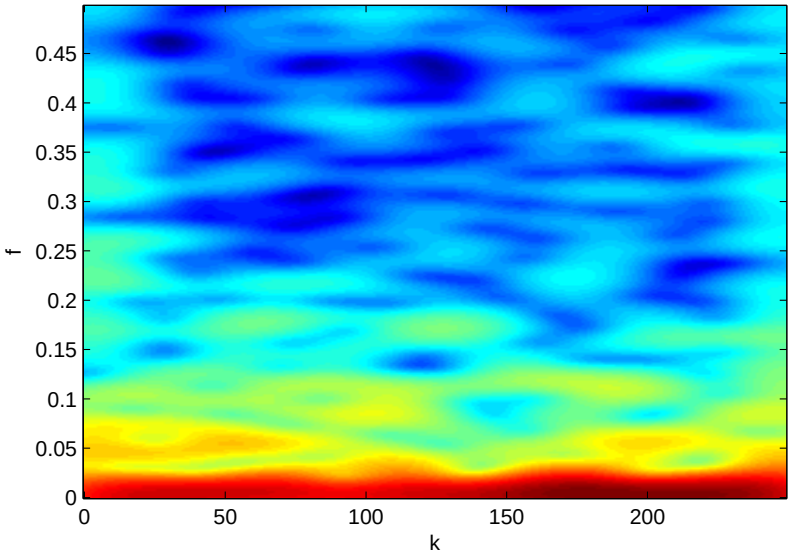

Figure 6.14: The estimate $|\widehat{P}_{XX^*}[k,f)|$ on a log scale for an FBM process with $H = 0.5$.

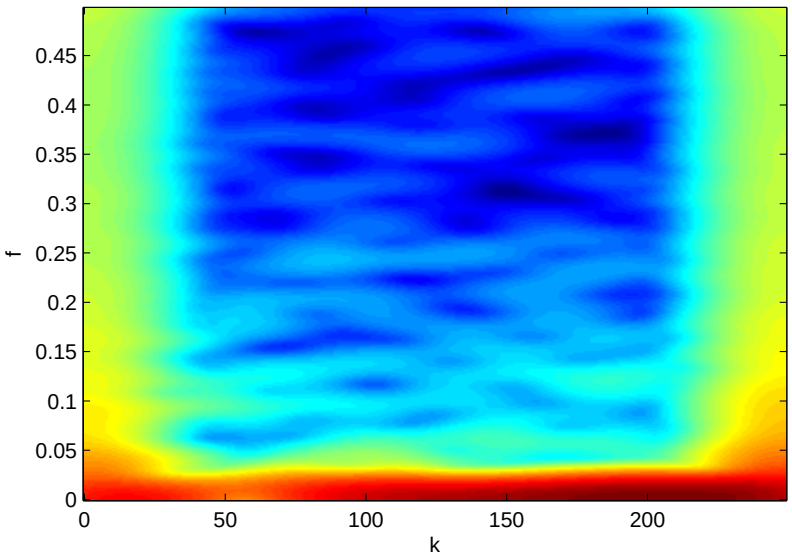

Figure 6.15: The estimate $|\widehat{P}_{XX^*}[k,f)|$ on a log scale for an FBM process with $H = 0.8$.

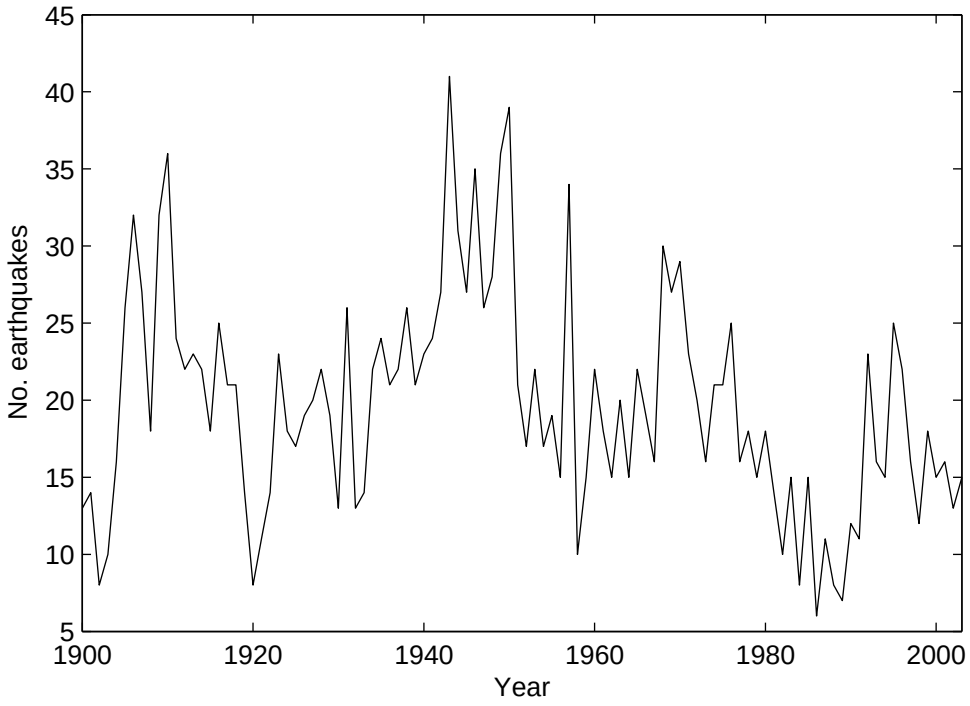

Figure 6.16: Number of earthquakes of magnitude larger than 7.0 on the Richter's scale per year.

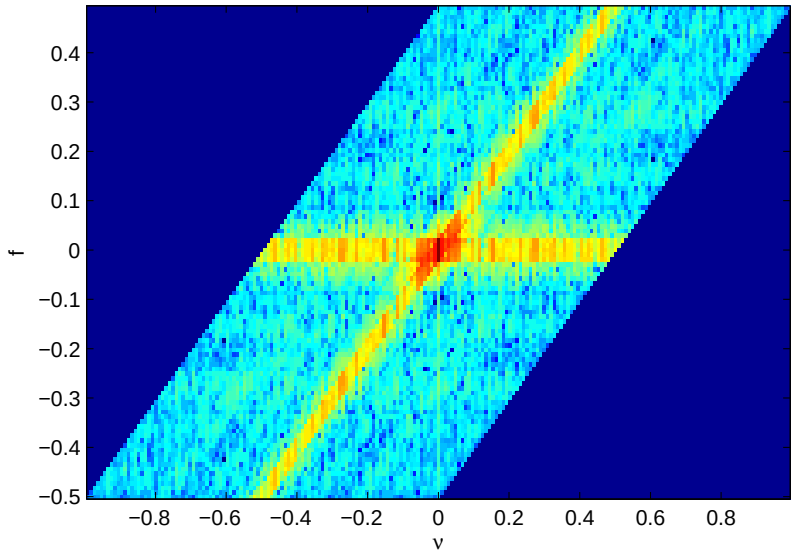

Figure 6.17: The estimate $|\widehat{S}_{XX^*}(\nu, f)|$ on a log scale for the earthquake data.

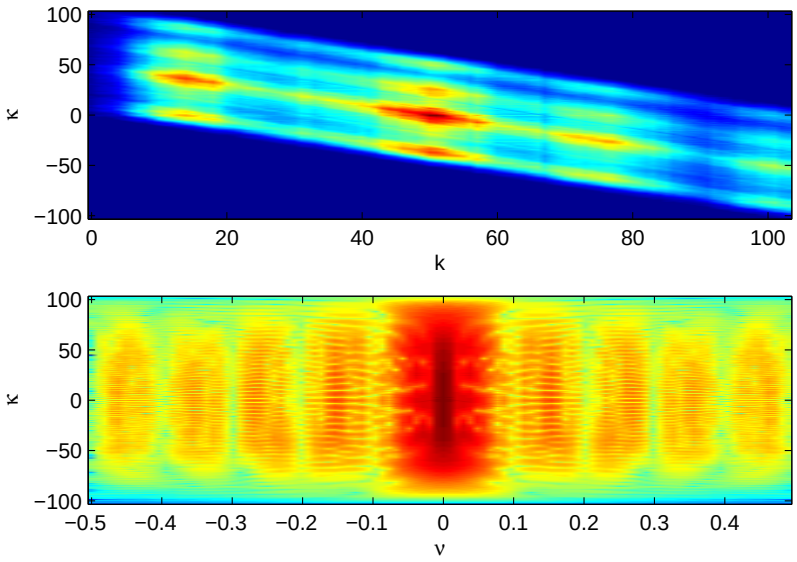

Figure 6.18: Estimates of the moment function and the ambiguity function of the earthquake data. Top: $\widehat{M}_{XX^*}[k, \kappa]$. Bottom: $|\widehat{A}_{XX^*}(\nu, \kappa]|$ on a log scale.

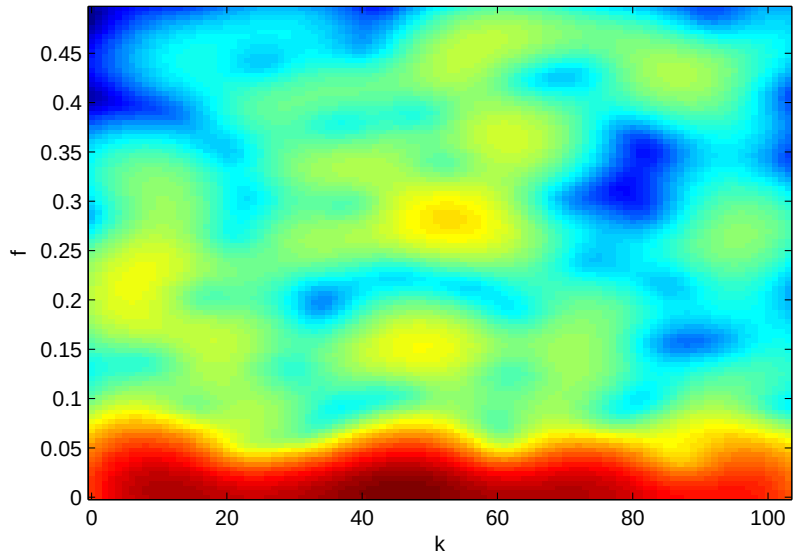

Figure 6.19: The estimate $|\widehat{P}_{XX^*}[k, f)|$ on a log scale for the earthquake data.

Chapter 7

Coherences

The increment process $dZ(f)$ of a harmonizable process $X(t)$ has non-orthogonal increments. Thus, we want to quantify the correlation between the increment process at different frequencies. The frequency content of harmonizable processes changes with time, such that the correlation between the process and its increment process is also of interest. To obtain objective measures of these correlations, we introduce the concept of coherence. A measure of coherence of the process should be restricted to values between zero and one.

7.1 Mean square estimation

We are interested in estimating the value of a complex random variable Z in terms of the observation of another complex random variable W.

In linear mean square estimation (LMSE), Z is estimated as a linear function of W. We choose the constant α such that the estimate $\widehat{Z} = \alpha W$ minimizes the mean square error $\mathbb{E}\left[|Z - \widehat{Z}|^2\right]$ [Picinbono, 1993]. By taking the derivative of the mean square error with respect to α, setting the result to zero and solving for α, we find

$$\alpha = \frac{\mathbb{E}[ZW^*]}{\mathbb{E}[|W|^2]}. \tag{7.1}$$

This minimal mean square error will be

$$\begin{aligned} \epsilon_{_L}^2 &= \mathbb{E}\left[|Z|^2\right] - \mathbb{E}\left[|\widehat{Z}|^2\right] \\ &= \mathbb{E}\left[|Z|^2\right]\left(1 - |\rho_{_L}|^2\right), \end{aligned} \tag{7.2}$$

where

$$|\rho_{_L}|^2 = \frac{|\mathbb{E}[ZW^*]|^2}{\mathbb{E}[|Z|^2]\,\mathbb{E}[|W|^2]}. \tag{7.3}$$

Note that this solution for α leads to $\mathbb{E}\left[(Z - \widehat{Z})W^*\right] = 0$. This is the orthogo-

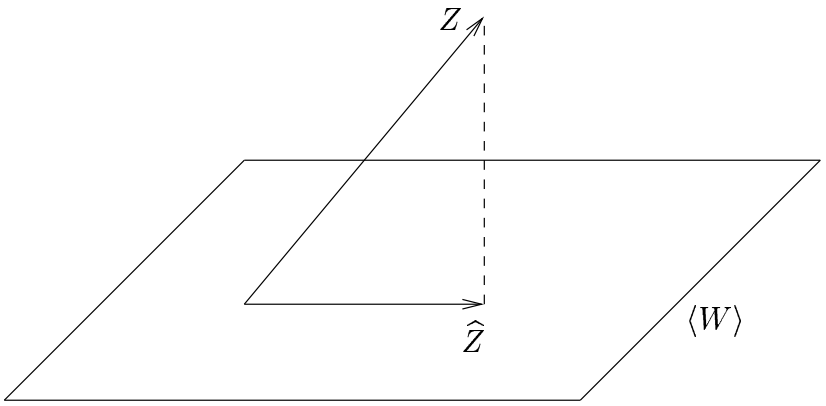

Figure 7.1: The projection of Z onto the vector space spanned by W.

nality condition [Picinbono, 1993], which states that the mean square error of the best linear estimate of Z is orthogonal to the observation of W. We can think of $\widehat{Z}$ as the projection of Z onto the vector space spanned by W, as illustrated in Figure 7.1. The correlation coefficient will then be the magnitude squared cosine of the angle associated with the Hilbert space inner product $\langle Z, W \rangle$ [Picinbono, 1993].

The mean square error ϵ_L^2 is a measure of how close our estimated value $\widehat{Z}$ will be to the actual value of Z. A small mean square error suggests that Z is estimable by W as a linear function, i.e., that there is a linear relationship between the two random variables. Likewise, a large mean square error implies that our estimate is poor. Obviously, the mean square error is non-negative, but it is upper bounded by $\mathbb{E}[|Z|^2]$. However, by using Schwartz' inequality it is easy to show that $0 \leq |\rho_L|^2 \leq 1$. The quantity $|\rho_L|^2$ is often called the correlation coefficient. We compare the mean square errors of estimating Z from the observation of two different random variables W_1 and W_2. Any difference in the two mean square errors is due to the term $|\rho_L|^2$, since $\mathbb{E}[|Z|^2]$ is constant. Lets say that the mean square error of estimating Z from W_1 is smaller than the mean square error of estimating Z from W_2. The correlation coefficient of W_1 will then be larger than the correlation coefficient of W_2. Thus, the larger the correlation coefficient, the better we can estimate Z from W.

For complex random variables, we should not limit ourselves to estimate Z as a linear function of W. In widely linear mean square estimation (WLMSE) we estimate Z as a widely linear function of the observation of W and its complex conjugate W^* [Picinbono and Chevalier, 1995]. As in LMSE, we choose the con-

stants α, β such that the estimate $\widehat{Z} = \alpha W + \beta W^*$ minimizes the mean square error $\mathbb{E}\left[|Z - \widehat{Z}|^2\right]$. By taking the partial derivative of the mean square error with respect to α and β, setting the result to zero and solving for α and β, we find

$$\alpha = \frac{\mathbb{E}[ZW^*]\,\mathbb{E}[|W|^2] - \mathbb{E}[WZ]\,(\mathbb{E}[W^2])^*}{(\mathbb{E}[|W|^2])^2 - |\mathbb{E}[W^2]|^2} \tag{7.4}$$

and

$$\beta = \frac{\mathbb{E}[ZW]\,\mathbb{E}[|W|^2] - \mathbb{E}[ZW^*]\,\mathbb{E}[W^2]}{(\mathbb{E}[|W|^2])^2 - |\mathbb{E}[W^2]|^2}. \tag{7.5}$$

The minimal mean square error is then

$$\begin{aligned} \epsilon_{WL}^2 &= \mathbb{E}\left[|Z|^2\right] - \mathbb{E}\left[|\widehat{Z}|^2\right] \\ &= \mathbb{E}\left[|Z|^2\right]\left(1 - |\rho_{WL}|^2\right). \end{aligned} \tag{7.6}$$

Here,

$$|\rho_{WL}|^2 = \frac{\xi}{\eta}, \tag{7.7}$$

with

$$\begin{aligned} \xi = &\left(|\mathbb{E}[WZ^*]|^2 + |\mathbb{E}[WZ]|^2\right)\mathbb{E}\left[|W|^2\right] \\ &- 2\Re\left\{\left(\mathbb{E}\left[W^2\right]\right)^*\mathbb{E}[WZ^*]\,\mathbb{E}[WZ]\right\} \end{aligned} \tag{7.8}$$

and

$$\eta = \mathbb{E}\left[|Z|^2\right]\left(\left(\mathbb{E}\left[|W|^2\right]\right)^2 - \left|\mathbb{E}\left[W^2\right]\right|^2\right). \tag{7.9}$$

This solution for α and β leads to the orthogonality principle of WLMSE where now $\mathbb{E}\left[(Z - \widehat{Z})W^*\right] = 0$ and $\mathbb{E}\left[(Z - \widehat{Z})W\right] = 0$. Thus, the mean square error of the best widely linear estimate of Z is orthogonal to both the observation W and its complex conjugate W^* [Picinbono and Chevalier, 1995]. Again, we can think of $\widehat{Z}$ as the projection of Z onto the vector space spanned by W and W^*.

To compare the mean square error associated with LMSE and the mean square error associated with WLMSE, we define the quantity

$$\begin{aligned} \Delta\epsilon^2 &= \epsilon_L^2 - \epsilon_{WL}^2 \\ &= \frac{\left|\mathbb{E}[WZ]\,\mathbb{E}[|W|^2] - \mathbb{E}[W^2]\,\mathbb{E}[W^*Z]\right|^2}{\mathbb{E}[|Z|^2]\left((\mathbb{E}[|W|^2])^2 - |\mathbb{E}[W^2]|^2\right)}. \end{aligned} \tag{7.10}$$

Obviously, the numerator of $\Delta\epsilon^2$ is non-negative. By Schwartz' inequality, the denominator of $\Delta\epsilon^2$ will also be non-negative, such that $\epsilon_L^2 \geq \epsilon_{WL}^2$. Since ϵ_{WL}^2 and $\Delta\epsilon^2$ is non-negative, we have $0 \leq |\rho_{WL}|^2 \leq 1$. As for LMSE, the quantity $|\rho_{WL}|^2$ will have values close to one if $\widehat{Z}$ is a good estimate of Z, i.e., Z is estimable as a widely linear function of W.

7.2 Dual-frequency coherence

We want a useful measure of the dual-frequency coherence of a harmonizable process $X(t)$, i.e., we want to quantify the correlation between $dZ(f)$ and $dZ(f-\nu)$. If $dZ(f)$ and $dZ(f-\nu)$ are correlated, $dZ(f-\nu)$ should be linearly estimable from $dZ(f)$. We argued that in using LMSE, the quantity $|\rho_{_L}|^2$ will have values close to one if the two variables are linearly estimable from each other and values close to zero if they are not. If we estimate $Z = dZ(f-\nu)$ from $W = dZ(f)$, we have

$$\begin{aligned} |\rho_{_{X,L}}(\nu,f)|^2 &= \frac{|\mathbb{E}[dZ(f)dZ^*(f-\nu)]\,|^2}{\mathbb{E}[|dZ(f)|^2]\;\mathbb{E}[|dZ(f-\nu)|^2]} \\ &= \frac{|S_{XX^*}(\nu,f)|^2}{S_{XX^*}(0,f)\,S_{XX^*}(0,f-v)}. \end{aligned} \tag{7.11}$$

The quantity $|\rho_{_{X,L}}(\nu,f)|^2$ is the magnitude squared cosine of the angle associated with the Hilbert space inner product $\langle dZ(f), dZ(f-\nu)\rangle$, which is the Hermitian f-f spectrum of a harmonizable process. Thus, we use $|\rho_{_{X,L}}(\nu,f)|^2$ as a measure of the dual-frequency coherence of a harmonizable process [Hanssen and Scharf, 2003].

Since the increment process of a harmonizable process is complex-valued, we can estimate $dZ(f-\nu)$ as a widely linear function of $dZ(f)$. The correlation coefficient associated with WLMSE will have high values if $dZ(f-\nu)$ is widely linear estimable from $dZ(f)$. Likewise, the correlation coefficient will have values close to zero if we are not able to estimate $dZ(f-\nu)$ as a widely linear function of $dZ(f)$. By using WLMSE to estimate $Z = dZ(f-\nu)$ from $W = dZ(f)$, we obtain the correlation coefficient

$$|\rho_{_{X,WL}}(\nu,f)|^2 = \frac{\xi(\nu,f)}{\eta(\nu,f)}, \tag{7.12}$$

where

$$\begin{aligned} \xi(\nu,f) = &\left(|S_{XX^*}(\nu,f)|^2 + |S_{XX}(2f-\nu,f)|^2\right) S_{XX^*}(0,f) \\ &- 2\Re\left\{S^*_{XX}(2f,f)S_{XX}(2f-\nu,f)S_{XX^*}(\nu,f)\right\} \end{aligned} \tag{7.13}$$

and

$$\eta(\nu,f) = S_{XX^*}(0,f-\nu)\left[|S_{XX^*}(0,f)|^2 - |S_{XX}(2f,f)|^2\right]. \tag{7.14}$$

We propose the quantity $|\rho_{_{X,WL}}(\nu,f)|^2$ as an alternative measure of the dual-frequency coherence of a harmonizable process. For complex-valued processes,

the measure in (7.12) has the obvious advantage that it utilizes both the Hermitian and the complementary f-f spectrum. If the complex-valued process $X(t)$ is proper, $S_{XX}(\nu, f)$ is zero everywhere and $|\rho_{X,WL}(\nu, f)|^2$ reduces to $|\rho_{X,L}(\nu, f)|^2$. A real-valued process cannot be proper, and the Hermitian and complementary quantities of real-valued processes are equal. The quantity $|\rho_{X,WL}(\nu, f)|^2$ is an alternative measure of coherence for both real-valued harmonizable processes and improper, complex-valued harmonizable processes. However, for real-valued process we have to take into account that both $\xi(\nu, f)$ and $\eta(\nu, f)$ will be zero for $f = 0$.

7.3 Time-frequency coherence

The time-frequency coherence of a harmonizable process $X(t)$ measures the coherence between the process $X(t)$ and the modulated increment process $dZ(f)e^{j2\pi ft}$. Time-frequency coherence can be seen as an estimation problem, where we measure the degree that we are able to estimate the process $Z = X(t)$ from the modulated increment process $W = dZ(f)e^{j2\pi ft}$. Using LMSE we define

$$\begin{aligned} |\gamma_{X,L}(t, f)|^2 &= \frac{\left|\mathbb{E}\left[X^*(t)dZ(f)e^{j2\pi ft}\right]\right|^2}{\mathbb{E}[|X(t)|^2]\,\mathbb{E}[|dZ(f)|^2]} \\ &= \frac{|P_{XX^*}(t, f)|^2}{M_{XX^*}(t, 0)S_{XX^*}(0, f)}. \end{aligned} \tag{7.15}$$

Again, $|\gamma_{X,L}(t, f)|^2$ is the magnitude squared cosine of the angle associated with the Hilbert space inner product $\left\langle dZ(f)e^{j2\pi ft}, X(t)\right\rangle$, which is the Hermitian t-f spectrum of a harmonizable process. We use the quantity $|\gamma_{X,L}(t, f)|^2$ as a measure of the time-frequency coherence of harmonizable processes [Hanssen and Scharf, 2003].

We can also estimate the process $X(t)$ as a widely linear function of the modulated increment process. The corresponding correlation coefficient will measure how good this estimate will be, with values close to one if the estimate is good and values close to zero if the estimate is poor. If we use WLMSE to estimate $Z = X(t)$ from $W = dZ(f)e^{j2\pi ft}$, we get the correlation coefficient

$$|\gamma_{X,WL}(t, f)|^2 = \frac{\xi(t, f)}{\eta(t, f)}, \tag{7.16}$$

where

$$\begin{aligned} \xi(t, f) = &\left(|P_{XX^*}(t, f)|^2 + |P_{XX}(t, f)|^2\right) S_{XX^*}(0, f) \\ &- 2\Re\left\{e^{-j4\pi ft} S^*_{XX}(2f, f)P_{XX}(t, f)P_{XX^*}(t, f)\right\} \end{aligned} \tag{7.17}$$

and

$$\eta(t,f) = M_{XX^*}(t,0)\left[|S_{XX^*}(0,f)|^2 - |S_{XX}(2f,f)|^2\right]. \tag{7.18}$$

We propose the quantity $|\gamma_{X,W_L}(t,f)|^2$ as an alternative measure of the time-frequency coherence of a harmonizable process. This quantity is a function of both the Hermitian and the complementary functions of the process. If the complex-valued process $X(t)$ is proper, the complementary functions will be zero everywhere and $|\gamma_{X,W_L}(t,f)|^2$ reduces to $|\gamma_{X,L}(t,f)|^2$. The time-frequency coherence measure in (7.16) is also valid for real-valued processes, since $dZ(f)e^{j2\pi ft}$ still has complex values. Note that, for real-valued processes, both $\eta(t,f)$ and $\xi(t,f)$ will be zero for $f = 0$.

7.4 Numerical examples

We want to test these coherence measures on some random processes. This can of course be done by calculating the exact expressions for a known process. However, we cannot use stationary or cyclostationary processes since this would result in delta functions in the denominator of the coherences. The chirp with Gaussian envelope from Section 3.9 is a good candidate for evaluating the coherences from the calculated expressions. But if we calculate $|\rho_{X,L}(t,f)|^2$, $|\rho_{X,W_L}(t,f)|^2$, $|\gamma_{X,L}(t,f)|^2$ and $|\gamma_{X,W_L}(t,f)|^2$ for this process, we obtain that the coherences equals unity everywhere.

Therefore, we turn to estimating the quantities required in the coherence measures. Since the moment functions, the t-f spectra, and the f-f spectra are estimated with different methods, the values of these estimates are not comparable, and the time-frequency coherence measures based on these estimates will not be properly normalized. The dual-frequency coherence measures, however, only contain Hermitian and complementary f-f spectra, and the f-f spectra are estimated with comparable methods. We will examine the dual-frequency coherences of some processes based on numerical data.

7.4.1 Estimation of the dual-frequency coherence

We will estimate the dual-frequency coherence of a chirp process

$$X(t) = \exp\left[j\pi(2\alpha t + \beta t^2 + \Psi)\right]. \tag{7.19}$$

Here, $K = 250$ samples $x[k]$, $k = 0, \ldots, K-1$, are generated from the process with $\alpha = -0.3$, $\beta = 0.002$ and a random phase Ψ uniformly distributed on $[-1, 1]$. The f-f spectra are estimated using a time-bandwidth product of $KW = 7$.

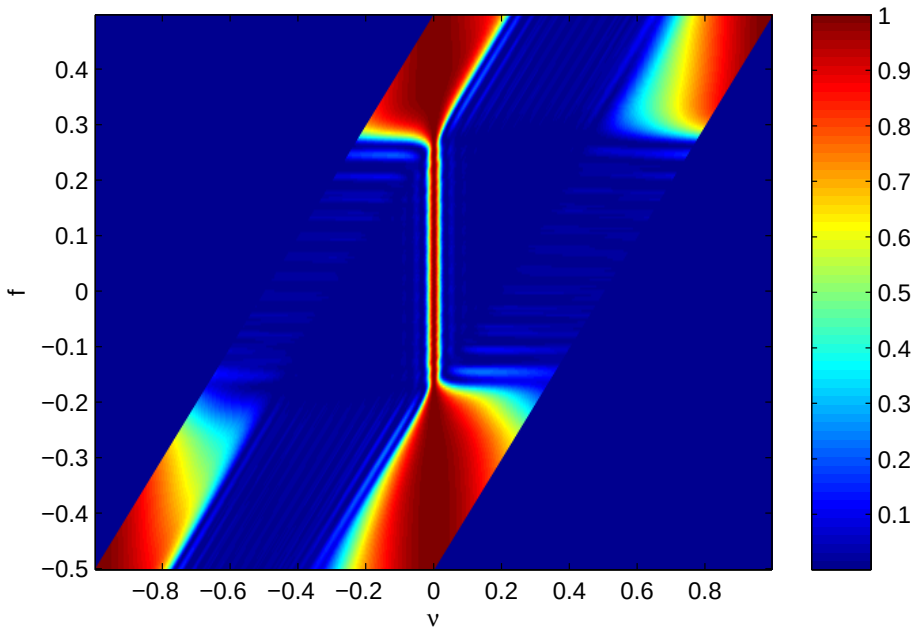

Figure 7.2: Estimate of the dual-frequency coherence $|\rho_{X,L}(\nu, f)|^2$ of a complex-valued chirp.

Figure 7.2 and 7.3 shows the estimate of $|\rho_{X,L}(\nu, f)|^2$ and $|\rho_{X,WL}(\nu, f)|^2$, respectively. The chirp has a starting instantaneous frequency -0.2, and by the last sample the frequency will be 0.3. We see that for $-0.2 \leq f \leq 0.3$, both coherence measures are concentrated in a small area around $\nu = 0$. In this area, the coherence is reasonably constant. Thus, in the frequency range of the chirp, neighboring frequencies are strongly correlated. The estimate of $|\rho_{X,WL}(\nu, f)|^2$ has the disadvantage that it has considerably more noise in this range than the estimate of $|\rho_{X,L}(\nu, f)|^2$.

We would also expect high coherence in the areas of the f-ν plane where both f and $f - \nu$ are outside of the frequency range of the chirp, such that both $dZ(f)$ and $dZ(f-\nu)$ will be zero. These areas are defined more correctly in the estimate of $|\rho_{X,WL}(\nu, f)|^2$ than in the estimate of $|\rho_{X,L}(\nu, f)|^2$.

We stated that $|\rho_{X,WL}(\nu, f)|^2$ also would be an alternative measure of the dual-frequency coherence for real-valued processes. We therefore examine the real-valued chirp process

$$X(t) = \cos\left[\pi(2\alpha t + \beta t^2) + \Psi\right], \tag{7.20}$$

We generated $K = 250$ samples $x[k]$, $k = 0, \ldots, K-1$, of $X(t)$ with $\alpha = -0.2$, $\beta = 0.002$ and a random phase Ψ uniformly distributed on $[-\pi, \pi]$. The es-

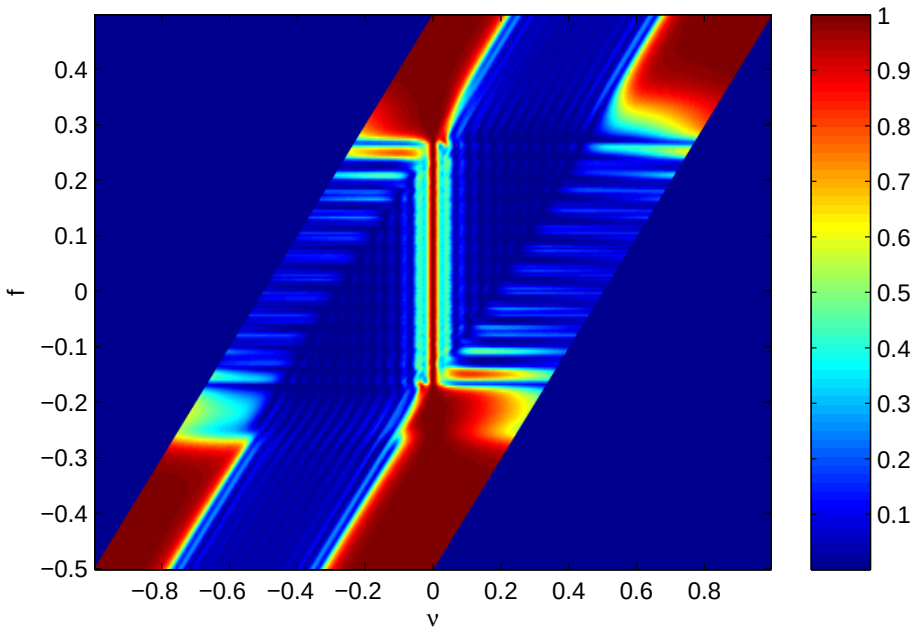

Figure 7.3: Estimate of the dual-frequency coherence $|\rho_{X,WL}(\nu, f)|^2$ of a complex-valued chirp.

timates with a time-bandwidth product $KW = 4$ based on these samples are shown in Figure 7.4 and 7.5. When dealing with real-valued processes, we define $|\rho_{X,WL}(\nu, 0)|^2 = 0$ in order to avoid the singularities at $f = 0$.

As for the complex-valued chirp, we expect high coherence in the areas where both f and $f - \nu$ are not in the frequency range of the chirp. This is a real-valued process, so the increment process of $X(t)$ will have a Hermitian symmetry such that the frequency range of the chirp is $[-0.3, 0.3]$. Again, we see that these areas are better defined in the estimate of $|\rho_{X,WL}(\nu, f)|^2$ than in the estimate of $|\rho_{X,L}(\nu, f)|^2$.

We have high coherence in a small area around $\nu = 0$ in the frequency range of the chirp. Since $X(t)$ is a real-valued process, $dZ(f)$ and $dZ(-f)$ should be strongly correlated. Thus, we should have high coherence in a small area around the line $\nu = 2f$ in the frequency range of the chirp. Both estimates of the dual-frequency coherence of the process have these features. We would expect the value of the coherence of the real-valued chirp in these areas to be constant, as it was for the complex-valued chirp. While $|\rho_{X,WL}(\nu, f)|^2$ is reasonably constant in these areas, $|\rho_{X,L}(\nu, f)|^2$ exhibits quite large variations. But also for this process, there is considerably more noise in $|\rho_{X,WL}(\nu, f)|^2$ in this range.

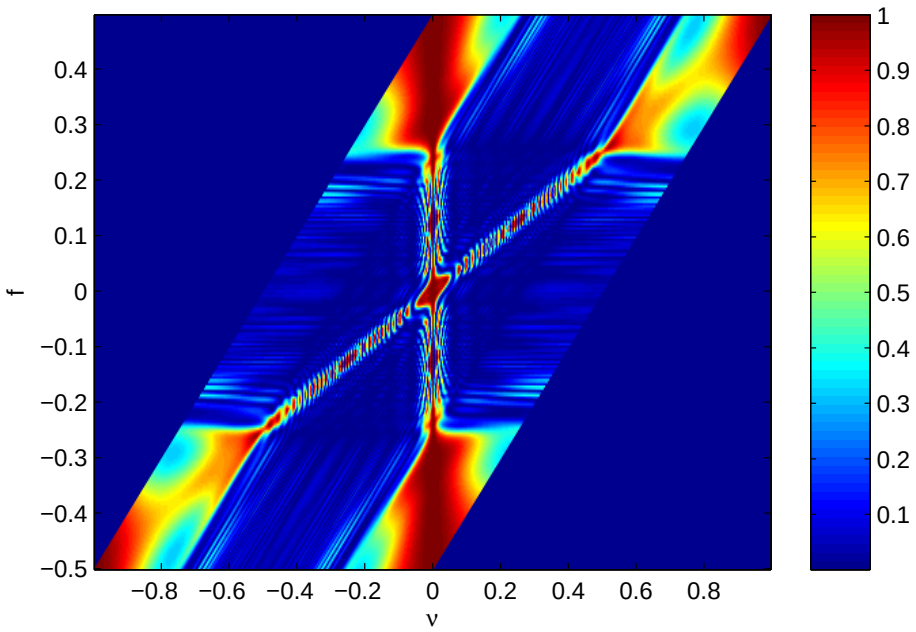

Figure 7.4: Estimate of the dual-frequency coherence $|\rho_{X,L}(\nu, f)|^2$ of a real-valued chirp.

Next, we estimate the dual-frequency coherence of an FBM process. Figure 7.6 and Figure 7.7 shows the estimate of the dual-frequency coherence based on $K = 250$ samples of an FBM process with Hurst parameter $H = 0.1$ using a time-bandwidth product $KW = 4$.

Both coherence estimates have values equal to one on the line $\nu = 0$. Since the FBM process is a real-valued process, we should have strong coherence on the line $\nu = 2f$ as well. In the estimate of $|\rho_{X,L}(\nu, f)|^2$, we can see that there is something happening on this line, but the coherence is far from one. Thus, the coherence based on LMSE could lead to the conclusion that this process is complex-valued. The estimate of $|\rho_{X,WL}(\nu, f)|^2$, however, has values equal to one for $\nu = 2f$.

Finally, the dual-frequency coherence of the earthquake data from Section 6.6 is estimated using a time-bandwidth product $KW = 3$. From Figure 7.8 and Figure 7.9, we see that both estimates have strong coherence on $\nu = 0$. The earthquake data is real-valued, so we expect strong coherence on $\nu = 2f$. We see that also for this process, only $|\rho_{X,WL}(\nu, f)|^2$ has values close to one on this line, whereas $|\rho_{X,L}(\nu, f)|^2$ misses this coherence.

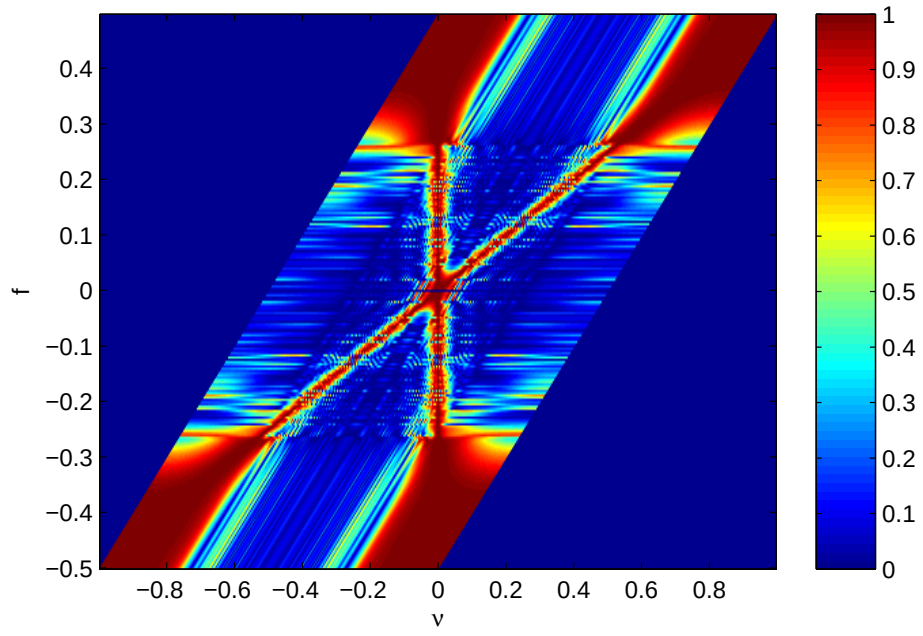

Figure 7.5: Estimate of the dual-frequency coherence $|\rho_{X,WL}(\nu, f)|^2$ of a real-valued chirp.

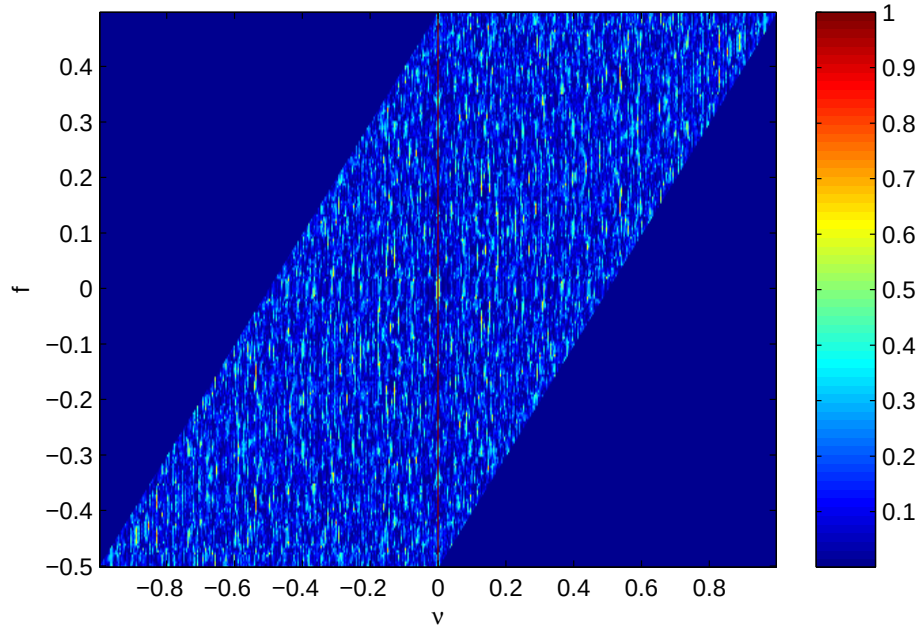

Figure 7.6: Estimate of the dual-frequency coherence $|\rho_{X,L}(\nu, f)|^2$ of an FBM process with Hurst parameter $H = 0.1$.

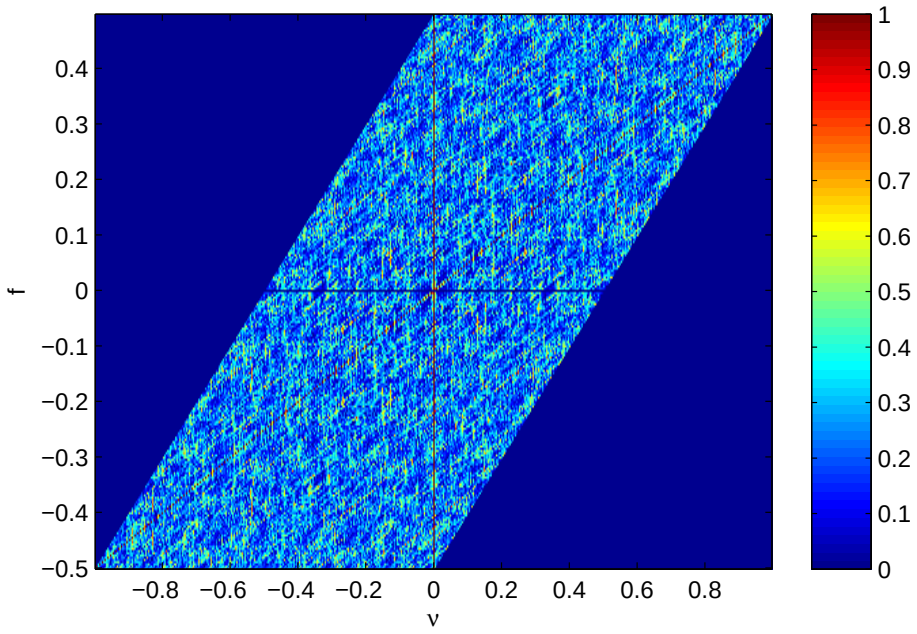

Figure 7.7: Estimate of the dual-frequency coherence $|\rho_{X,W_L}(\nu, f)|^2$ of an FBM process with Hurst parameter $H = 0.1$.

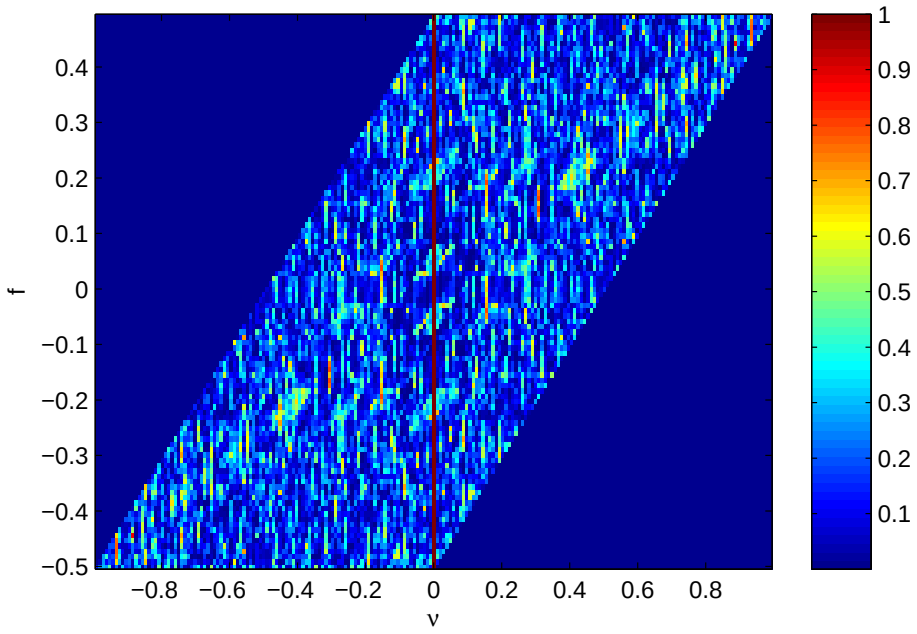

Figure 7.8: Estimate of the dual-frequency coherence $|\rho_{X,L}(\nu, f)|^2$ of the earthquake data.

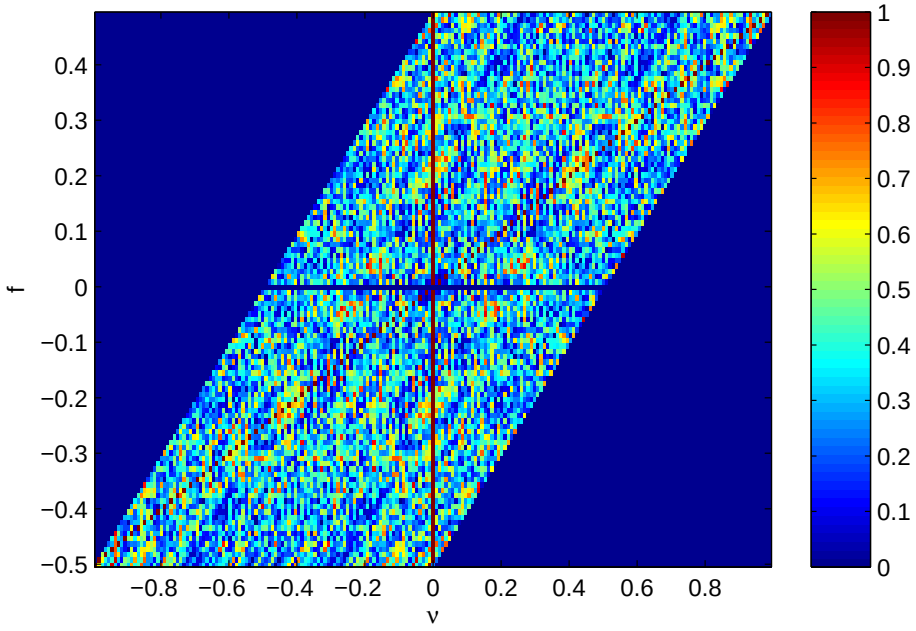

Figure 7.9: Estimate of the dual-frequency coherence $|\rho_{X,WL}(\nu, f)|^2$ of the earthquake data.

Chapter 8

Conclusion

In this thesis, we have studied the second-order statistical quantities of complex-valued harmonizable processes. We saw that the Hermitian second-order statistical quantities of complex-valued, harmonizable processes can be represented in four different domains, through the Hermitian temporal moment function, the Hermitian f-f spectrum, the Hermitian t-f spectrum and the Hermitian ambiguity function. In order to completely describe the second-order statistical quantities of improper complex-valued processes, the complementary moment function, the complementary f-f spectrum, the complementary t-f spectrum and the complementary ambiguity function have to be considered. It is common to assume that complex-valued processes are proper, but we have seen many examples of improper processes in this thesis.

We defined estimators of the moment functions, the ambiguity functions and the f-f spectra of complex-valued processes based on existing estimators for the corresponding quantities of real-valued processes. We implemented new estimators of the t-f spectra of complex-valued harmonizable processes. For these estimators, we have to choose data windows for a factorized kernel. We tested two possible kernels. The kernel with Hamming and Gaussian windows worked well for single-component processes, but exhibited interference terms in the estimates for multi-component processes. A kernel constructed from Kaiser-Bessel windows worked well for both single-component and multi-component processes.

We proposed alternative measures of the dual-frequency and the time-frequency coherence of real-valued and improper complex-valued harmonizable processes. This alternative coherence will depend on both the Hermitian and on the complementary functions of the process. We estimated both the alternative and the conventional dual-frequency coherence based on numerically generated data and on a real-world time series. One problem with the alternative coherence was that it was more noisy than than the conventional coherence. For two of the examined real-valued processes, however, the conventional coherence missed the coherence

due to the Hermitian symmetry of the increment process. This coherence was clearly present in the proposed generalized coherence. Thus, for many processes the alternative coherence is thought to be very useful, even for real-valued processes.

The results of this thesis illustrate the importance of the complementary functions of complex-valued processes. There is still work to be done on the understanding and interpreting of the complementary functions and on the extension to higher-order statistics and higher-order coherences of complex-valued processes.

Bibliography

P. O. Amblard and J. L. Lacoume. *Construction of fourth-order Cohen's class : a deductive approach*. In *Proc. IEEE Symposium on Time-Scale and Time-Frequency Analysis*, pp. 257–260. Victoria, Canada, October 4-6. 1992.

P. O. Amblard and J. L. Lacoume. *A deductive construction of third-order time-frequency distributions*. *Signal Processing*, **36**: 277–286, April 1994.

P. O. Amblard, M. Gaeta and J. L. Lacoume. *Statistics for complex variables and signals - part II: Signals*. *Signal Processing*, **42**: 15–25, November 1996.

F. Auger, P. Flandrin, P. Goncalvès and O. Lemoine. *Time-Frequency Toolbox for use with Matlab*. CNRS (France), Rice University (USA), 1996. The toolbox is available for free download at http://gdr-isis.org/Applications/tftb/iutsn.univ-nantes.fr/auger/tftb.html.

W. R. Bennett. *Statistics of regenerative digital transmission*. *Bell Syst. Tech J.*, **37**: 1501–1542, November 1958.

Y. Birkelund, A. Hanssen and E. J. Powers. *Multitaper estimators of polyspectra*. *Signal Processing*, **83**: 545–559, March 2002.

R. N. Bracewell. *The Fourier Transform and its Applications*. New York, NY: McGraw-Hill, Second Edition, 1986.

S. Cambanis and B. Liu. *On harmonizable stochastic processes*. *Information and Control*, **17**: 183–202, 1970.

L. Cohen. *Generalized phase-space distribution functions*. *J. Math. Phys.*, **7**: 781–786, May 1966.

L. Cohen. *Time-Frequency Analysis*. Englewood Cliffs, NJ: Prentice Hall, 1995.

H. Cramér. *On the theory of stationary random processes*. *Ann. Math.*, **41**: 215–230, January 1940.

A. V. Dandawaté and G. B. Giannakis. *Nonparametric polyspectral estimators for kth-order (almost) cyclostationary processes*. *IEEE Trans. Inform. Theory*, **40**: 67–84, January 1994.

J. L. Doob. *Stochastic Processes*. New York, NY: Wiley, 1953.

A. Einstein. *Method for the determination of the statistical values of observations concerning quantities subject to irregular fluctuations. Archives de Sciences Physiques et Naturales*, **37**: 254–256, 1914. An English translation, originally by AT&T Laboratories, and further edited by W.A. Gardner is available in IEEE ASSP Magazine, October 1987.

P. Flandrin. *Time-Frequency/Time-Scale Analysis*. San Diego, CA: Academic Press, 1999.

J. Fonollosa and C. Nikias. *Wigner higher-order moments spectra: definition, properties, computation and application to transient detection. IEEE Trans. Signal Proc.*, **41**: 245–266, January 1993.

W. A. Gardner and C. Spooner. *The cumulant theory of cyclostationary time-series, part I: Foundation. IEEE Trans. Signal Proc.*, **42**: 3387–3408, December 1994.

E. G. Gladyshev. *Periodically correlated random sequences. Sov. Math.*, **2**: 385–388, March 1961.

C. Granger and M. Hatanaka. *Spectral Analysis of Economic Time Series*. Princeton, NJ: Princeton Univ. Press, 1964.

U. Grenander and M. Rosenblatt. *Statistical Analysis of Stationary Time Series*. New York, NY: Chelsea Publishing Co., Second Edition, 1984.

A. Hanssen and L. L. Scharf. *A theory of polyspectra for nonstationary stochastic processes. IEEE Trans. Signal Proc.*, **51**: 1243–1252, May 2003.

F. J. Harris. *On the use of windows for harmonic analysis with the discrete Fourier transform. Proc. IEEE*, **66**: 51–83, January 1978.

H. Hindberg, R. E. Hansen, T. O. Sæbø and H. J. Callow. *Time-frequency analysis in synthetic aperture sonar*. Technical Report FFI/NOTAT-2004/03365, Norwegian Defence Research Establishment, Kjeller, Norway, November 2004.

F. Hlawatsch. *Time-Frequency Analysis and Synthesis of Linear Signal Spaces: Time-frequency Filters, Signal Detection and Estimation, and Range-Doppler Estimation*. Boston, MA: Kluwer Academic Publishers, 1998.

L. Izzo and A. Napolitano. *The higher order theory of generalized almost-cyclostationary time series. IEEE Trans. Signal Proc.*, **46**: 2975–2989, November 1998.

J. F. Kaiser. *Digital filters*. In *System Analysis by Digital Computer*, edited by F. F. Kuo and J. F. Kaiser, pp. 218–285. New York, NY: Wiley, 1966.

A. Khintchine. *Korrelationstheorie der stationären stochastischen prozesse. Math. Ann.*, **109**: 604–615, 1934.

Y. Larsen. *Spectral properties of harmonizable random processes and fields*. Ph.D. thesis, Department of Physics, Univ. of Tromsø, Norway, 2003.

K. Lii and M. Rosenblatt. *Spectral analysis for harmonizable processes. Ann. of Statistics*, **30**: 258–297, 2002.

M. Loève. *Sur le fonctions aléatoire de second ordre. Rev. Sci.*, **83**: 297–303, 1945.

M. Loève. *Sur le fonctions aléatoire de second ordre. Rev. Sci.*, **84**: 195–206, 1946.

M. Loève. *Probability Theory*. New York, NY: Springer-Verlag, Fourth Edition, 1978.

S. B. Lowen. *Efficient generation of fractional Brownian motion for simulation of infrared focal-plane array calibration drift. Meth. Comp. Appl. Prob.*, **1**: 445–456, 2000.

S. Mallat. *A Wavelet Tour of Signal Processing*. San Diego, CA: Academic Press, 1998.

B. B. Mandelbrot and J. W. Van Ness. *Fractional Brownian motions, fractional noises and applications. SIAM Rev.*, **10**: 422–437, October 1968.

W. Martin and P. Flandrin. *Wigner-Ville spectral analysis of nonstationary processes. IEEE Trans. Acoustics, Speech, Signal Proc.*, **33**: 1461–1470, December 1985.

F. D. Neeser and J. Massey. *Proper complex random processes with applications to information theory. IEEE Trans. Inform. Theory*, **39**: 1293–1302, July 1993.

C. L. Nikias and A. P. Petropulu. *Higher-Order Spectra Analysis. A Nonlinear Signal Processing Framework*. Englewood Cliffs, NJ: Prentice-Hall, 1993.

H. Nyquist. *Certain factors affecting telegraph speed. Bell Syst. Tech. J.*, **3**: 324–346, 1924.

T. A. Øigård. *Statistical analysis and representation of non-trivial signals and random processes*. Ph.D. thesis, Department of Mathematics and Statistics, Univ. of Tromsø, Norway, 2004.

P. Z. Peebles. *Probability, Random Variables and Random Signal Principles*. New York, NY: McGraw-Hill, Fourth Edition, 2001.

D. B. Percival and A. T. Walden. *Spectral Analysis for Physical Applications: Multivariate and Conventional Univariate Techniques*. Cambridge, U.K.: Cambridge Univ. Press, 1993.

B. Picinbono. *Random Signals and Systems*. Englewood Cliffs, NJ: Prentice-Hall, 1993.

B. Picinbono. *On circularity. IEEE Trans. Signal Proc.*, **42**: 3473–3482, December 1994.

B. Picinbono and P. Bondon. *Second-order statistics of complex signals. IEEE Trans. Signal Proc.*, **45**: 411–420, February 1997.

B. Picinbono and P. Chevalier. *Widely linear estimation with complex data. IEEE Trans. Signal Proc.*, **43**: 2030–2033, August 1995.

M. B. Priestley. *Evolutionary spectra and non-stationary processes. Roy. Stat. Soc.*, **B 47**(2): 204–237, 1965.

M. B. Priestley. *Non-Linear and Non-Stationary Time Series Analysis*. London, U.K.: Academic, 1988.

J. G. Proakis and M. Salehi. *Communication Systems Engineering*. Upper Saddle River, NJ: Prentice-Hall, Second Edition, 2002.

A. Rihaczek. *Signal energy distribution in time and frequency. IEEE Trans. Inform. Theory*, **14**: 369–374, May 1968.

M. Rosenblatt. *Stationary Sequences and Random Fields*. Boston, MA: Birkhäuser, 1985.

L. L. Scharf, B. Friedlander, P. Flandrin and A. Hanssen. *The Hilbert space geometry of the stochastic Rihaczek distribution*. In *Proc. 35th Asilomar Conf. on Signals, Systems, Comput.*, pp. 720–725. Pacific Grove, CA, November 4-7. 2001.

L. L. Scharf, P. J. Schreier and A. Hanssen. *The Hilbert space geometry of the Rihaczek distribution for stochastic analytic signals. IEEE Signal Proc. Lett.*, **12**: 297–300, April 2005.

P. J. Schreier and L. L. Scharf. *Second-order analysis of improper complex random vectors and processes. IEEE Trans. on Signal Processing*, **51**: 714–725, March 2003a.

P. J. Schreier and L. L. Scharf. *Stochastic time-frequency analysis using the analytic signal: Why the complementary distribution matters. IEEE Trans. Signal Proc.*, **51**: 3071–3079, December 2003b.

C. E. Shannon. *Communications in the presence of noise. Proc. IRE*, **37**: 10–21, January 1949.

D. Slepian. *Prolate spheroidal wave functions, Fourier analysis and uncertainty V: the discrete case. Bell Syst. Tech. J.*, **57**: 1371–1429, 1978.

C. M. Spooner and W. A. Gardner. *The cumulant theory of cyclostationary time-series, part II: Development and applications. IEEE Trans. Signal Proc.*, **42**: 3409–3429, December 1994.

A. Swami, G. B. Giannakis and G. Zhou. *Bibliography on higher-order statistics. Signal Processing*, **60**: 65–126, July 1997.

D. J. Thomson. *Spectrum estimation and harmonic analysis. Proc. IEEE*, **70**: 1055–1096, September 1982.

D. J. Thomson. *Multi-window bispectrum estimates.* In *Proc. IEEE Workshop on Higher-Order Spectral Analysis*. Vail, CO, June 28-30. 1989.

J. Ville. *Théorie et applications de la notion de signal analytique. Cables et Trans.*, **2**(1): 61–74, 1948.

N. Wiener. *Generalized harmonic analysis. Acta Math.*, **55**: 117–258, 1930.

E. P. Wigner. *On the quantum correction for thermodynamic equilibrium. Phys. Rev.*, **40**: 749–759, 1932.

A. M. Yaglom. *An Introduction to the Theory of Stationary Random Functions*. Englewood Cliffs, NJ: Prentice Hall, 1962.

A. M. Yaglom. *Correlation Theory of Stationary and Related Random Functions*. New York, NY: Springer-Verlag, 1987.